Electron-electron Collisions and Drift Velocity Fluctuations in n-GaAs at T=80 K

R. Raguotis

Centre of Physical Sciences and Technology Semiconductor Physics Institute, Vilnius, Lithuania
E-mail: romasr@pfi.lt

Abstract: Modified combined scattering rate Monte Carlo technique is proposed. Electron collisions with phonons, impurities and among themselves are taken into account. The proposed technique avoids the short-time-step procedure inherent to conventional ensemble Monte Carlo method. All *N* modeled electrons move using the total probability for the scattering of each electron by the thermal bath and mutual scattering between electrons pairs ("events in the electron system"). The quantitative fitting to the available experimental data on the spectral density is achieved and the range of moderate fields is defined for interparticle collisions to manifest themselves in the noise. In the second part of the presented report a drift velocity correlator is investigated numerically by Monte Carlo simulation and for the fist time analytically by a phenomenological approach taking into account electron-phonon and electron-electron scattering between free carriers. The thermodynamic approach is investigated. The results of the velocity-to-velocity correlation functions and electron noise spectrum obtained analytically are in quite good agreement with those given by the Monte Carlo method.
Keywords: Monte Carlo, Electron-electron collisions, Drift velocity fluctuations, Spectral density.

1. Introduction

Fluctuations phenomena in semiconductors have been intensively investigated during the last three decades [1-3]. Fluctuation effects have been conventionally investigated without an account on the Coulomb electron-electron (e-e) scattering. However at sufficiently high electron densities, it is necessary to take into account e-e scattering to the total distribution function and related correlators.
Interparticle collisions though conserving energy and momentum of the electron system have an indirect effect on transport and – even more direct – on velocity correlations. In the presented report the 'combined scattering method' (CSR) Monte Carlo method [4] is used to interpret the results of microwave noise.

The important role of e-e collisions is demonstrated, and velocity-velocity cross-correlation under non-e1uilibrium conditions is calculated. In the second part drift velocity correlation functions are investigated analytically in a phenomenological approach and numerically through Monte Carlo simulation.

Thermodynamic equilibrium state is investigated. Analytical results are in good agreement with those obtained by Monte Carlo method in the GaAs crystals.

2. Electron-electron collisions. Drift velocity fluctuations

It can be shown [4] that the "time of free flight" for independent scattering events of the N electron system with $\mathbf{k}_i$ wave-vectors is defined by the combined scattering rate:

$$\lambda_{comb}(\mathbf{k}_1, \mathbf{k}_2, ..., \mathbf{k}_N) = \sum_{i=1}^{N} \lambda_i(\mathbf{k}_i) + \frac{1}{N-1} \sum_{i=1}^{N-1} \sum_{j=i+1}^{N} \lambda_{ij}^{ee}(\mathbf{k}_i, \mathbf{k}_j) \qquad (1)$$

where $\lambda_i(\mathbf{k}_i)$ and $\lambda_{ij}^{ee}(\mathbf{k}_i, \mathbf{k}_j)$ are conventional integral rates of scattering of the ith electron by the thermal bath and by the jth electron respectively [5]. Equation (1) reduces to that written down in [6] for N=2. All N electrons move without scattering for the "time of free flight of the system" between two successive events of an electron by the thermal bath or mutual collision between two electrons occurs. The "time of free flight" is defined from the sum of the each electon scattering rate on the thermal bath and on the all remaining electrons. CSR technique avoids the short-time step procedure and a large electron number inherent to conventional ensemble MC simulation.
The time-displaced drift-velocity correlation function is

$$\Phi_{total} = N\overline{\delta v_d(t_1 + t)\delta v_d(t_1)} = \Phi_{auto} + \Phi_{cross}\ , \qquad (2)$$

where the auto- and cross-correlation functions are defined as:

$$\Phi_{auto} = \overline{\frac{1}{N}\sum_i \delta v_i(t_1 + t)\delta v_i(t_1)},\ \ \Phi_{cross} = \overline{\frac{1}{N}\sum_{i \neq j} \delta v_i(t_1 + t)\delta v_j(t_1)}\ , \qquad (3)$$

In order to demonstrate the effect of e-e collisions on fluctuations the calculated velocity correlation functions in heating electric field are shown in Figure 1 for a model corresponding to n-type GaAs with the impurity scattering neglected. In our case $\tau_{ee} \leq \tau_p$ strong cross-correlation appears. The equal-time cross-correlation also appears in non-equilibrium system as it was predicted in [1]. The auto-correlation decreases mainly in time τ_{ee}. The decay of Φ_{total} is caused by the electron interaction with thermostat. In thermodynamic equilibrium, when $\Phi_{cross}(0) = 0$, the latter is equal to $\Phi_{total}(0) = \Phi_{auto}(0) = \overline{V^2} = kT/m$.

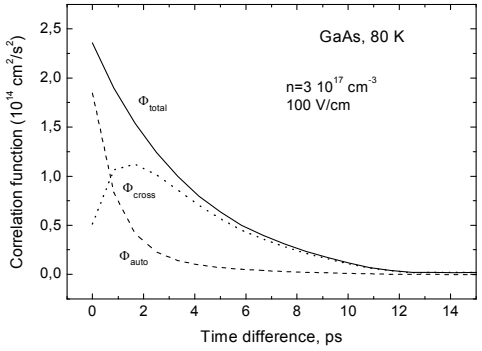

Fig. 1. Drift-velocity correlation functions: total (solid line), auto-correlation (dashed line) and cross-correlation (dotted line). Phonon and interelectron scattering is taken into account, impurity scattering is neglected

The results of the spectral density on the spectral density of drift velocity fluctuations are presented in Figure 2. The experimental data are obtained from the current fluctuations data through normalization at zero field by using mobility data and Nyquist formula [7]. One can see that the most pronounced effect is obtained at intermediate fields ranging from 5 V/cm to 500 V/cm

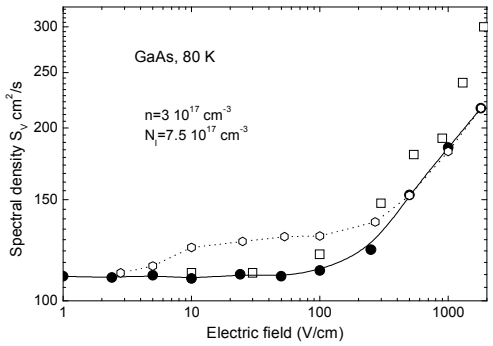

Fig. 2. Dependence of the spectral density of electron drift velocity fluctuations in compensated n-GaAs. MC with phonon, impurity and e-e scattering: (closed circles), without e-e scattering (diamonds). Experimental data–open squares [7].

The nearly constant behavior at fields up to 100 V/cm can be explained by enhanced energy loss by electrons on optical phonons in the presence of e-e collisions. The role of e-e collisions diminishes at higher field.

3. Drift velocity correlations in semiconductors in the thermodynamic equilibrium state.

The values of correlators at the thermodynamic equilibrium have been calculated for the parabolic model of Γ valley in GaAs. The material parameters correspond to these listed in [8]. Electron scattering on non-elastic acoustic and optical modes of lattice vibrations, as well as e-e scattering ($n_e = 10^{15}$ cm^{-3}) is taken into account. Inter-electron collisions are treated in the Brooks-Herring approximation. Standard expressions for electron scattering rates are used [5]. The calculations are performed by the CSR method.

Let us start with the simplified Boltzmann-Langevin equation for the fluctuation distribution function. In the state of thermodynamic equilibrium it can be written as

$$\frac{d\delta F_p(t)}{dt} = -\frac{\delta F_p(t)}{\tau_p} - \frac{\delta F_p(t) - \delta F_p^M(t)}{\tau_{ee}} + y_p(t) \qquad (4)$$

Here $F_p(t)$ is the instantaneous electron momentum distribution function, $F_p^M(t)$ is the drifted Maxwellian distribution corresponding to the $F_p(t)$ at time t, $y_p(t)$ describes the Langevin random force. In our case the rate of fluctuation relaxation is governed by the lattice and e-e scattering mechanisms.

The first term on the right-hand side of equation (4) ensures the relaxation of instantaneous distribution $F_p(t)$ to the equilibrium distribution during lattice relaxation time τ_p. The second term is written in accordance with the Gross-Bhatnager-Krook approach [9]. Its form is based on the property of the instantaneous electron distribution function to acquire symmetric form (the drifted Maxwellian distribution) in the e-e scattering time τ_{ee} under the influence of e-e scattering. R. Liboff in his textbook [10] gives considerable attention to this approach (see also [11]). Electron momentum can be intensively scattered by impurity centers too, but the energy of electrons is conserved in this scattering process. Even in this simple approach we cannot predict the final distribution that will result under the influence of impurity scattering. Therefore, we will omit further the impurity scattering.

The therm $\delta F_p^M(t)$ describes the deviation of a drifted Maxwellian distribution.

E-e scattering does not tend to bring either $F_p^M(t)$ or $F_p(t)$ to the thermodynamic equilibrium, because the average energy and momentum do not

change during e-e collisions. So, the drifted Maxwellian distribution is supposed to relax only under the influence of lattice scattering during the corresponding scattering time τ_p. Therefore, we have used $\delta F_p^M(t) = \delta F_p^M(0)\exp(-t/\tau_p)$.
Then, we multiply the equation (4) by the initial distribution function fluctuation $\delta F_{p1}(t_1)$, and average the product. Let us denote the correlator $\overline{\delta F_{p1}(t_1)\delta F_p(t_1+t)}$ as $\overline{\delta F_{p1}(0)\delta F_p(t)}$). Now we write the dynamic equation:

$$\frac{d\overline{\delta F_{p1}(0)\delta F_p(t)}}{dt} = -\frac{\overline{\delta F_{p1}(0)\delta F_p(t)}}{\tau_p} - \frac{\overline{\delta F_{p1}(0)\delta F_p(t)} - \overline{\delta F_{p1}(0)\delta F_p^M(0)}\exp(-t/\tau_p)}{\tau_{ee}} \tag{5}$$

The last term in Eq. (3) representing a random force vanishes because this force is δ-correlated in time. Initial fluctuations of an actual distribution and the drifted Maxwellian distribution are related in the following way:

$$\delta F_p^M(0) = \delta F_p(0) + \Delta F_p(0) \tag{6}$$

where $\Delta F_p(0)$ is deviation between them. Because of the chaotic behaviour of $\Delta F_p(0)$ we assume that

$$\overline{\delta F_{p1}(0)\delta F_p^M(0)} = \overline{\delta F_{p1}(0)\delta F_p(0)} \tag{7}$$

We are interested in the velocity-to-velocity correlators; therefore we multiply the equation (4) by $V_{i1}(0)V_j(t)$ and sum it up by p_1 and p. Finally, we obtain the phenomenological equation describing the relaxation of the total velocity-to-velocity correlator coefficient $c_{total}(t) = c_{auto}(t) + c_{cross}(t)$ in the thermodynamic equilibrium:

$$\frac{dc_{total}(t)}{dt} = -\frac{c_{total}(t)}{\tau_p} - \frac{c_{total}(t) - c_{total}(0)\exp(-t/\tau_p)}{\tau_{ee}} \tag{8}$$

The first-order linear differential equations for the velocity-to-velocity correlator coefficients can be then written as

$$\frac{dc_{auto}(t)}{dt} = -\frac{c_{auto}(t)}{\tau_p} - \frac{c_{auto}(t)}{\tau_{ee}}$$
$$\frac{dc_{cross}(t)}{dt} = -\frac{c_{cross}(t)}{\tau_p} - \frac{c_{cross}(t)}{\tau_{ee}} + \frac{\exp(-t/\tau_p)}{\tau_{ee}} \quad (9)$$

Taking into account the known initial conditions [1] under equilibrium: $c_{auto}(0) = 1$, and $c_{cross}(0) = 0$, the correlation coefficients are given as

$$c_{auto}(t) = e^{-t/\tau_c},$$
$$c_{cross}(t) = e^{-t/\tau_p}(1 - e^{-t/\tau_{ee}}). \quad (10)$$

As it seen the auto-correlation coefficient in equilibrium decreases exponentially with a combined relaxation time $\tau_c = \tau_p \tau_{ee}/(\tau_p + \tau_{ee})$. This result describes conventionally the relaxation of the probe particle velocity correlator. We obtain from the second equation that the cross-correlation coefficient tends to increase during the time τ_{ee}, but then decreases to zero per lattice scattering time.
One can see an important result of the total correlation coefficient:

$$c_{total}(t) = c_{auto}(t) + c_{cross}(t) = \exp(-t/\tau_p), \quad (11)$$

which shows that it does not depend on e-e scattering.
The analytical dependencies calculated with equation (11) reasonably well coincide with those from the MC data (Fig. 3).

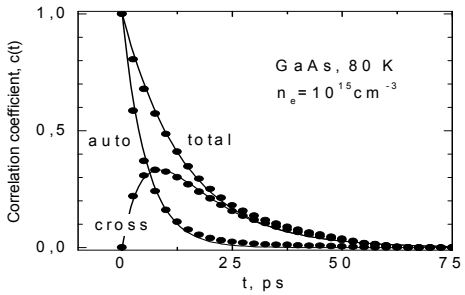

Fig. 3. Relaxation of velocity correlation coefficients in n-GaAs. Points - MC, curves by equations (1).

The characteristic time at which the cross-correlation function reaches its maximum in the case of $\tau_{ee} \le \tau_p$ is $t_{\max} \approx \tau_{ee} \ln(1 + \tau_p/\tau_{ee})$. The more details of the corelation functions bechavior (spectral density, etc.) can be found in [12].

4. Conclusions

The presented MC procedure was demonstrated to be an efficient tool for studying electron noise in the presence of e-e scattering. Taking them in accordance is crucial for explanation of experimental data on microwave noise in doped GaAs.

The results of analytical approach are in good agreement with the Monte Carlo simulation, what confirms the usefulness of our simple analytical model. Till now only the single particle autocorrelation behavior has been describe analytically in the textbooks of fluctuation phenomena (for example, see [13]).

References

1. S. V. Gantsevich, V.L.Gurevich, Katilius. R. *Riv. Nuovo Cimento* 2: 1-87, 1979.
2. Sh. Kogan. *Electronic Noise and Fluctuations in Solids.*Cambridge University Press, Cambrige, Ghap. 3, 1996.
3. H. L. Hartnagel, R. Katilius and A. Matulionis. *Microwave noise in Semiconductor Devices*, Wiley & Sons, New York, 2001.
4. A. Matulionis, R. Raguotis, and R. Katilius. *Phys. Rev. B 56*: 2052–2057, 1997.
5. C. Jacoboni and P. Lugli. *The Monte Carlo method for semiconductor Device Simulation.* Springer-Verlag, Wien, 1989.
6. A. Hasegawa, K. Miyatsuji, K. Tanaguchi, and C. Hamaguhi. *Solid-State Electron.* 31: 547-550, 1988.
7. V. Ainkevičius, V. Bareikis, J. Liberis, A. Matulionis, and P. Sakalas. *Solid-State Electron 36*: 1339- 1343, 1993.
8. K. Brennan and K. Hess K. *Solid-State Electron*. 27: 347 1984
9. E. Gross E, D. Bhatnager, M Krook *Phys. Rev*. 94: 511, 1954
10. R. L. Liboff . *Introduction to the theory of kinetic equations*, Wiley, N.Y., 1969.
11. Ned S. Wingreen, C. J. Stanton , and J. W. Wilkins. *Phys. Rev. Lett.* 57: 1084, 1986.
12. R. Raguotis. *J. Phys. Condens. Matter*. 16: 3973-3670, 2004.
13. L. D. Landau and E. M. Lifshitz. *Statistical physics*, Pergamon Press LTD 5, 1958.


Proceedings, 4th Chaotic Modeling and Simulation International Conference
31 May – 3 June 2011, Agios Nikolaos, Crete Greece

Angular Momentum Method for Analysis of Irregular Time Series

Zoran Rajilić

University of Banja Luka, M. Stojanovića 2, 51000 Banja Luka,
Republic of Srpska, Bosnia and Herzegovina
(E-mail: ZoranRajilic@netscape.net)

Abstract. A quantity formally similar to averaged angular momentum is computed for many chaotic scalar time series with additional Gaussian noise. Considered time series are constructed using iterative maps, three-dimensional ODEs and computer generated noise. Using proposed method we can distinguish chaos with noise from pure noise, if level of noise in time series is low enough. Some types of chaos can be detected in short time series with very high level of noise. Application of the method on real time series is demonstrated.
Keywords: Chaos, noise, time series.

1 Introduction

Identifying chaos in time series is a very difficult task arising in physics, fluid mechanics, astronomy, geophysics, meteorology, ecology, life sciences and finance. One can try to solve this task using time delay embedding [1,2] and correlation dimension algorithm [3] or estimating entropies [4] and Lyapunov exponents [5,6]. There are methods for analysis of irregular time series (chaotic and stochastic) based on short-term predictability (chaotic systems follow definite rules), detection of nonlinearity, reversibility, surrogate data and transportation distance function [7]. It is important for understanding, modeling and forecasting of complex processes [8].
We compute here a quantity looks like the averaged component of the angular momentum of a particle. The aim is to develop a new approach in the analysis of irregular time series in other to have the value of this quantity as an additional indicator of chaos, in a specific time series, beside other indicators obtained by different methods. Our mechanical view on time series is similar to Tuncay's mechanics of stock exchange, where he introduces potential and kinetic energies for prices [9].

2 Angular Momentum

For a time series α_j $(1 \leq j \leq N+3)$, we compute

$$x_j = \frac{\alpha_j}{\alpha_{max}} \tag{1}$$

where

$$\alpha_{max} = max\{|\alpha_j|; j = 1, 2, ..., N + 3\} \tag{2}$$

Then we take

$$y_j = x_{j+3}, \quad 1 \leq j \leq N \tag{3}$$

(it is not so important if time delay is 1, 2 or 3) and compute components of velocity in discrete time

$$v_{xj} = x_j - x_{j-1}, \quad v_{yj} = y_j - y_{j-1}, \quad 2 \leq j \leq N \tag{4}$$

We can now find out values of z component of the angular momentum

$$L_{zj} = x_j v_{yj} - y_j v_{xj}, \quad 2 \leq j \leq N \tag{5}$$

For a particle of unit mass with coordinates x_j and y_j, the quantity

$$L = \frac{1}{N-1} \sum_{j=2}^{N} L_{zj} \tag{6}$$

would be the angular momentum averaged in discrete time. We will see that the level of noise in a time series significantly influences the value of L.

3 Time Series Constructed Using Feigenbaum Map and Lorenz Equations

We compute here

$$\alpha_j = (1 - b)\xi_j + b\xi_{max} G_j \tag{7}$$

where

$$\xi_j = 1 - q\xi_{j-1}^2 \tag{8}$$

(Feigenbaum map) and

$$\xi_{max} = max\{|\xi_j|; j = 1, 2, ..., N + 3\} \tag{9}$$

G_j is computer generated Gaussian noise where distribution mean is zero and scale parameter is one. The level of noise is denoted by b. For low enough b, we can distinguish chaotic time series with noise from clean noise if the averaged angular momentum (L) is computed (figures 1 and 2).
We also use the relations (7) and (9) after replacement

$$\xi_j \longrightarrow \xi(jh) \tag{10}$$

where $\xi(jh)$ satisfies equations (Lorenz)

$$\frac{d\xi}{dt} = 10(\eta - \xi), \quad \frac{d\eta}{dt} = r\xi - \eta - \xi\zeta, \quad \frac{d\zeta}{dt} = \xi\eta - \frac{8}{3}\zeta \tag{11}$$

Again we can distinguish chaotic time series with noise from clean noise, for low enough noise level (figure 3).

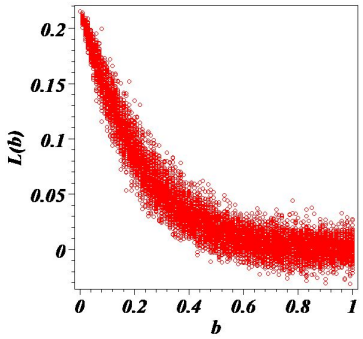

Fig. 1. Averaged angular momentum (L) of a very short time series ($N = 300$) constructed using Feigenbaum map (8) with $q = 1.94$ and $\xi_0 = 0.6$. For low enough noise level b, $L(b)$ is different from $L(1)$ (corresponding to clean Gaussian noise).

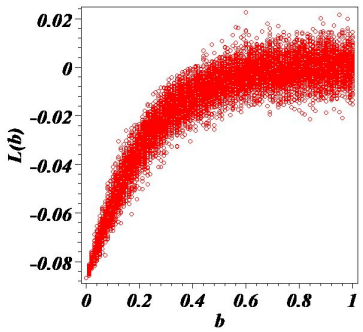

Fig. 2. L of time series with $N = 597$ constructed using Feigenbaum map (8) with $q = 1.67$ and $\xi_0 = 0.4$.

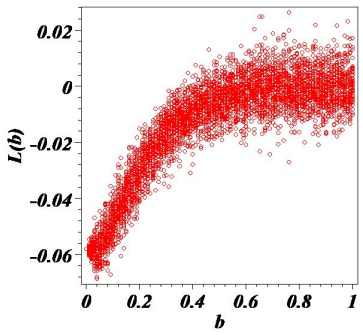

Fig. 3. Averaged angular momentum of time series with $N = 475$ constructed using Lorenz equations (11) with $r = 30$ and $\xi(0) = \eta(0) = \zeta(0) = 1$. Here $h = 0.1$.

4 LM Diagrams

Besides the averaged angular momentum L, the spread of angular momentum

$$M = max\{L_{zj}; j = 2, 3, ..., N\} - min\{L_{zj}; j = 2, 3, ..., N\} \qquad (12)$$

will be of crucial importance in our approach.
Here we consider time series (7) with (10) using three-dimensional ODEs like (11). We take

$$N = 3000, \quad 0.01 \leq h \leq 0.1, \quad -1 \leq \xi(0), \eta(0), \zeta(0) \leq 1 \qquad (13)$$

Values of $h, \xi(0), \eta(0), \zeta(0)$, restricted in this manner, we choose randomly.

We have computed L and M for 2800 different chaotic time series with additional Gaussian noise (red circles in figures 4,5,6,7). There are included:

- 200 different time series ($\alpha_j = (1-b)\xi(jh) + b\xi_{max}G_j$) constructed using Lorenz equations (11) with $r = 28$ and different values of b, h, $\xi(0)$, $\eta(0)$ and $\zeta(0)$ randomly chosen in given intervals
- 200 different time series constructed using Rössler equations

$$\frac{d\xi}{dt} = -\eta - \zeta, \quad \frac{d\eta}{dt} = \xi + 0.1\eta, \quad \frac{d\zeta}{dt} = 0.1 + \zeta(\xi - 10)$$

- 200 different time series constructed using Ueda equations

$$\frac{d\xi}{dt} = \eta, \quad \frac{d\eta}{dt} = -\xi^3 - k\eta + B\sin\zeta, \quad \frac{d\zeta}{dt} = 1$$

  with $k = 0.06$ and $B = 8.1$
- 200 different time series constructed using Rikitake equations

$$\frac{d\xi}{dt} = -\mu\xi + \zeta\eta, \quad \frac{d\eta}{dt} = -\mu\eta + (\zeta - a)\xi, \quad \frac{d\zeta}{dt} = 1 - \xi\eta$$

  with $\mu = 1$ and $a = 4$
- 200 different time series constructed using modified Lorenz equations [10]

$$\frac{d\xi}{dt} = 10(\eta - \xi), \quad \frac{d\eta}{dt} = (24 - 4\rho)\xi + \rho\eta - \xi\zeta, \quad \frac{d\zeta}{dt} = \xi\eta - \frac{8}{3}\zeta$$

  where $\rho = 6.4$
- 200 different time series constructed using modified Lorenz equations with another value of ρ corresponding to chaos
- etc.

We also have computed L and M for 3600 different stochastic time series (blue circles in figures 4,5,6,7) with $N = 3000$. There are included:

- 200 different time series with float random numbers between 6.9 and 25.3
- 200 different time series with rational random numbers between $-15/2$ and $15/2$
- 200 different time series with integer random numbers between -61 and -4
- 200 different time series with random numbers between other certain boundaries
- random series with Gaussian distribution ($b = 1$)
- etc.

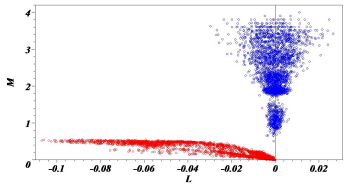

Fig. 4. Averaged angular momentum (L) and spread of the angular momentum (M) for chaotoc time series (red circles) and stochastic time series (blue circles). Here we take $b = 0$ (there is not noise in chaotic time series) and $N = 3000$.

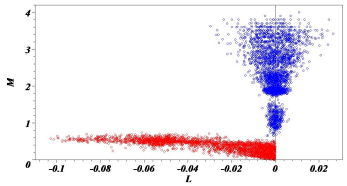

Fig. 5. L and M for chaotic time series with noise (red circles) and stochastic time series (blue circles). Here $0 \leq b \leq 0.05$ (the level of noise is randomly chosen) and $N = 3000$.

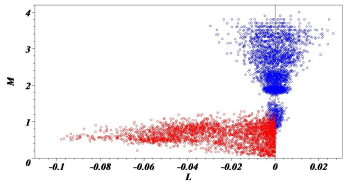

Fig. 6. Averaged angular momentum and spread of the angular momentum for chaotic time series with noise (red circles) and stochastic time series (blue circles). Here we take $0 \leq b \leq 0.15$ and $N = 3000$. Broadening of red area, compared with the previous figure, is a consequence of the increasing of maximal b.

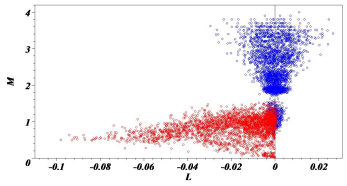

Fig. 7. L and M for chaotic time series with noise (red circles) and stochastic time series (blue circles). Here $0 \leq b \leq 0.3$ and $N = 3000$. If the point (L, M), for a real time series, is in the overlapping area of red and blue circles, we can not distinguish chaos from noise.

5 Real Time Series

If α_n $(1 \leq n \leq N+3)$ is vertical acceleration (nm/s^2) of the Kobe earthquake in nth second [11], recorded at Tasmania University on 16 January 1995, we find $L = -0.01$ and $M = 0.5$. Here $N = 3045$. The point $(-0.01, 0.5)$ is in red area of figure 5 so we conclude that we have an indication of chaos. We find, using angular momentum method, that considered real time series is chaotic one with the noise level $b \leq 0.05$. This is in agreement with two results published before. First, de Sousa Vieira found out that chaos is present in the symmetric two-block Burridge-Knopoff model for earthquakes [12]. Second, according to Iliopoulos et al. [13], the Hellenic lithospheric system appears to be in a state of early turbulence with a low dimensional universal attractor.

Considering monthly temperatures in England [11] for the yers 1723-1970 $(N = 2973)$, we get $L = -0.06$ and $M = 0.7$. One can see the point $(-0.06, 0.7)$ in red area of figure 5. Again we have chaos with noise of level $b \leq 0.05$. It is interesting that Berndtsson et al. [14] analyzed monthly temperature time series observed in Lund (1753-1990) and concluded that there are indications of a low dimensional chaotic component.

For daily brightness of a variable star on successive midnights [11] $(N = 597)$ it is found $L = -0.02$. If we use figure 2, we can conclude that there is a very large amount of noise in this time series. This is in agreement with the results found by Kiss et al. Power spectra of red supergiant stars show a single mode resolved into multiple peaks under a Lorenzian envelope, interpreted as evidence for stochastic oscillations caused by convection and pulsations. A strong $1/f$ noise component in the power spectra is also found [15].

Considering monthly prices of gold in US Dollars from January of 1971 to October of 2010 [16] $(N = 475)$, we find out $L = -0.00013$. For prices in Yens we get $L = -0.00074$. We conclude that these time series are stochastic both (figure 3). It is often in econometrics that time series are assumed to be stochastic [17].

6 Conclusion

The proposed angular momentum method can give us an indication of low-dimensional chaos in a noisy time series. It is possible sometimes distinguish chaos from noise in a very short time series. We have analyzed some real time series using the angular momentum method and our results are in agreement with the published results obtained by some other methods. We are restricted here on certain types of chaos and noise so there are time series we can not analyze using the method. The upgrade of LM diagrams is possible and the method can be more efficient, but never absolutely efficient.

References

1.N. Packard, J. Crutchfield, D. Farmer, and R. Shaw. Geometry from a time series. *Phys. Rev. Lett.*, 45:712, 1980.
2.H.F. Astudillo, F.A. Borotto, and R. Abarca-del-Rio. Embedding reconstruction methodology for short time series - application to large El Niño events. *Nonlin. Processes Geophys.*, 17:753, 2010.
3.P. Grassberger and I. Procaccia. Characterization of strange attractors. *Phys. Rev. Lett.*, 50:346, 1983.
4.S.Q. Zhang, Y.C. Zhao, J. Jia, L.G. Zhang, and H.L. Shanguan. Research on the chaos recognition method based on differential entropy. *Chin. Phys. B*, 19:060514, 2010.
5.J.B. Gao, J. Hu, W.W. Tung, and Y.H. Cao. Distinguishing chaos from noise by scale-dependent Lyapunov exponent. *Phys. Rev. E*, 74:066204, 2006.
6.T.Q.D. Khoa, N. Yuichi, and N. Masahiro. Recognizing brain motor imagery activities by identifying chaos properties of oxy-hemoglobin dynamics time series. *Chaos, Solitons & Fractals*, 42:422, 2009.
7.S. Basu and E. Foufoula-Georgiou. Detection of nonlinearity and chaoticity in time series using the transportation distance function. *Phys. Lett. A*, 301:413, 2002.
8.L. Lacasa and R. Toral. Description of stochastic and chaotic series using visibility graphs. *Phys. Rev. E*, 82:036120, 2010.
9.Ç. Tuncay. Stock Mechanics: Predicting Recession in S&P500, DJIA and NASDAQ. *Cent. Eur. J. Phys.*, 4:58, 2006.
10.K. Sun and J.C. Sprott. Dynamics of a simplified Lorenz system. *Int. J. Bif. Chaos*, 19:1357, 2009.
11.R. Hyndman. Time Series Data Library. http://robjhyndman.com/TSDL
12.M. de Sousa Vieira. Chaos and Synchronized Chaos in an Earthquake Model. *Phys. Rev. Lett.*, 82:201, 1999.
13.A.C. Iliopoulos, G.P. Pavlos, and M.A. Athanasiu. Spatiotemporal Chaos into the Hellenic Seismogenesis: Evidence for a Global Seismic Strange Attractor. *Nonlinear Phenomena in Complex Systems*, 11:274, 2008.
14.R. Berndtsson, C. Uvo, M. Matsumoto, K. Jinno, A. Kawamura, S. Xu, and J. Olsson. Solar-Climatic Relationship and Implications for Hydrology. *Nordic Hydrology*, 32:65, 2001.

15.L.L. Kiss, G.M. Szabó, and T.R. Bedding. Variability in red supergiant stars: pulsations, long secondary periods and convection noise. *Mon. Not. R. Astron. Soc.*, 372:1721, 2006.
16.Gold Research and Statistics, http://www.research.gold.org/prices/monthly
17.E. Otranto. Clustering heteroskedastic time series by model-based procedures. *Computational Statistics & Data Analysis*, 52:4685, 2008.

Proceedings, 4th Chaotic Modeling and Simulation International Conference
31 May – 3 June 2011, Agios Nikolaos, Crete Greece

Evidence of Deterministic Behavior in the Financial Markets: Classification of Underlying Dynamics

L. Romano[1], G. Greco[2], P. Pattitoni[3,4] and R. Rosa[1,5]

[1] Department of Statistical Sciences, University of Bologna, Italy
(E-mail: sololaluna85@hotmail.it)
[2] INAF-Astronomical Observatory of Bologna, Italy
[3] Department of Management, University of Bologna, Italy
[4] The Rimini Centre for Economic Analysis (RCEA), Rimini, Italy
[5] CNR-IMM, Department of Bologna, Bologna, Italy

Abstract. *Aim.* This work aims to find evidence of deterministic dynamics in Financial Markets combining the advanced spectral method of the Singular-Spectrum Analysis (SSA) with the classical tools provided by the chaos theory. We focus on return and realized volatility series of several stock indexes (i.e., FTSE ITALIA MIB STORICO, DAX 30, CAC 40, FTSE ALL SHARE, S&P500, NASDAQ 100, NIKKEI ALL STOCKS and EURO STOXX).

Methods. Initially, a Monte Carlo SSA (MC-SSA) tests significance against a red-noise null-hypothesis ($AR(1)$, first-order autoregressive process) is performed. Specifically, the error bars computed for each empirical orthogonal function represent 95% of the range of variance found in the state-space direction defined by that empirical orthogonal function in an ensemble of 1000 red-noise realizations. Thus, the bars represent the interval between the 0.5% and 99.5% percentiles, and eigenvalues that lie outside this range are significantly different (at the 5% level) from those generated by the red-noise process against which they are tested. Then, the eigenvalues lie outside this interval are used to reconstruct the time series of the stock indexes. Finally, we apply the chaotic analysis on the reconstructed time series.

Results. Despite the extremely complex morphologies observed in the vast majority of the Financial Markets time series, here we show that the fundamental dynamic appears to be governed by a well-defined fractal attractor. A universal strange attractor –underlying the nontrivial financial time structures– suggests that the mechanism of production of such phenomena is governed by some inherent deterministic processes with a few degrees of freedom. In conclusion, we discuss the stock indexes of FTSE ITALIA MIB STORICO and the NIKKEI ALL STOCKS in which the Monte Carlo SSA test does not distinguish the signals from a relatively significant red-noise.
Keywords: Financial Time Series, Chaos, Singular Spectrum Analysis.

1 Introduction and Purpose

Chaos theory has been applied to many different fields, from predicting weather patterns to the stock market. However, the stochastic random noise

present in several physical processes affect the possibility of using this analysis and, more generally, to treat the system with a relative low number of dimensions [1]. In this paper, we treat the financial time series as natural dynamic process with the purpose of extracting the deterministic signal from a pure noisy. The de-noise time series is then analyzed with the classical tools provided by the chaos theory. The experiment is performed by using several stock indexes. Excepted in the cases of the `FTSE ITALIA MIB STORICO` and the `NIKKEI ALL STOCKS` indexes, all time series analyzed here show an universal strange attractor with a correlation dimension, $D_2 \lesssim 2$. This fact point out that the mechanism of production of such phenomena is governed by some inherent deterministic processes with a few degrees of freedom making the financial signal more *tractable* from a mathematical point of view. Furthermore, the evidence of small positive maximum Lyapunov exponents found here, $0.01 < \lambda_{max} < 0.003$, provide an useful constraint on making prediction. Lyapunov exponents, in fact, are inversely proportional to the predictability horizon.

In this work, we only present the detailed analysis of the `EURO STOXX`. The complete Singular Spectrum Analysis, as well as, the chaotic investigation of the entire sample will be publish by Romano et al. (in preparation).

2 Data

We focus our analysis on return and realized volatility series of several stock indexes, `FTSE ITALIA MIB STORICO`, `DAX 30`, `CAC 40`, `FTSE ALL SHARE`, `EURO STOXX NASDAQ 100`, `S&P500`, and `NIKKEI ALL STOCKS`. The analyzed frequency is daily for a period ranging from **01/01/1990** to **31/03/2010**. All time series are temporally coincident with the exception of the Japanese index ranging from **01/01/1991** to **31/03/2010**. Before addressing the statistical chaotic analysis, we test the non-linearity of time series under consideration using the BDS test. The null hypothesis H_0: the time series are independent and identically distributed, is rejected for all stock indexes analyzed here.

3 Method

In this work we combining the advanced spectral method of the Singular-Spectrum Analysis (SSA) with the classical tools provided by the chaos theory. Our analysis is briefly summarized in what follows.

(I) Initially, a Monte Carlo SSA (MC-SSA) tests significance against a $AR(1)$ null-hypothesis H_0 is performed. Specifically, the error bars computed for each empirical orthogonal function represent 95% of the range of variance found in the state-space direction defined by that empirical orthogonal function in an ensemble of 1000 red-noise realizations. Thus, the bars represent the interval between the 0.5% and 99.5% percentiles, and eigenvalues that

lie outside this range are significantly different (at the 5% level) from those generated by the red-noise process against which they are tested.

(II) By using these *de-noise* eigenvalues we reconstruct the time series of the stock indexes.

(III) Finally, on the reconstructed time series we apply the classical chaotic analysis: attractor reconstruction, correlation dimension, D_2 and maximum Lyapunov exponent λ_{max}.

3.1 Singular Spectrum Analysis

Singular Spectrum Analysis (SSA) is a recent and alternative time series method [2].

Based on principal component analysis, the SSA method generates a set of eigenvalues and eigenvectors from a symmetric covariance matrix obtained by setting a specified window length M. The window length M should be chosen to be longer than number of data points. In general, the window length be less than about $N/5$ where N is the number of points in the time series. The choice of window length sets the dimension of the lag autocorrelation matrix to be constructed and diagonalized by SSA, and thus determines the computational burden of the application. Larger values of M correspond to higher spectral resolution, although there is no direct equivalence between them. Robustness of results to M is an important test of their validity. We test different settings of the window length ($3 < N < 10$) without observing significant changes in our analysis.

The eigenvalues quantify the variance associated with each eigenvector or empirical orthogonal function (EOF). Projection of the data onto a set of EOFs allows its reconstruction for selected components, such as those above the noise floor accounting for most of the significant signal.

The application of SSA in combination with this red-noise test is known as Monte Carlo SSA [3]. The *SSA-MTM TOOLKIT* freeware software[1] was used for the analysis [4].

3.2 Monte Carlo SSA

The Monte Carlo SSA test (MC-SSA) was used to distinguish deterministic signals from red noise. Red-noise, is known to be significant relevant in several natural system. It is dominated by cycles of low frequency (long period) in its power spectrum and exhibits significant autocorrelations that decay over time. For red-noise, we specifically consider here a first-order autoregressive process, $AR(1)$, given by $x_t{=}\phi x_{t-1}{+}\varepsilon_t$ with $0{<}\phi{<}1$ and ϵ_t independent identically distributed normal errors.

A total of 1000 randomizations were used for the computation of MC-SSA. MC-SSA estimates the parameters of the $AR(1)$ model from the time series itself by using a maximum-likelihood criterion [5].

[1] http://www.atmos.ucla.edu/tcd/ssa/

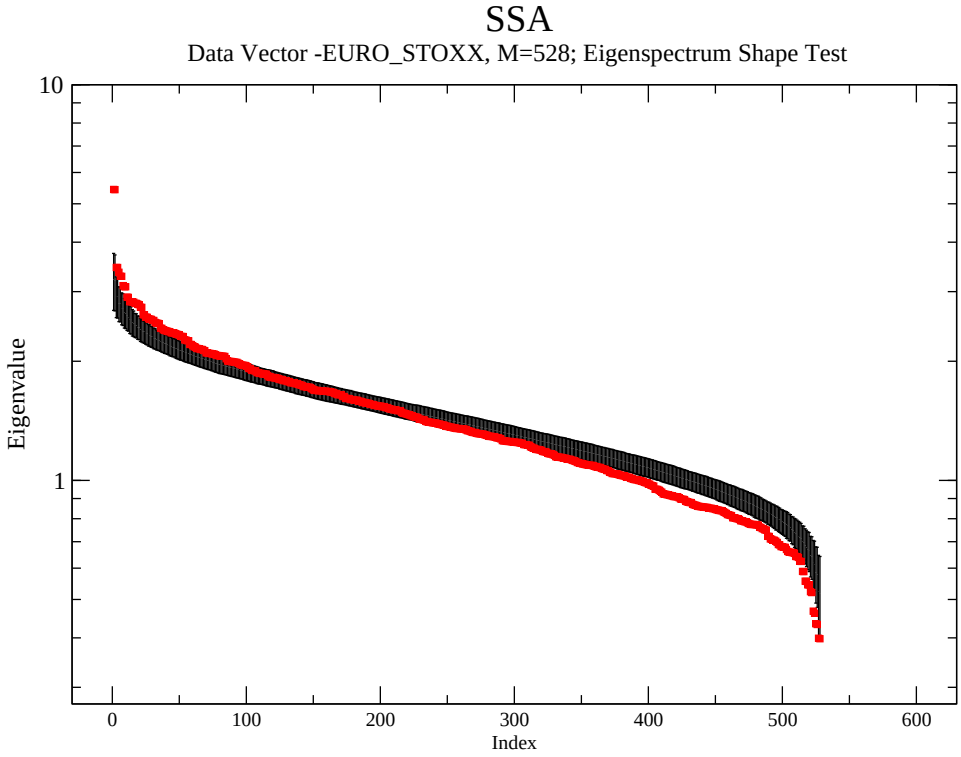

Fig. 1. Eigen-spectrum Shape Test of `EURO STOXX` index. The eigenvalues are ranked by order of importance according to the variance. The bars specify the 95% confidence intervals generated with Monte Carlo simulations of red-noise.

4 Results

Fig. 1 shows the eigenvalues decomposition (eigen-spectrum) obtained by MC-SSA for the `EURO STOXX` index. The eigenvalues are ranked by order of importance according to the variance. Specifically, the error bars computed for each empirical orthogonal function represent 95% of the range of variance found in the state-space direction defined by that empirical orthogonal function in an ensemble of 1000 red-noise realizations. The 95% confidence intervals are defined by the values expected for a red noise process with similar decorrelation time $\tau = -1/\log(r)$, where r is the lag-one autocorrelation value (see §3). Thus, the bars represent the interval between the 0.5% and 99.5% percentiles, and eigenvalues lying outside this range are significantly

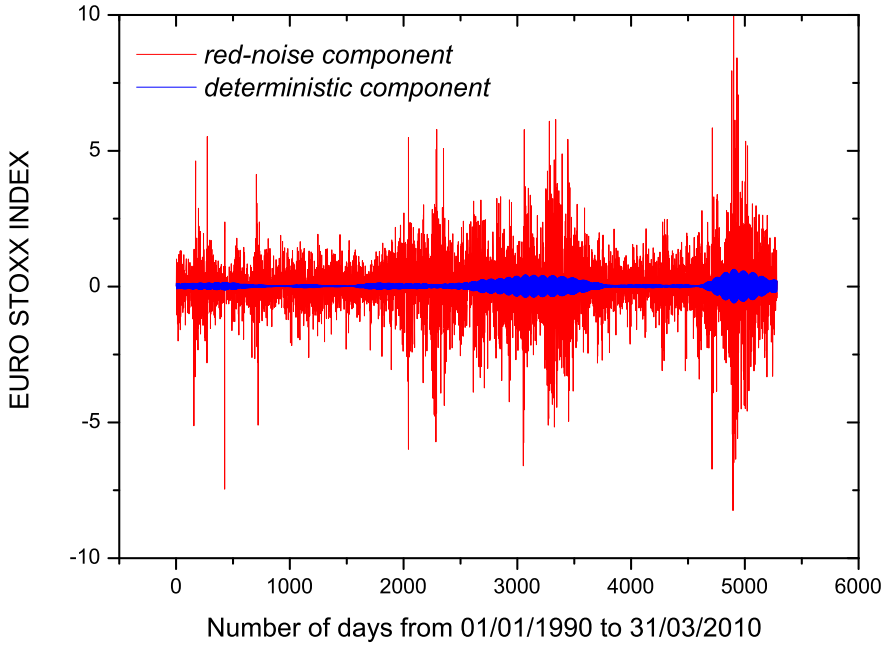

Fig. 2. `EURO STOXX` index: in red we show the the noise sub-components as reported in the the eigen-spectrum shape (MC-SSA); in blue the deterministic part of the signal is reconstructed.

different (at the 5% level) from those generated by the red-noise process against which they are tested. The first two eigenvalues are dominant and lie outside this interval and their variances are significantly different from the noise-variance. These eigenvalues are used to reconstruct the de-noise time series plotted in blue color inside the original signal (see Fig. 2) The strange attractors of the `EURO STOXX` index is plotted in Fig. 3. In particular, the Fig. 4 shows the Strange Attractor of the `EURO STOXX` index from **01/01/1995 to 01/01/2005** in which we perform the research for the maximum Lyapunov exponent. The values of the correlation dimension and the maximun Lyapunov Exponent are $D_2 = 1.87$ and $\lambda_{max} = 0.006$, respectively (see Figs. 5-6). Excepted in the cases of the `FTSE ITALIA MIB STORICO` and the `NIKKEI ALL STOCKS` indexes, all stock indexes reported in §2 show an universal strange attractor with a correlation dimension, $D_2 \lesssim 2$ and $0.01 < \lambda_{max} < 0.003$ (Romano et al. in preparation).

5 Conclusion

The advanced spectral method of the Singular-Spectrum Analysis (SSA) with the classical tools provided in the chaos theory prove largely successful to de-

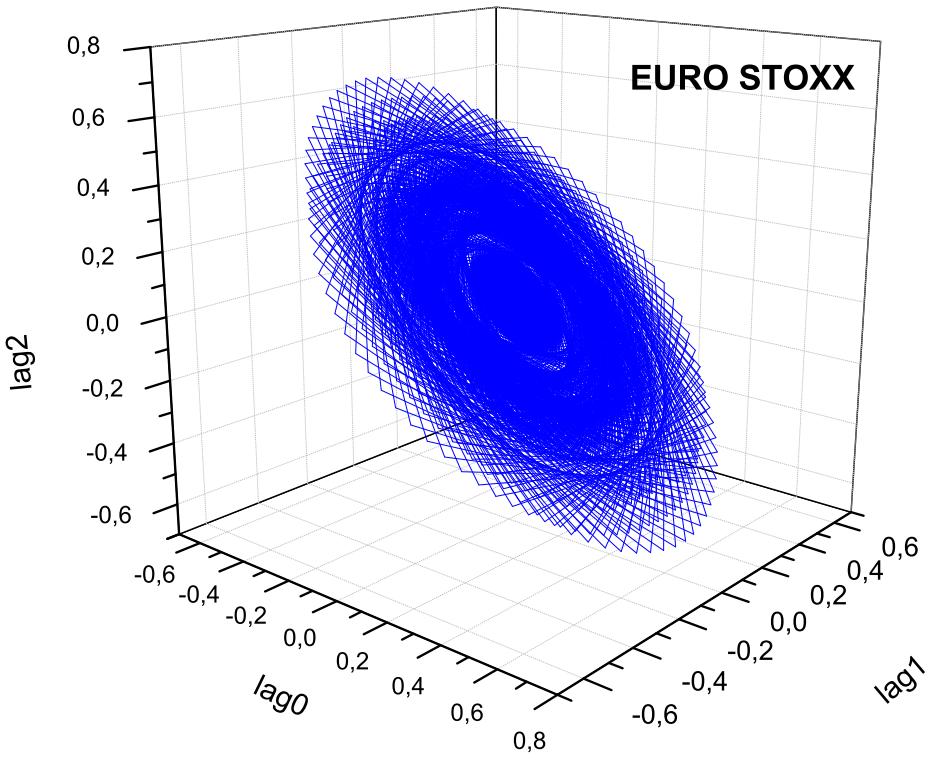

Fig. 3. Strange Attractor of the EURO STOXX index after removing the noise subcomponents from the eigen-spectrum shape. See text for more details.

scribe and classify the financial time series. Despite the extremely complex morphologies observed in the vast majority of the Financial Markets time series, here we show that the fundamental dynamic appears to be governed by a well-defined fractal attractor. A universal strange attractor underlying the nontrivial financial time structures suggests that the mechanism of production of such phenomena is governed by some inherent deterministic processes with a few degrees of freedom.

Clearly our analysis shows two types of markets (**i**) the financial signal is separable from a stochastic noise (DAX 30, CAC 40, FTSE ALL SHARE, S&P500, NASDAQ 100, and EURO STOXX) (**ii**) the dynamic process of the time series is completely affected by random phenomena (FTSE ITALIA MIB STORICO and NIKKEI ALL STOCKS). This in principle gives us the opportunity to make more accurate econometric analysis because *a priori* we know the

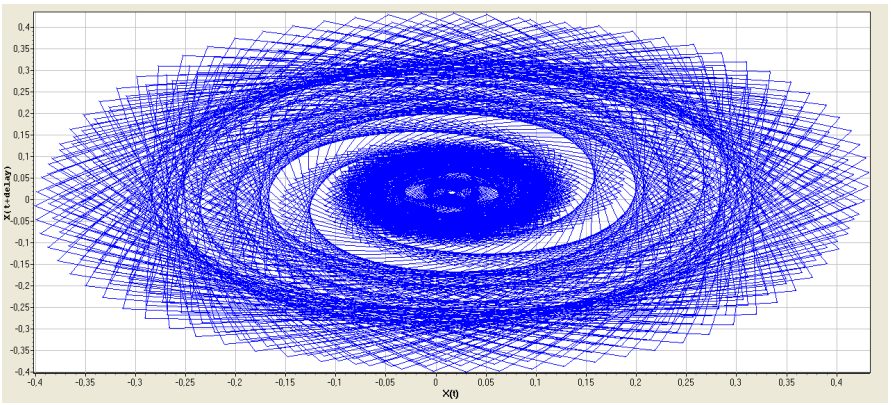

Fig. 4. Strange Attractor of the EURO STOXX index from **01/01/1995 to 01/01/2005**. In this time period we perform the research for the maximum Lyapunov exponent.

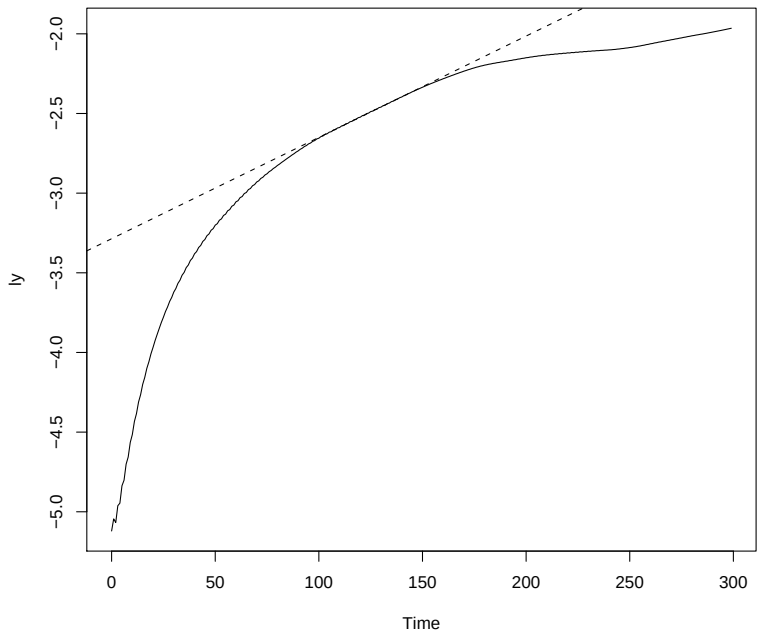

Fig. 5. Maximum Lyapunov exponent of EURO STOXX index, λ_{max}=0.006. We use the *tseriesChaos* package of *R software* to estimate the largest Lyapunov exponent.

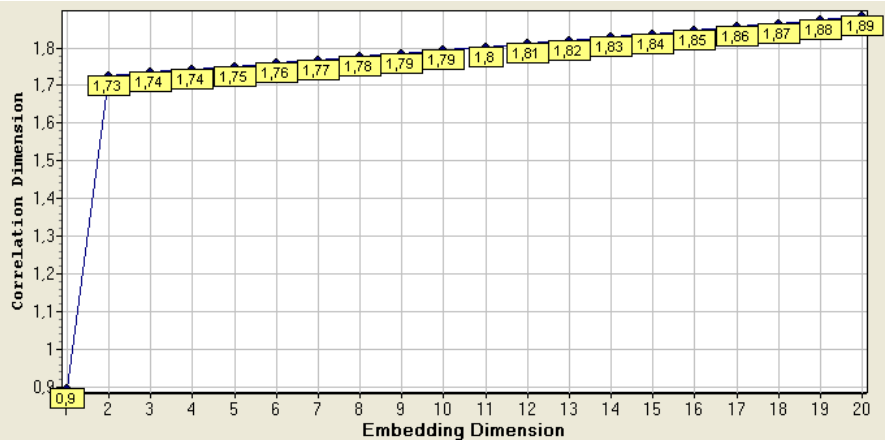

Fig. 6. Correlation Dimension of `EURO STOXX` index, D_2=1.8. We use the Grassberger-Procaccia method implemented in *Visual Recurrence Analysis Software*, http://nonlinear.110mb.com/vra/.

underlying process involving in time series under examinantion. This different behavior may be a reflection of the various marketing strategies adapted by different countries during the *dynamic financial evolution*.

Acknowledgments

This work is supported from the Department of Statistical Sciences and INAF-Astronomical Observatory of Bologna. G. G. acknowledges the **Fondazione Carisbo di Bologna** for the essential support.

References

1.Hegger, R., Kantz, H., and Schreiber, T. Practical implementation of nonlinear time series methods: The TISEAN package. *Chaos*, 413 (1999); doi:10.1063:1.166424, 1999.
2.Vautard, R., Yiou, P., and Ghil, M. Singular-spectrum analysis: A toolkit for short, noisy chaotic signals. *Physica D*, 58, 95:126, 1992.
3.Ghil M., R. M. Allen, M. D. Dettinger, K. Ide, D. Kondrashov, M. E. Mann, A. Robertson, A. Saunders, Y. Tian, F. Varadi, and P. Yiou. Advanced spectral methods for climatic time series. *Rev. Geophys*, 3.1:3.41, 2002.
4.Dettinger, M. D., Ghil, M., Strong, C. M., Weibel, W., and Yiou, P. Software expedites singular-spectrum analysis of noisy time series. *Eos, Trans. American Geophysical Union*, v. 76(2), 12:21, 1995.
5.Allen, M .R., and Smith, L. A. Monte Carlo SSA: detecting oscillations in the presence of coloured noise. *J. Climate*, 9, 3373:3404, 1996.


Proceedings, 4th Chaotic Modeling and Simulation International Conference
31 May – 3 June 2011, Agios Nikolaos, Crete Greece

Toward a reliable use of the nonlinearity detection and the noise titration technique

Elise Roulin[1], Ubiratan Santos Freitas[2] and Christophe Letellier[1]

[1] CORIA UMR 6614 — Universit et INSA de Rouen, BP. 12, 76801 Saint-Etienne du Rouvray cedex, France
(E-mail: roulin@coria.fr)
[2] ADIR Association — EA GRHV 3830, France
(E-mail: freitas@coria.fr)

Abstract. Even if noise titration cannot be used to prove the presence of chaos, it can still be used to detect nonlinear component in dynamics. Nevertheless, since the technique is based on nonlinear models for one-step-ahead predictions, it requires an acute choice of modelling parameters, that is the number of terms and the nonlinearity degree of the models. Based on illustrative examples, we propose conditions under which the noise titration can be reliably applied to characterize nonlinearity governing the dynamics underlying the measured time series. Moreover, we found that investigating nonlinear dynamics in the entire phase space or in a Poincaré section does not necessarily lead to similar results.
Keywords: noise titration technique, time series analysis.

Identifying chaotic dynamics from biological data still remains a great challenge, mainly because it requires a conclusive proof for a global determinism governing the whole system, that was never provided until now (Glass [1]). To overcome this difficulty, a technique to identify and to quantify chaos from short time series was proposed by C.-S. Poon and M. Barahona [2]. Unfortunately, the so-called "noise titration technique", based on the comparison between one-step-ahead predictions given by linear and nonlinear models, is not always able to distinguish some coloured noise from a purely deterministic chaotic dynamics (Freitas *et al.* [3]). Thus this method is not able to provide a conclusive proof of a chaotic behaviour. Nevertheless it can still be used to detect a nonlinear process — deterministic or stochastic — which governs the dynamics. In fact, this technique was used to discriminate healthy subjects from patients suffering from different cardiac failures, by comparing the strength of the nonlinearity underlying the data (Freitas *et al.* [4]). On the other hand, the results obtained with the noise titration applied to some spontaneous respiratory dynamics (Fiamma *et al.* [5]), or some breathing patterns of patients assisted by mechanical ventilation (Mangin *et al.* [6]), remains valid if one ignores the references to chaos in the conclusions. Nevertheless, this technique has to be applied according to some precautions, relative to the sampling of the data set, the choice of the modelling parameters, the choice of the observable, and so on. These guidelines are described section 1.

When the detection of the nonlinear component (Barahona *et al.* [7]) is applied, the probability p for having better predictions with a nonlinear model is computed. A p value greater than 0.99 ensure that the dynamics is nonlinear, while p around 0.50 means there is no gain to use a nonlinear model. Nevertheless, in the case of p around 0, encountered in the case of atrial fibrillation (Freitas *et al.* [4]), it is not so clear which kind of dynamics can lead to such results. We therefore propose to check whether relaxation oscillations could not be a good candidate to understand this case. Relaxation oscillations were already observed on a cellular scale (Tyson and Kauffman[8], Guevara *et al.* [9]) but also on the scale of a whole organism, considering physiological (Van Der Pol [10]) or biological (Barlow [11]) rhythms, or even on a collective, behavioural approach (Liu *et al.* [12]). These oscillations can present a fast increase of their amplitude, followed by a slow relaxation to a basis value. Typically, the slow part can be reproduced by a linear process, while the fast dynamics is controlled by a nonlinear process, driving notably the amplitude fluctuations. This type of dynamics is hard to analyse, because of its intrinsic dual behaviour. In order to better understand the phenomenon, we built a caricature of relaxation oscillations, based on periodical oscillations whose amplitude is modulated by the logistic function. The time series provided is a pathological case for data analysis, due to the fact that the nonlinearity only acts by very brief impulses. We showed that the nonlinearity detection, proposed in Barahona *et al.* [7], failed to detect the nonlinear component of this so-built dynamics.

1 The noise titration technique

The noise titration technique (Poon and Barahona [2]) is conditioned by a nonlinearity detection based on estimations of one-step-ahead polynomial predictors (Barahona and Poon [7]). Once this detection achieved, and only if a nonlinearity is detected ($p > 0.99$), the noise titration is applied. A white Gaussian noise is then gradually added to the data, until the nonlinearity goes undetected according to the predictors. These two steps are detailed in the following two subsections.

1.1 Detecting nonlinearity

A time series $\{y_n\}_{n=1}^{N}$ is investigated by comparing one step ahead predictions obtained with linear and nonlinear parametric models. These models are not built to reproduce the global dynamics but only to be optimal for one-step-

ahead predictions. The general form of these models is:

$$\begin{aligned}\tilde{y}_n(d,M) &= a_0 + a_1\, y_{n-1} + a_2\, y_{n-2} + ... \\ &\quad + a_{\kappa+1}\, y_{n-1}^2 + a_{\kappa+2}\, y_{n-1}\, y_{n-2} + ... + a_{M-1}\, y_{n-\kappa}^d \\ &= \sum_{m=0}^{M-1} a_m z_m(n)\end{aligned} \tag{1}$$

where $\{z_m(n)\}_{m=1}^{M}$, $M \in \mathbb{N}$, is the functional basis made of all distinct combinations of delay coordinates $\{y_{n-k}\}_{k=1}^{\kappa}$, $\kappa \in \mathbb{N}$, up to the maximum allowed degree d. There is thus $M = \frac{(\kappa+d)!}{(d!\kappa!)}$ terms. The models are thus defined by the two parameters d and M, from which the order κ of the model can be obtained. For a linear model ($d = 1$), $\kappa = M - 1$.

Coefficients a_m of model (1) are estimated using a least squares technique in order to minimize the squared prediction error

$$\epsilon^2 = \frac{\sum_{n=1}^{N} (\tilde{y}_n - y_n)^2}{\sum_{n=1}^{N} (y_n - \overline{y})^2} \tag{2}$$

where $\overline{y} = \frac{1}{N}\sum_{n=1}^{N} y_n$. This error was used to assess the quality of the model from the one-step-ahead prediction point of view. This error can be also used for selecting the most important term in the model as follows (Chen *et al.* [13]): The maximum squared prediction error $\max(\epsilon^2)$ is achieved when no terms are included in the model, that is, when $M = 0$. In this case, $\epsilon^2 = \max(\epsilon^2) = 1$. The inclusion of the nth term in the auxiliary model (1) induces a reduction in ϵ^2. Expressing this reduction as a percentage of $\max(\epsilon^2)$ yields the error reduction ratio (ERR) (Chen *et al.* [13]). The terms with large ERR values are thus selected to form the model.

Among each class of models parametrized by (d, M), we retained the best nonlinear model (δ, m_{nl}) where $\delta \leq d$, and $m_{nl} \leq M$, which was compared to the best linear model parametrized by $(1, m_l)$ selected among $(1, M)$ models. Obviously $m_l \leq M$. Thus, when we assess the performance of a nonlinear model (d, M), this always means that the performance of the best nonlinear model (δ, m_{nl}) for one-step-ahead predictions is compared to the performance of the best linear model $(1, m_l)$. For short, we will say that models parametrized by (d, M) are tested.

Once the best linear $(1, m_l)$ and the best nonlinear (δ, m_{nl}) models are selected, the null hypothesis (the best linear model) is then tested against the alternate hypothesis (the best nonlinear model) using the non-parametric Mann-Whitney statistical test. So the probability p for the best nonlinear model to provide better one-step-ahead predictions than those provided by

the linear model is calculated. When the probability p is around 50%, this means that there is no advantage to choose a nonlinear model rather than a linear one. Nevertheless, when p is greater than 99%, a nonlinearity — or a nonlinear component — is detected among the data, and the noise titration can then be applied.

1.2 Noise titration

To titrate the noise in a time series, a Gaussian distributed white noise ν_n of the same standard deviation as y_n with increasing amplitude A ($0 \leq A \leq 1$) is added to the data until its nonlinearity goes undetected (within a prescribed level of statistical confidence). If the nonlinearity detection persists to be conclusive, parameter A is increased. This process continues until the p-value goes under the threshold of 0.99. The corresponding noise amplitude A defines the Noise Limit (N_L).

We would like to insist on the fact that this nonlinearity test is actually able to detect nonlinear relations between two states of the system delayed in time, using models which were selected only to ensure good one-step-ahead predictions. This not necessarily involves an underlying determinism (Freitas *et al.* [3]), since one-step-ahead prediction cannot provide such a proof (Dafilis *et al.* [14]).

1.3 Recommendations for an optimal use

We showed that the results provided by the noise titration technique could strongly depend on some modelling parameters on one side, or to the time series on the other side (Roulin *et al.* [15]). The modelling parameters d and M cannot be chosen too small or too big, because it could leads to false results. We showed some examples where wrong negative and wrong positive answers can be obtained (Freitas *et al.* [4]), and such a feature is our main argument to ban the use of the noise titration to proove the chaotic nature of a dynamics. The nonlinearity degree has to be at least equal to 3, and the number of terms at least equal to 20 or 30, but it should not exceed 100, to avoid over parametrization. On the other hand, the noise limit is sensitive to the noise realization used for the titration. It becomes necessary to consider a mean value of several titrations (we recommend at least 5 titrations). We also showed (Roulin *et al.* [15]) that the choice of the variable describing the dynamics may affect the results according to the observability coefficients (Letellier and Aguirre [16]). Indeed, there are better variables than others to investigate a dynamics, and the noise titration is sensitive to that choice, as many other techniques. Moreover, we found that investigating nonlinear dynamics using a trajectory in the phase space or using a Poincaré section does not necessarily lead to similar results (Letellier [17]).

Finally, when the probability p is equal to 0.50, this means that the choice between a linear and a nonlinear model is not obvious, and that the pertinence

of both types of models is equivalent. When p is above 0.99, the use of a nonlinear model is required to describe the one-step-ahead dynamics, and we conclude about the underlying nonlinearity of the system. If p is about 0, in principle, the dynamics is mainly linear, but this was never proved. So we wanted to test this last case.

2 Slow/fast dynamics with chaotic amplitude modulation

The nonlinearity detection applied on cardiac data revealed different kinds of dynamical behaviour for patients suffering from congestive heart failure ($p \approx 1$), for others suffering from atrial fibrillation ($p \approx 0$), and for healthy patients ($p \approx 0.75$) (Freitas *et al.* [4]). Surprisingly, the nonlinearity detection seemed to show that the cardiac dynamics was strongly linear in the case of atrial fibrillation, as revealed by the very low p-values (Fig. 1).

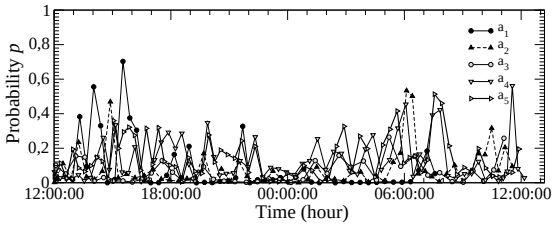

Fig. 1. Probability p calculated from $\Delta \mathrm{RR}_n = \mathrm{RR}_{n+1} - \mathrm{RR}_n$ for 5 patients suffering from atrial fibrillation. Modelling parameters: $(d, M) = (3, 50)$. From Freitas *et al.* [4].

We consider here the time series generated by a periodic behaviour, whose amplitude is modulated by the logistic function in a chaotic regime. The periodic component corresponds to a triangular signal, for which the linear decrease is slow in comparison to the fast increase. Indeed, only one iteration is sufficient to reach the maximal amplitude of the ith cycle, given by:

$$A_i = \frac{n}{20}\left(1 + \frac{y_i}{10}\right) \tag{3}$$

where n gives the number of iterations in one oscillation and y_i is a solution of the logistic function

$$y_{n+1} = \mu y_n \left(1 - y_n\right) . \tag{4}$$

The time series $\{x_k\}$ is then built according to

$$x_{k+1} = \begin{cases} x_k - \dfrac{A_i}{n} & \text{si} \quad x_k > 0 \\ A_i & \text{si} \quad x_k \leq 0 \, . \end{cases} \tag{5}$$

where $i = [\frac{k}{n}]$. To each cycle i corresponds only one A_i value; the oscillation period remains constant, and does not depend on the amplitude value, which is varying between two successive cycles. A typical time series is shown Fig. 2.

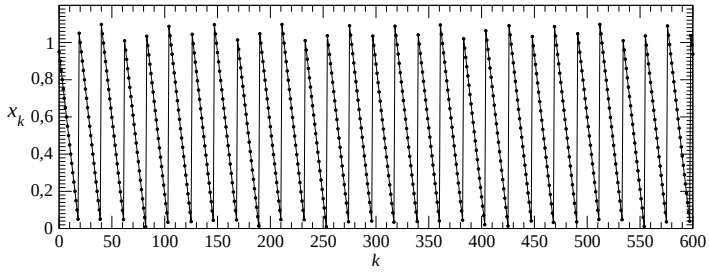

Fig. 2. Time series of the slow/fast dynamics with chaotic amplitude modulation. Parameter values: $\mu = 3.9$ and $n = 20$.

This time series is mainly governed by the linear behaviour defined by the first equation of process (5). But, very briefly, a nonlinear component drives the amplitude of the signal. From the time series point of view, the system is mainly linear, but a first-return map to a Poincaré section provides a parabola similar to the logistic function's hallmark (Fig. 3).

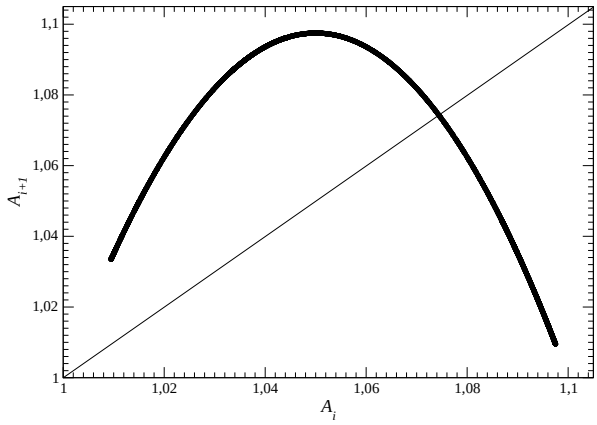

Fig. 3. First-return map of the slow/fast dynamics with chaotic amplitude modulation. Parameter values: $\mu = 3,9$ and $n = 20$.

2.1 Results

The nonlinearity detection technique described in section 1 was then applied to the time series $\{x_k\}$. The modelling parameters were chosen as $(d, M) = (3, 50)$, and a mean value over 5 detections is computed for each p value. We observed that the probability p for the best nonlinear model to be better for the one-step-ahead prediction than the best linear model were always equal to 0. This value never changed when we varied the number α of relaxation oscillations in the data's window considered for the detection. We tested the nonlinearity for a time series where $n = 20$ and $\alpha \geq 12$, that is, a window of 240 points for the models estimation. Even if α was equal to 30, p remained around zero. This means that the nonlinear component was acting too sporadically to be detected on the basis of one-step-ahead predictions. Typically, a linear model would furnish a bad prediction only during the stiff increase of the amplitude. But larger n is, less the error weight on the statistics, and since with $n = 20$ the technique already failed to detect the nonlinear component, this remain true for layer n.

The so-built time series is then presented as a "pathological" case: since the nonlinearity acts on very brief impulses, the noise titration technique fails to detect the nonlinear component of the dynamics, and only shows its linear component. However, we noted that if the problem was approached in a Poincaré section, p values were always equal to 1, as it was observed with the logistic function, evidencing the presence of a nonlinear component. This example was certainly a caricature, but it showed the non-equivalence to work in the phase space, or in a Poincaré section. Such a difference was already revealed while estimating a Shannon entropy (Letellier [17]).

3 Conclusion

In addition to the guidelines we provided to carefully use the nonlinearity detection, we showed here that using the nonlinearity detection to search for a nonlinear component failed when the time series results from a dynamics where the nonlinearity only acts very briefly. Our caricatural dynamics appeared to be a typical case to test the robustness of any analysis. In addition, the non-equivalence to analyse a trajectory in the phase space and in a Poincaré section is once again confirmed here, for the nonlinearity detection in particular.

References

1.L. Glass, Introduction to controversial topics in nonlinear science: Is the heart rate chaotic?, *Chaos*, **19**, 028501 (2009).
2.C.-S. Poon & M. Barahona, Titration of chaos with added noise, *Proceedings of the National Academy of Sciences* (USA), **98**, 7107-7112 (2001).

3.U. S. Freitas, L. Aguirre & C. Letellier, Failure for distinguishing coloured noise from chaos by the "Noise titration" technique, *Physical Review E.*, **79**, 035201 (2009).
4.U. S. Freitas, E. Roulin, J.-F. Muir & C. Letellier, Identifying determinism underlying heart rate: the right task?, *Chaos*, **19**, 028505 (2009).
5.M.-N. Fiamma, C. Straus, S. Thibault, M. Wysocki, P. Baconnier & T. Similowski, Effects of hypercapnia and hypocapnia on ventilatory variability and the chaotic dynamics of ventilatory flow in humans, *American Journal of Physiology-Regulatory Integrative and Comparative Physiology*, **292**, R1985-R1993 (2007).
6.L. Mangin, M.-N. Fiamma, C. Straus, J.-P. Derenne, M. Zelter, C. Clerici & T. Similowski, Source of human ventilatory chaos: Lessons from switching controlled mechanical ventilation to inspiratory pressure support in critically ill patients, *Respiratory Physiology & Neurobiology*, **161** (2), 189-196 (2008).
7.M. Barahona & C.-S. Poon, Detection of nonlinear dynamics in short noisy time series, *Nature*, **381**, 215-217 (1996).
8.J. Tyson & S. Kauffman, Control of mitosis by a continuous biochemical oscillation: synchronisation: spatially inhomogeneous oscillations, *Journal of Mathematical Biology*, **1**, 289-310 (1975).
9.M. R. Guevara, L. Glass & A. Shrier, Phase locking, period-doubling bifurcations, and irregular dynamics in periodically stimulated cardiac cells, *Science*, **214**, 1350-1353 (1981).
10.B. van der Pol, Biological rhythms considered as relaxation oscillations, *Acta Medica Scandinavica*, **103** (S108), 76 (1940).
11.J. S. Barlow, A phase-comparator model for the diurnal rhythm of emergence of *Drosophila*, *Annals of the New-York Academy of Science*, **98**, 788-805 (1962).
12.W. Liu, D. Xiao & Y. Yi, Relaxation oscillations in a class of predator-prey systems, *Journal of Differential Equations*, **188**, 306-331 (2003).
13.S. Chen, S. A. Billings & W. Luo, Orthogonal least squares methods and their application to non-linear system identification , *International Journal of Control*, **50** (5), 1873-1896 (1989).
14.M. P. Dafilis, N. C. Sinclair, P. J. Cadusch & D. T. J. Liley, Re-evaluating the performance of the nonlinear prediction error for the detection of deterministic dynamics, *Physica D*, **240**, 695-700 (2011).
15.E. Roulin, U.S. Freitas and C. Letellier. Working conditions for safe detection of nonlinearity and noise titration. *Physical Review E*, in press.
16.C. Letellier & L. A. Aguirre, Graphical interpretation of observability in terms of feedback circuits, *Physical Review E*, **72**, 056202 (2005).
17.C. Letellier, Estimating the Shannon entropy: recurrence plots versus symbolic dynamics, *Physical Review Letters*, **96**, 254102 (2006).

Proceedings, 4th Chaotic Modeling and Simulation International Conference
31 May – 3 June 2011, Agios Nikolaos, Crete Greece

"Quantum" Chaos and Stability Condition of Soliton-like Waves of Nuclear Burning in Neutron-Multiplicating Media

V.D. Rusov[1,2], *E.P.Linnik*[1], *V.A. Tarasov*[1], *T.N. Zelentsova*[1],
I.V. Sharf[1], *S.A. Chernezhenko*[1], *O.A. Byegunova*[1,2],

[1]*Odessa National Polytechnic University, 65044, Odessa, Ukraine*
[2]*Bielefeld University, D-33615, Bielefeld, Germany*

Abstract

We show that the stability condition for the soliton-like wave of nuclear burning in neutron-multiplicating medium is determined in general by two conditions. The first condition (necessary) is determined by relationship between the equilibrium concentration and critical concentration of active (fissile) isotope, that is a consequence of the Bohr-Sommerfeld quantization condition. The second condition (sufficient) is set by the so-called Wigner quantum statistics, or more accurately, by a ststistics of the Gaussian simplectic ensembles with respect to the parameter that describes the squared width of burning wave front of nuclear fuel active component.

PACS number(s): 25.85.Ec; 28.50.-k; 05.45.Mt; 05.45.Yv

* Corresponding author: Rusov V.D., E-mail: siiis@te.net.ua

I. INTRODUCTION

In spite of obvious efficiency and allurement of the nuclear power engineering of next generation, the main difficulties of its perception are predetermined by non-trivial properties which future ideal nuclear reactor must possess. At first, the natural, i.e. unenriched uranium or thorium must be used as a nuclear fuel. Secondly, the reactivity regulation system of reactor by traditional control rods is completely absents, but for all that a reactor must possess the property of so-called inner safety. It means that the critical state of reactor core must be permanently maintained in any situation, i.e. the reactor normal operation is automatically maintained not as a result of operator activity, but by virtue of physical reasons-laws preventing the explosive development of chain reaction by the natural way. Figuratively speaking, the reactor with inner safety it is “the nuclear installation which never explode” [1].

$$^{238}U(n,\gamma)\rightarrow{}^{239}U\xrightarrow{\beta^-}{}^{239}Np\xrightarrow{\beta^-}{}^{239}Pu(n,\ fission) \qquad (1)$$

Strangely enough, but reactors satisfying such unusual requirements are possible in the reality. For the first time the idea of such reactor was proposed by Feoktistov [2] and independently by Teller, Ishikawa and Wood [3].

The main idea of reactor with inner safety consists in the selection of fuel composition so that, at first, the characteristic time τ_β of the nuclear burning of fuel active (fissile) component is substantially greater than the characteristic time of delayed neutrons production and, secondly, necessary self-regulation conditions are meet during the reactor operation (that always take place, when the equilibrium concentration $\tilde{n}_{fis}$ of fuel active component is greater than critical concentration n_{crit} [2]). These very important conditions can practically always to be attained, if among other reactions in the reactor the chain of nuclear transformations of the Feoktistov uranium-plutonium cycle type [2]

$$^{238}U(n,\gamma)\rightarrow{}^{239}U\xrightarrow{\beta^-}{}^{239}Np\xrightarrow{\beta^-}{}^{239}Pu(n,\ fission) \qquad (1)$$

or the Teller-Ishikawa-Wood thorium-uranium cycle type [3]

$$^{232}Th(n,\gamma)\rightarrow{}^{233}Pa\xrightarrow{\beta^-}{}^{233}U(n,\ fission)\,, \qquad (2)$$

will be enough appreciable.

In both cases the produced fissile isotopes of ^{239}Pu or ^{233}U are the active components of nuclear fuel. The characteristic time of such reaction, i.e. the time of proper β-decays, is approximately equal to τ_β =2.3/ln2≈3.3 days for reaction (1) and τ_β ≈39.5 days and for reaction (2), that is several orders greater than the time of delayed neutrons production.

The self-regulation of nuclear burning process is stipulated by the fact that such system left by itself can not pass from a critical state to reactor acceleration mode, because a critical concentration is bounded from above by the finite equilibrium concentration of nuclear fuel fissile component (plutonium for (1) or uranium for (2)), i.e. $\tilde{n}_{fis} > n_{crit}$ (Feoktistov's stability condition [2]). On phenomenological level the self-regulation of nuclear burning is manifested as follows. The increase of neutron flux due to some reasons will result in the rapid burnup of nuclear fuel fissile component (plutonium for (1) or uranium for (2)), i.e. its concentration as well as the neutron flux will decrease, while the new nuclei of corresponding fissile component of nuclear fuel are produced with the same generation rate during time τ_β. And vice versa, if the neutron flux is sharply decreased due to external action, the burnup rate decrease too, and the accumulation rate of fuel fissile component will be increased as well as the number of neutron production after a while τ_β.

However, as is known [2], the Feoktistov stability condition is only necessary but insufficient condition. Therefore full generalization of the Feoktistov stability condition for critical waves of nuclear burning in neutron-multiplicating mediums is the purpose of this paper.

II. PROPERTIES OF STABILITY CONDITION FOR CRITICAL WAVE OF NUCLEAR BURNING ACCORDING TO FEOKTISTOV

Following [2], let us consider the known "polygon" system of kinetic equations for neutrons and nuclei in the reaction chain (1) with respect to the normalized autowave variable $z=(x+ut)/L$:

$$\frac{d^2 n_*}{dz^2} = \left[1 - \frac{n_{Pu}}{n_{crit}^{Pu}}\right] n_*, \tag{3}$$

$$\Lambda \frac{dn_8}{dz} = -\left[n_8 - n_9 - n_{Pu}\right] n_*, \tag{4}$$

$$\Lambda \frac{dn_9}{dz} = \left(n_8 - n_9\right) n_* - n_9, \tag{5}$$

$$\Lambda \frac{dn_{Pu}}{dz} = n_9 - \frac{n_{Pu}}{\tilde{n}_{Pu}} n_*, \tag{6}$$

where u is phase velocity of the steady running wave, L is the neutron average diffusion length, $n_*(z,t)$ is the neutron density, $D=\upsilon/3\Sigma_s= L^2/\tau$ is neutron diffusion constant, $cm^2\cdot s^{-1}$; υ is neutron velocity in the one-group approximation, $cm\cdot s^{-1}$; Σ_s is neutron microscopic scattering cross-section, cm^{-1}; $\tau = 1/\upsilon\sum\sigma_a^i N_i$ is neutron lifetime in medium, s; $\Lambda= u\tau_\beta /L$ is dimensionless constant, $n_{crit}^{Pu} = N_{crit}/N_8(-\infty)$ = = $\sum\sigma_a^i n_i)/(\nu-1)\sigma_f^{Pu}$ is the plutonium relative critical concentration, N_{crit} is the plutonium critical concentration, N_8 is the U^{238} concentration, σ_a and σ_f are the microscopic neutron capture cross-section and fission cross-section, respectively, n_8 and n_9 are the concentrations of U^{238} and U^{239} normalized to U^{238} initial concentration, i.e., to $N_8(-\infty)$, ν is the average number of prompt neutrons produced per plutonium nucleus fission.

Solving these equations Feoktistov was based on the analogy of diffusion equation and the Schrödinger steady-state equation in quasi-classical approximation [2]. Naturally, in this case (see Eq. (3)) the stationarity condition of solution is satisfied integrally, because there are points where $n_{Pu} > n_{crit,}$ and there are points where $n_{Pu} < n_{crit}$. In this sense, the region at $n_{Pu} > n_{crit}$ corresponds as it were to allowed region, while the region at $n_{Pu} < n_{crit}$ corresponds to subbarrier region. In other words, the inverted profile of plutonium concentration in the ^{238}U medium plays the role of potential well (Fig. 1(a) [4]).

In the region at front of wave ($z =-\infty$) the approximate solution looks like

$$n = C\exp z, \tag{7}$$

$$n_8 = \exp\left(-\frac{C}{\Lambda}\exp z\right), \tag{8}$$

$$n_9 = \frac{C}{1+\Lambda}\exp z, \tag{9}$$

$$n_{Pu} = \frac{\tilde{n}_{Pu}}{1+\Lambda}\left[1-\exp\left(-\frac{C}{\Lambda\tilde{n}_{Pu}}\exp z\right)\right]. \tag{10}$$

Let us remind that obtaining this solution, we have neglected summands n_9 and n_{Pu} whose values are determined by edge condition $n_8\cong 1$. Then assuming that the subbarrier region ends at $z=0$, we have $n_{Pu} = n_{crit}$ at this point. This allows us to determinate the value of constant C. At the point $z=a$, according to the Bohr-Sommerfeld quantization condition, we have the following equality

$$\int_0^a \sqrt{\frac{n_{Pu}}{n_{crit}^{Pu}}-1}dz = \frac{\pi}{2}, \tag{11}$$

where the integral is taken over the supercritical region ($n_{Pu}>n_{crit}$). At the same time condition (11) plays also the role of condition for finding the point a at $n_{Pu} = n_{crit}$, i.e., when the transition into subbarrier region happens due to burn-up (see Fig. 1(a) and Fig.2)[1].

Executing the ordinary for quasi-classical approximation linkage with the supercriticality region ($n_{Pu}>n_{crit}$) we will come to calculation of Λ.

As a critical state is automatically maintained at $n_{Pu} > n_{crit}$ [2] (that is the direct consequence of the Bohr-Sommerfeld quantization condition), we can use this fact for generalization of the following inequality:

$$\tilde{n}_{Pu} > n_{Pu} > n_{crit}^{Pu}, \tag{12}$$

Thus, Feoktistov shown for the first time [2] that the soliton-like propagation of neutron-fission wave of nuclear burning is possible in ^{238}U medium only under the condition of a certain ratio between equilibrium and critical plutonium concentrations ($\tilde{n}_{Pu} > n_{crit}$), which is characterized by the Bohr-Sommerfeld quantization condition. In other words, only in this case the critical (quasi-stationary) state of system (reactor core) can automatically maintained without any external intervention, and, consequently, only in this case the reactor fully and unambiguously possesses the inner safety properties.

It is appropriate here to pay an attention to very important Feoktistov's parameter, which, as shown below, is basis for ideology of the stability of soliton-like wave of nuclear burning:

$$\Lambda(a) = \frac{u\tau_\beta}{L}, \tag{13}$$

where a is the width of permitted range of integration in the Bohr-Sommerfeld condition (11), where the inequality $n_{Pu} > n_{crit}$ (Fig. 2) and $\tilde{n}_{Pu} > n_{crit}$,, respectively, are satisfied; $\Lambda(a)$ is dimensionless coefficient, which appears within the framework of simplified diffusion model of the Feoktistov reactor (3)-(6).

[1] Note that the model calculations of the Feoktistov problem by the system of equations (3)-(6) really show [4] that at steady-state conditions the Bohr-Sommerfeld quantization condition is fulfiled with an accuracy up to a few percents (!!!). Authors [4] note that there are no grounds to expect the more exact coincidence because a quantization condition for lower level is approximate.

Obviously, Eq. (11) due to its physical meaning is a key factor which predetermines the phase velocity of soliton-like burning wave. Therefore, this equation exists regardless of an idealization degree of reactor core model and should appear in explicit or implicit form in any model whose the system of kinetics equations for neutrons and nuclei has soliton-like solutions for neutrons. At the same time, as the average width of soliton wave has an order of $2L$, the maximum values of the dimensionless coefficient $\Lambda(a)$ and wave velocity u are determined by the following approximate equality

$$\frac{1}{b}\Lambda_{\max}(a) = \frac{u_{\max}\tau_\beta}{bL} = 1, \tag{14}$$

where coefficient is $b\sim 2$ although a final estimation will be done below.

From analysis of Eq. (14) it follows that the velocity of stable propagation of soliton-like wave is not necessarily equal to the diffusion rate $u=L/\tau_\beta$. It can be considerably slower or faster due to very strong domination either of the nonlinearity parameter or dispersion parameter, which in its turn reflects the peculiarities of nuclear transformation kinetics, for example, in the chain (1) and/or in (2). In practice they manifest itself as higher or lower degree of fuel burn-up.

In other words, when the wave velocity and consequently the degree of fuel burnup are low, the wave stops due to the following reasons. Neutrons from an external source, which take place in the initial stage of wave initiation, burn out the plutonium on medium bondary and simultaneously transmute the uranium into ^{239}Np. Neptunium with time starts to produce the plutonium but it can not create the required high concentration, while the ^{239}Pu production decreases due to the uranium burnup. More and more thick layer without both ^{238}U and ^{239}Pu grows on the medium boundary. The neutron diffusion through this layer does not provide the increase of plutonium concentration in next layers, and the wave does not arise even at $n_{Pu}(x,0)= n_{crit}$.

Conversely, when the wave velocity and degree of fuel burn-up are high, the wave stops also because of the scarce (or more exactly, delayed) plutonium production which takes place due to another reason. Figuratively speaking, the situation resembles the fire in the forest under strong wind, when only tree crowns burn. When the wind speed increases, it could extinguish the fire at all. We have the similar situation, when there is a velocity, at which in the early stage (when $x\approx 0$) the front of neutron soliton wave outruns the front of plutonium production wave, and this advance exceeds the neutron diffusion length. This leads, in fact, to transformation of fast wave into slow wave or to its full stop. It is interesting to note that this case not studied in the literature (with the exception of [4,5]), but it is possible to postulate that it corresponds to

some hypothetical situation, when the nuclear burning wave forms in highly-enriched fuel which has the ultra-low critical concentration of fuel fissile component.

Thus, the lag (Fig. 1(b)) or advance of neutron wave front relative to the plutonium wave front for a distance considerably exceeding the neutron diffusion length will leads to stop and total degradation of these waves. This means that degradation of waves with very low or very high initial phase velocity will exhibits as the tendency to zero of Eq. (11) at very low or very high values of *a*. Therefore taking into account Eq. (14), we can conclude that Eq. (11) is true in the range $0 \le (1/b)\Lambda(a) \le 1$. Based on this generalization, we can make an important assumption that the expression $(1/b)\Lambda(a)$ means the certain probability density distribution $p(a)$ with respect to a:

$$\frac{u\tau_\beta}{bL} = p(a). \tag{15}$$

Let us consider and substantiate the type and main properties of such a statistics, and also show the results of its verification based on the known computational experiments on simulation of nuclear burning wave in the U–Pu (1) and Th–U (2) fuel cycles.

III. CHAOS AND INTEGRABILITY IN NONLINEAR DYNAMIC OF REACTOR CORE

In order to solve the assigned task we use the known analogy between the neutron diffusion equation and the Schrödinger steady-state equation in quasiclassical approximation. We would remind that this analogy was used earlier to solve the system of kinetics equation for neutrons and nuclei (3)-(6) in the reaction chain (1) of the U–Pu fuel cycle. Since the system of equations for neutrons and nuclei in the Th–U fuel cycle (2) is structurally identical to the system equation for the U–Pu fuel cycle (1), the computed “quantum mechanical” solution, which describes the statistics (15), will be general for both fuel cycles, except for a few details.

Now, let us remind that earlier we have used the Bohr-Sommerfeld quantization condition which in the case of the one-dimensional systems determines in the explicit form the energy eigenvalues E_n

$$\oint p(x)dx = \oint \sqrt{2m(E_n - V(x)}dx = 2\pi\hbar\left(n + \frac{1}{2}\right), \quad n = 0, 1, 2\ldots, \tag{16}$$

where m and $p(x)$ are the mass and momentum of particle in the field of some smooth potential $V(x)$.

For the Feoktistov nearly integrable system of the equations (3)-(6) or for the anologous Teller system of equations, for which it is assumed that m=1/2, $V(x)$=1 and n=0, this condition is applied in the form

$$\int_0^a \sqrt{E_0 - 1}dz = \frac{\pi}{2}, \quad E_0 = \frac{n_{fis}}{n_{crit}^{fis}}, \tag{17}$$

where index *fis* denotes the fissionable isotope, for example, the ^{239}Pu in the Feoktistov U–Pu fuel cycle (1) or the ^{233}U in the Teller Th–U fuel cycle.

However, in describing the real evolution of fast reactor core, the corresponding systems of equations for neutrons and nuclei are nonintegrable almost without exception. This, in its turn, means that according to the Kolmogorov-Arnold-Moser theorem [6,7] quasiclassical quantization formulas are inapplicable for the system, where the motion in phase space is not limited by multidimentional tori. This is stipulated by the fact that in the Hamiltonian nonintegrable systems the more and more number of tori collapse in phase space with perturbation (nonintegrability) growth. As a result, the trajectories of majority of bound states gets entangled, the motion becomes mainly chaotic, and bound states themselves and their energies, can not be described by the rules of quasiclassical quiantization, for example, such as the Einstein-Brillouin-Keller (EBK) quantization rule for multidimentional case [7,8], which generalizes the Bohr-Sommerfeld quiantization rule. Note that nowdays a notion “quantum chaos” is included the circle of problems related to quantum-mechanical description of systems chaotic in a classic limit [9**,** 10].

Since the results of random matrices theory will be used for research of chaotic properties of the statistics (11), we first give an overview of the main concepts of this theory.

First, following [9,10], let us shortly consider a nature of so-called universality classes and the Gaussian ensemble types. As is known, the Hamilton operator matrix in possession of any kind of a symmetry can be reduced to the block-diagonal form. At the same time, matrix elements in each block are specified by a certain quantum number set. For the sake of simplicity we assume that the Schrödinger equation $i\hbar(\partial\psi/\partial t) = \hat{H}\psi$ is expressed for states belonging to the one block. At the same time the size of the operator $\hat{H}$ matrix is finite and equal to an integer.

As shown in [9,10], these universality classes separate physical systems into groups according to their relation to orthogonal, unitary or simplectic transformation, which leave the $\hat{H}$ matrix invariant. In other words, as it postulated in [9]:

• the Hamiltonian of spinless system possessing a symmetry with respect to time inversion is invariant under orthogonal transformations and can be represented by real matrix;

• the Hamiltonian of spinless system not possessing a symmetry with respect to time inversion is invariant under unitary transformations and can be represented by the Hermitian matrix;

• the Hamiltonian of the system with spin of 1/2 possessing a symmetry with respect to time inversion is invariant under simplectic transformations and can be represented by quaternion real matrix.

Now let us talk about the Gaussian ensembles. If the matrix element distribution function is invariant under one of indicated transformations, this means that the sets of all matrices with elements described by these distribution functions form the Gaussian orthogonal ensemble (GOE), the Gaussian unitary ensemble (GUE) and the Gaussian simplectic ensemble (GSE), respectively.

At the same time it should be noted the one very substantial detail. The matrix element distribution function of the Gaussian ensembles can not be directly measured, since the experiment can give us information about the energy levels of investigated quantum-mechanical system only. In other words, just the energy eigenvalues distribution function is of greater interest from the practical point of view.

Derivation of corresponding equations for the considered types of the Gaussian ensembles can be found in [10]. At the same time, the correlated distribution function of energy eigenvalues it is possible to write down in the sufficiently universal form for all ensemble types :

$$P(E_1,...,E_N) \sim \prod_{n>m}(E_n - E_m)^{\nu} \exp(-A\sum_n E_n^2), \tag{18}$$

where ν is an universality index, which takes on the value of 1, 2 and 4 for GOE, GUE and GSE statistics, respectively. At ν=0 energy eigenvalues are not correlated. In this case, the energy level spacing distribution function is described by the Poisson statistics, and the matrix ensemble itself is called the Poisson ensemble.

So long as the energy level spacing distribution function is the most studied property of chaotic systems, following [9], we give a calculation only for relatively simple case of the Gaussian ensemble with matrixes 2×2 in size. Let us calculate the energy level spacing distribution function $p_W(s)$ substituting the function $P(E_1, E_2)$ in (18):

$$p_W(s) = \int_{-\infty}^{+\infty} dE_1 \int_{-\infty}^{+\infty} dE_2 P(E_1, E_2)\delta(s - |E_1 - E_2|) =$$

$$= C \int_{-\infty}^{+\infty} dE_1 \int_{-\infty}^{+\infty} dE_2 \left|E_1 - E_2\right|^{\nu} \exp(-A\sum_n E_n^2)\delta(s - \left|E_1 - E_2\right|). \quad (19)$$

Constants *A* and *C* are defined by the two normalization conditions:

$$\int_0^{\infty} p_W(s)ds = 1, \quad (20)$$

$$\int_0^{\infty} sp_W(s)ds = 1. \quad (21)$$

The first condition is normalization of the total probability, and the second condition is normalization of the average energy level spacing. Integration of (19) gives us the so-called Wigner energy level spacing distribution functions, which correspond to the different Gaussian ensembles:

$$p_W(s) = \begin{cases} \frac{\pi}{2} s \exp(-\frac{\pi}{4} s^2), & \nu = 1(GOE); \\ \frac{32}{\pi} s^2 \exp(-\frac{\pi}{4} s^2), & \nu = 2(GUE); \\ \left(\frac{8}{3\sqrt{\pi}}\right)^6 s^4 \exp(-\frac{64}{9\pi} s^2), & \nu = 4(GSE). \end{cases} \quad (22)$$

Despite the fact that these functions were obtained for the Gaussian ensemble with matrixes 2×2 in size, they describe with sufficient accuracy the spectra of arbitrary size matrices [9].

Note that random matrix theory at first was developed to find some regularities of heavy nucleus energy spectra [10,11], but it attracted keen interest after the Bohigas, Giannoni and Schmit conclusion [12] that this theory can be applied to any chaotic system.

We now turn to our problem of determination of statistics (15) type and will try to use the considered statistics properties of the Gaussian ensembles.

IV. THE WIGNER QUANTUM STATISTICS AND GENERALIZED STABILITY CONDITION

Now, in the framework of nearly integrable system, to which the system of equations describing the nuclear burning kinetics of the Feoktistov U–Pu fuel cycle (1) or the Taylor Th–U

fuel cycle (2) belongs, we formally introduce the "energy" eigenvalue of stationary state as $(\tilde{n}_{fis0}/n_{crit}^{fis})=E_0$ and "energy" eigenvalue of quasistationary state as $(n_{fiss}^{semi}/n_{crit}^{fis})=E_{semi}$ (where $E_0 \geq E_{semi}$ and $\tilde{n}_{fis0}$ is the current equilibrium concentration of fissile isotope limited from above by its initial equilibrium concentration, i.e., $\tilde{n}_{fis0} < \tilde{n}_{fiss}$). In general case, to describe the wave mode of nuclear burning, when the reactor is maintained in the near-critical state, we can consider that $E_{semi} \to 1$. Then in the framework of quantum-mechanical analogy, this means that the evolution of nuclear burning "energy" spectrum in allowed region is described by some quasi-equivalent two-level scheme (Fig. 3).

Then, for the nearly-integrable system which describes the nuclear transformation kinetics for the Feoktistov (1) or for the Teller (2) fuel cycle in general case we can use the Bohr-Sommerfeld approximate condition in the form

$$\int_0^a \sqrt{\frac{n_{fis}}{n_{crit}^{fis}} - 1}\, dz \approx a\sqrt{E_0 - E_{semi}} \sim \frac{\pi}{2}. \tag{23}$$

It follows that, we can postulate one obvious and important assertion: by virtue of the Bohr-Sommerfeld condition (23) the type of the Wigner energy level spacing statistics unambiguously predetermines the analogous statistics type of parameter, which characterizes the squared width (a^2) of concentration wave front of active (fissile) material.

Note that we have not any information about the value of energy E_0 before the experiment, whereas it is possible to consider that $E_{semi} = 1$. If to add also, that in the steady-state mode all wave kinetic parameters are predetermined by the initial equilibrium $\tilde{n}_{fis}$ and critical n_{crit}^{fis} concentration of active (fissile) isotope (whose values are known before experiment), the physical meaning and the necessity of following change

$$a\sqrt{E_0 - E_{semi}} = a_* \sqrt{\frac{\tilde{n}_{fis}}{n_{crit}^{fis}} - 1} \tag{24}$$

become apparent.

It is obvious that the conditions (23) and (24) make it possible to obtain the expression for parameter a_*:

$$a_*^2 \sim \frac{\pi^2}{4} \frac{n_{crit}}{\tilde{n}_{Pu} - n_{crit}}. \tag{25}$$

The next step for determining the statistics $p(a_*)$ of Eq. (15) type consists in the experimental validation of proposed hypothesis. For that we have compared the Gaussian

ensemble statistics (22) with the calculated data of well-known computational experiments [4,13-17] and have obtained a good accordance of calculation data with theoretical dependence, which is described by the Gaussian simplectic ensemble statistics (see Table I and Fig. 4).

Thus, we can conclude that the wave velocity (15) is predetermined by the following approximate equality

$$\frac{u\tau_\beta}{2L} \cong p_W^s(a_*) = \left(\frac{8}{3\sqrt{\pi}}\right)^6 a_*^4 \exp\left(-\frac{64}{9\pi}a_*^2\right), \quad a_*^2 \cong \frac{\pi^2}{4}\cdot\frac{n_{crit}^{Pu}}{\tilde{n}_{Pu}-n_{crit}^{Pu}}, \tag{26}$$

where coefficient b = 2 (see Eq.(15)); τ_β is the delay time caused by active (fissile) isotope production, which is equal to the β–decay time of compound nuclei in the Feoktistov (1) or the Teller (2) fuel cycle; $p_W^S(a_*)$ is the Wigner symplectic statistics.

Thus, based on the verification results of Eq.(26) we can make a conclusion, which generalizes the physical conditions of existence of Feoktistov's wave mode: the velocity of soliton-like wave propagation in neutron-multiplicating mediumin must be determined in general case by two conditions. The first condition (necessary) is predetermined by relationship between the equilibrium concentration and critical concentration of active (fissile) isotope $(\tilde{n}_{pu}/n_{crit})>1)$ or, more exactly, by the Bohr-Sommerfeld quantization condition. The second condition (sufficient) is set by statistics of the Gaussian simplectic ensembles with respect to the parameter *a*, which describes the burning concentration wave width of active (fissile) component of nuclear fuel.

V. COMPUTATION 3D-EXPERIMENT AND VERIFICATION OF THE WIGNER QUANTUM STATISTICS

Let us consider the simplified diffusion model of neutrons and nuclei kinetics in the chain (1) in the one-group approximation (neutron energy is ~ 1 MeV) and cylindrical geometry. Then, taking into account delayed neutrons, the respective system of differential equations, which describes the kinetics of Feoktistov's U-Pu fuel cycle, i.e., the kinetics of initiation and propagation of neutron-fission wave $n(x, t)$, is as follows [13]:

$$\frac{\partial n(x,t)}{\partial t} = D\Delta n(x,t) + q(x.t), \tag{27}$$

where

$$q(x,t) = \left[\nu(1-p)-1\right]\cdot n(x,t)\cdot \upsilon_n \cdot \sigma_f^{Pu}\cdot N_{Pu}(x,t) + \sum_{i=1}^{6}\frac{\tilde{N}_i \ln 2}{T_{1/2}^i} -$$

$$- n(x,t)\cdot \upsilon_n \cdot \left[\sum_{8,9,Pu}\sigma_a^i \cdot N_i(x,t) + \sum_{i=1}^{6}\sigma_a^i \cdot \tilde{N}_i(x,t) + \sum_{i=осколки}\sigma_a^i \cdot \overline{N}_i(x,t)\right],$$

$$\frac{\partial N_8(x,t)}{\partial t} = -\upsilon_n \cdot n(x,t)\cdot \sigma_a^8 \cdot N_8(x,t), \tag{28}$$

$$\frac{\partial N_9(x,t)}{\partial t} = \upsilon_n \cdot n(x,t)\cdot \sigma_a^8 \cdot N_8(x,t) - \frac{1}{\tau_\beta} N_9(x,t), \tag{29}$$

$$\frac{\partial N_{Pu}(x,t)}{\partial t} = \frac{1}{\tau_\beta} N_9(x,t) - \upsilon_n \cdot n(x,t)\cdot\left(\sigma_a^{Pu} + \sigma_f^{Pu}\right)\cdot N_{Pu}(x,t)\,, \tag{30}$$

$$\frac{\partial \tilde{N}_i}{\partial t} = p_i \cdot \upsilon_n \cdot n(x,t)\cdot \sigma_f^{Pu}\cdot N_{Pu}(x,t) - \frac{\ln 2 \cdot \tilde{N}_i}{T_{1/2}^i}, \quad i = 1,\ 6\,. \tag{31}$$

To determine the last term $q(x, t)$ on the right-hand-side of Eq.(27), we use the effective additional neutron absorber approximation:

$$n(x,t)\cdot \upsilon_n \cdot \sum_{i=осколки}\sigma_a^i \cdot \overline{N}_i(x,t) = n(x,t)\cdot \upsilon_n \cdot \sigma_a^{eff}\cdot \overline{N}(x,t)\,. \tag{32}$$

Taking into account the fact that fission with two fragment formation is most probable, the kinetic equation for $\overline{N}(x,t)$ becomes

$$\frac{\partial \overline{N}(x,t)}{\partial t} = 2\left(1-\sum_{i=1}^{6} p_i\right)\cdot n(x,t)\cdot \upsilon_n \cdot \sigma_f^{Pu}\cdot N_{Pu}(x,t) + \sum_{i=1}^{6}\frac{\tilde{N}_i \ln 2}{T_{1/2}^i}\,. \tag{33}$$

Here $n(x,t)$ is the neutron density; D is the diffusion constant of neutrons; υ_n is the neutron velocity (E_n =1 MeV in the one-group approximation); $\tilde{N}_i$ are the concentrations of neutron-rich fission fragments of the ^{239}Pu nuclei; N_8, N_9, N_{Pu} are the ^{238}U , ^{239}U, ^{239}Pu concentrations; $\overline{N}_i$ are the concentrations of rest fission fragments of the ^{239}Pu nuclei; σ_a is the neutron-capture microcross-section; σ_f is the fission microcross-section; τ_β is the nucleus life time with respect to the β–decay; p_i($p = \sum_{i=1}^{6} p_i$) are the parameters characterizing delayed neutrons groups for main fuel fissionable nuclides [18].

The boundary conditions for the system of differential equations (27)-(31) are

$$n(x,t)\big|_{x=0} = \Phi_0 / \upsilon_n\,, \quad n(x,t)\big|_{x=l} = 0\,, \tag{34}$$

where Φ_0 is the neutron density of plane diffusion source of neutrons which is located on the boundary x=0; l is the uranium block length.

An estimation of the neutron flux density Φ_0 from the external source on the boundary can be obtained from an estimation of the Pu critical concentration which is of order of 10%:

$$4\tau_\beta \Phi_0 \sigma_a^8 N_8(x,t)\big|_{t=0} = 0{,}1 N_8(x,t)\big|_{t=0}\ , \tag{35}$$

and therefore

$$\Phi_0 \approx 0.1 \big/ 4\tau_\beta \sigma_a^8\,. \tag{36}$$

Here we note that Eq. (36) is only an estimation of Φ_0. The results of computational experiment show that it can be substantially smaller in reality.

In general, different boundary conditions can be used, depending on physical conditions under which nuclear burning is initiated by the source neutrons, for example, the Dirichlet condition of (36) type, the Neumann condition or the so-called third-kind boundary condition, which summarizes the first two conditions. Use of the third-kind boundary condition is recommended in neutron transport theory [18]. Here we use this condition in the simple case which is known as Milne's problem, or more precisely, it is the linear combination of the neutron concentration $n(x,t)$ and its spatial derivative $\partial n/\partial x(x,t)$ on the boundary:

$$n(0,t) - 0.7104\lambda n^{(1,0)}(0,t) = 0\,, \tag{37}$$

where λ is the range of neutrons and $n^{(1,0)}(0, t) \equiv \partial n/\partial x\ (0, t)$.

Although the behavior of the "neutron source-nuclear fuel" system depends on the boundary conditions near the boundary, computational experiments show that in reactor core, i.e., far from the boundary, the system is asymptotically independent of the boundary conditions. This confirms the independence of wave propagation in reactor volume on the boundary conditions and parameters of nuclear fuel "ignition". In this sense the problem of determining the optimum parameters of nuclear fuel "ignition" in "neutron source-nuclear fuel" system is a nontrivial and extraordinarily vital issue, which requires a separate examination.

The initial conditions for the system of differential equations (27)-(31) are

$$n(x,t)\big|_{x,t=0} = \Phi_0 / \upsilon_n\,, \quad n(x,t)\big|_{x,t=0} = 0\,; \tag{38}$$

$$N_8(x,t)\Big|_{t=0} = \frac{\rho_8}{\mu_8} N_A \approx \frac{19}{238} N_A\,, \tag{39}$$

$$N_9(x,t)\big|_{t=0} = 0\,, \quad N_{Pu}(x,t)\big|_{t=0} = 0\,, \quad \tilde{N}_i(x,t)\big|_{t=0} = 0\,, \quad \overline{N}(x,t)\big|_{t=0} = 0\,, \tag{40}$$

where ρ_8 is the density, which is expressed in the units of g·cm^{-3}; N_A is the Avogadro constant.

The following values of constants were used for simulation:

$$\sigma_f^{Pu} = 2{,}0 \cdot 10^{-24} cm^2\,;\ \sigma_f^{8} = {,}55 \cdot 10^{-24} cm^2\,; \tag{41}$$

$$\sigma_a^8 = \sigma_a^i = \sigma_a^{fragments} = 5.38 \cdot 10^{-26}\ cm^2\,; \quad \sigma_a^9 = \sigma_a^{Pu} = 2.12 \cdot 10^{-26}\ cm^2\,; \tag{42}$$

$$\nu = 2{,}9\,;\ \tau_\beta \sim 3{,}3 \text{ days};\ \upsilon_n \approx 10^9 \text{ cm/s};\ D \approx 2.8 \cdot 10^9 \text{ cm}^2\text{/s}. \tag{43}$$

The system of equations (27)-(32) with boundary conditions (37)-(35), initial conditions (38)-(40) and the values of constants (41)-(43) is solved numerically using the software package Fortran Power Station 4.0. At the same time we use the DMOLCH subprogram from the IMSL Fortran Library. The DMOLCH subprogram solves a system of partial differential equations of the form $u_t = f(x,t,u_x,u_{xx})$ by the method of straight lines [13, 19]. The solutions of diffusion model of neutrons and nuclei kinetics in the chain (1) in the one-group approximation and cylindrical geomerty are presented in Fig.5.

Verification of the Wigner symplectic statistics consists in comparison of the experimental velocity of nuclear burning wave obtained by a computational 3D-experiment with its theoretical value obtained by Eq. (26). For this purpose we at first find the plutonium critical concentration n_{crit}^{fis} from the profile of space-time evolution of its experimental concentration distribution (Fig. 5). It is obvious, that the absolute value of critical concentration approximately is $N_{crit}^{Pu} \cong 8 \cdot 10^{20}$ cm^{-3}·(see Fig. 6(b)). It follows that the plutonium normalized critical concentration is

$$n_{crit}^{fis} = N_{crit}^{Pu} / N_8(x,0) = 0.0167\,, \tag{44}$$

where by virtue of Eq.(39) the initial uranium concentration is $N_8(x,0)= 4.79\cdot10^{22}$ cm^{-3}·and the value of a_* is equal to 0.704 by virtue of Eq. (25). In other words, the important case when $a_*<1$ takes a place (see Fig. 4).

Taking into account the plutonium normalized equilibrium concentration $\tilde{n}_{fis} = 0.1$, by virtue of Eq. (26) we have the theoretical value of the Wigner symplectic probability:

$$\frac{1}{2}\Lambda(a_*) = p_W^s(a_*) = 0.9303, \tag{45}$$

which corresponds to the velocity of nuclear burning wave of u_{theor} =2.82 cm/day at known parameters L=5 cm and τ_β =3.3 days.

Now we can simply determine the experimental values of nuclear burning wave velocity and, accordingly, the Wigner symplectic probability. In Fig. 6(a) the profile of space-time evolution of experimental concentration distribution of neutrons is shown. We can see that the wave crest has covered the distance of 600 cm during t=217 days. So, the velocity of nuclear burning neutron wave is

$$u_{simul} = 600/217 \cong 2.77 \quad cm/day. \tag{46}$$

This, in its turn, corresponds to the value of $(1/2)\Lambda(a_*) = p_W^s(a_*)$ =0.9141.

Thus, the approximate equality of the experimental and theoretical velocity of nuclear burning wave ($u_{theor}\cong u_{simul}$) makes it possible to conclude that the Wigner quantum (symplectic) statistics verified by computing 3D-experiment (see Fig. 4) satisfactorily describes experimental data characterized by the parameter $\Lambda(a_*)$.

Here we note that computing experiments show that the conditions of wave blocking, which describe the degradation and subsequent stop of wave, are predetermined by the degree of burn-up of the main nonfissionable (^{238}U) and fissionable (^{239}Pu) components of nuclear fuel in front of the wave by neutrons from external source in the initial stage of wave "ignition". This process is very important, since the high degree of fuel component burn-up in front of the wave will inhibit the wave from overcoming this region just as fire in the steppe can not cross the plowed in advance stripe of the land. It is obvious that in the initial stage of wave initiation the degree of fuel burn-up is determined first of all by the energy spectrum and intensity of neutrons from the external source and by the properties of nuclear fuel. The most important of these properties is the delay time τ_β of active (fissile) isotope generation due to the β–decay of compound nuclei in the Feoktistov U-Pu fuel cycle (1) or the Teller Th-U fuel cycle (2).

In spite of the general understanding of physics of nuclear burning wave blocking, it is obvious that indicated above difficulties in the describing this process testify to nontriviality of given problem. Unfortunately, the solving of this problem exceeds the scope of this work, but it will be a subject of future research.

CONCLUSIONS

The solutions of the system of diffusion type equations for neutrons and concomitant kinetic equations for nuclei obtained by numerical 3D-simulation persistently point to the regions where the stable soliton-like solutions for neutrons and solitary wave solutions for nuclei are existed. This is no wonder for nearly intergrable systems, to which the investigated system of equations for neutrons and nuclei belongs, whereas the existence of stable soliton-like solutions in three spatial dimensions causes a surprise for the following reason.

As is known, the derivation and solution of integrable nonlinear evolution partial differential equations in three spatial dimensions has been the holy grail in the field of integrability since the late 1970s. The celebrated Korteveg-de Vries and nonlinear Schrödinger equations, as well as Kadomtsev-Petviashvili and Davey-Stewertson equations, are prototypical examples of integrable evolution equations in the one and two spatial dimensions, respectively. Do there exist integrable analogs of these equations in three spatial dimensions?

As it has turned out, quite recently, in 2006, the method for finding of an analytical solutions of indicated above partial differential equations in three spatial dimensions was developed [20]. Therefore, the natural question arises: “To which from this equations does the diffusion equation for neutrons correspond, or, maybe, his is perfectly a new type of soliton partial differential equations in three spatial dimensions?”

ACKNOWLEDGMENT

The authors acknowledge the financial support of the DFG through SFB 701 “Spectral structures and topological methods in mathematics”, Bielefeld University (Germany), German-Ukrainian Project 436 UKR 113/94, and IGK Bielefeld (Germany).

REFERENCES

[1] L.P. Feoktistov, *From the Past towards the Future: from the Hopes of Bomb to the Safe Reactor* (RFNC-ANRISPh, Snezhinsk, 1998).

[2] L.P. Feoktistov, Dokl. Akad. Nauk SSSR **309,** 864 (1989).

[3] E. Teller, M. Ishikawa, L. Wood, R. Hyde, and J. Nuckols, in Proceedings of the International Conference on Emerging Nuclear Energy System (ICENEC'96), Obninsk, Russian,1996, p. 123 (available at http://www-phys.llnl.gov/adv_ energy_src/ICENES96.html); Lawrence Livermore National Laboratory, Preprint No. UCRL-JC-122708-RT2.

[4] Ershov, A.P., and V.F. Anisichkin, Combustion and Explosion Phys. (Russia), **39**, 121(2003).

[5] V.N. Pavlovich, E.N. Khotyaintseva, V.D. Rusov, V.N. Khotyaintsev, and A.S. Yurchenko, At. Energ.**102**, 181 (2007).

[6] Yu. Mozer, *KAM-theory and Stability Problems* (Publ. of Research-and-development Center "Regular and Chaotic Dynamics", Izhevsk, 2001).

[7] M. Tabor, *Chaos and Integrability in Nonlinear Dinamics* (J. Wiley, N.Y., 1989).

[8] I.C. Persival, Adv. Chem. Phys. **36**, 1 (1977).

[9] H.-J. Stokmann, *Quantum Chaos* (Cambridge University Press, 2000).

[10] H.A. Weidenmuller, Rev. Mod. Phys. **81**, 539 (2009).

[11] M.L. Mehta, *Random Matrices* (Academic Press, San Diego, 1991).

[12] O.Bohigas, M.J. Giannoni, and C. Schmit, Phys. Rev. Lett. **52**, 1 (1984).

[13] V.D. Rusov, V.N. Pavlovich, V.N. Vaschenko, V.A. Tarasov, T.N. Zelentsova, V.N. Bolshakov, D.A. Litvinov, S.I. Kosenko, and O.A. Byegunova, J. Geophys. Res. 112, B09203 (2007).

[14] H. Sekimoto, and Y. Udagava, J. Nucl. Sci. and Technolog. **43**, 189 (2006).

[15] S.P. Fomin, Y.P. Mel'nik, V.V. Pilipenko, and N.F. Shulga, Problems of Atom. Sci. and Technolog. **3,** 156 (2007).

[16] S.P. Fomin, Y.P. Mel'nik, V.V. Pilipenko, and N.F. Shulga, Ann. Nucl. Energ. **32**, 1435 (2005).

[17] E. Teller, M. Ishikawa, and L. Wood, in Proceedings of the Joint American Physical Society and American Association of Physics Teachers Texas Meeting "Frontiers in Physical Symposium", Lubbock, Texas, 1995.

[18] V.V. Smelov, *Lectures on Neutron Transport Theory* (Atomizdat, Moscow, 1978).

[19] V.D. Rusov, V.A. Tarasov, and D.A. Litvinov, *Reactor Antineutrinos Physics* (URSS, Moscow, 2008).

[20] A.S. Focas, Phys. Rev. Lett. **96**, 190201 (2006).

TABLE I. The parameters of nuclear burning wave

Parameter	U-Pu cycle							Th-U cycle
	References							
	Present paper	[14]	[15]	[15]	[16]	[4]	[17]	*)
$\frac{\tilde{n}^{fis}_{equil}}{n^{fis}_{crit}}$	$\frac{0.100}{0.017}$	$\frac{2.585}{1.750}$	$\frac{0.145}{0.080}$	$\frac{0.024}{0.015}$	$\frac{0.240}{0.105}$	$\frac{0.10}{0.05}$	$\frac{0.071}{0.032}$	$\frac{0.070}{0.035}$
a_*	0.704	2.274	1.743	2.028	1.385	1.571	1.423	1.571
u_{theor}/u_{simul} [cm/year]	1030/1012	2.9/3.1	125/130	21/22	622/620	293/331	46/~50	25

* Forecast for the Th−U fuel cycle in infinite medium at 10% enrichment of ^{233}U.

FIGURE CAPTIONS

FIG. 1. Time dependence of neutron concentration. Propagating wave (a) and locked wave (b): a segment of the curve of $n_{\mathrm{Pu}}(z)$ above the n_{cr} line is the reactor core; the scales of n_{cr} and n_{Pu} are given with $a\times10$ magnification [4].

FIG. 2. The schematic view of permitted and subbarier (gray colored) region corresponding to the conditions $n_{\mathrm{Pu}} > n_{\mathrm{crit}}$ and $n_{\mathrm{Pu}} < n_{\mathrm{crit}}$, respectively. The delineated by square region is considered more particularly in Fig. 3.

FIG. 3. Schematic description of the permitted and forbidden region boundaries of nuclear burning according to the Borh-Sommerfeld condition (a) and the corresponding quasi-equivalent two-level scheme (b).

FIG. 4. The theoretical (solid line)) and experimental (points) dependence of $\Lambda(a_*)$ on the parameter a_*.

FIG. 5. Concentration kinetics of neutrons, ^{238}U, ^{239}U and ^{239}Pu in the core of cylindrical reactor with radius of 125 cm and 1000 cm long at the time of 240 days. Here r is transverse spatial coordinate axis (cylinder radius), z is longitudinal spatial coordinate axis (cylinder length).

FIG. 6. (a) - The neutron concentration distribution at the cylinder axis at t = 217 days. The wave velocity is $u_{\mathrm{simul}} \approx 2{,}77$. (b) - The ^{239}Pu concentration distribution at the cylinder axis for $n_{Pu} = 0.1 n_{crit}^{Pu} n_{\mathrm{Pu}} = 0.0167$ at t = 217 days.

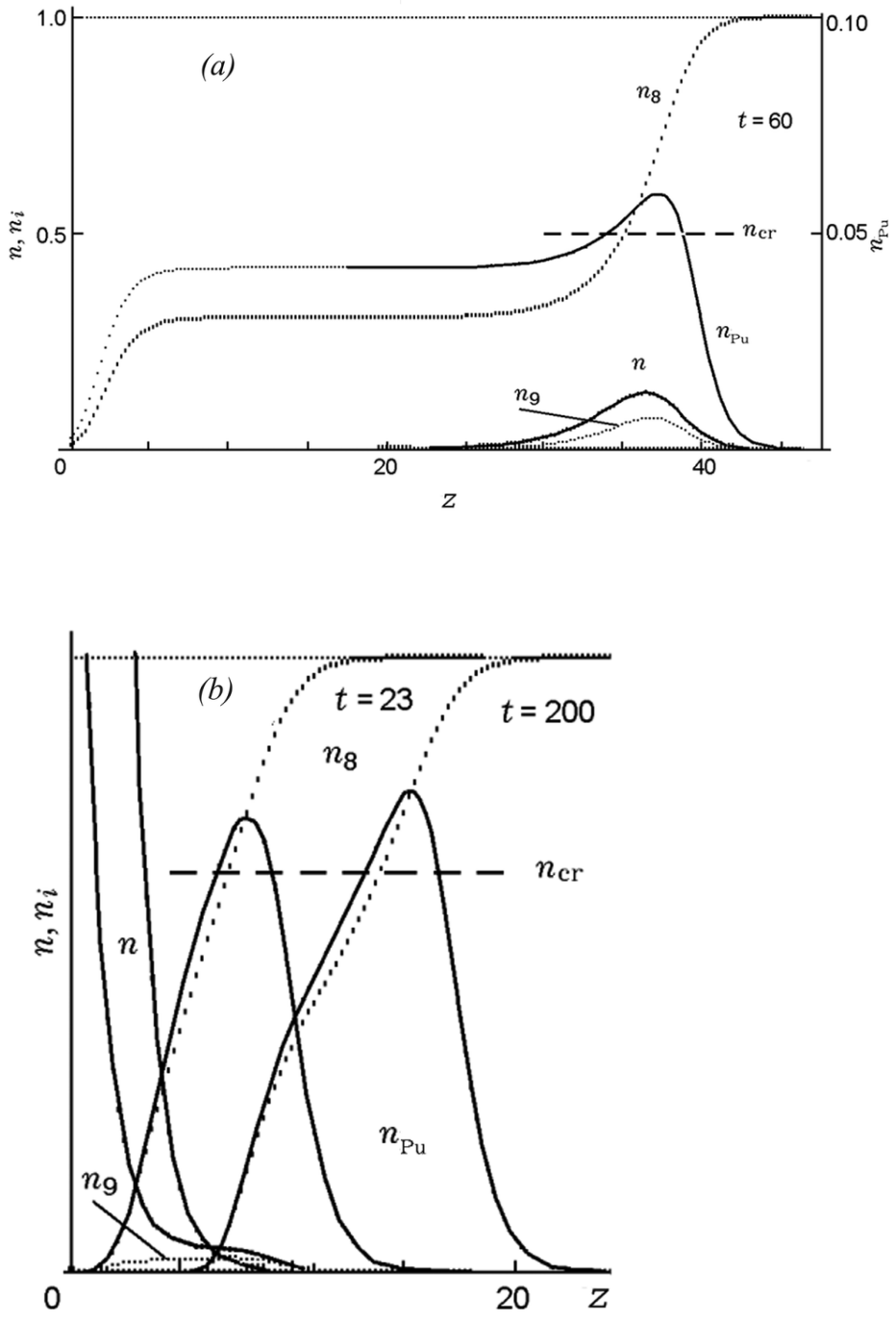
(a)
1.0
0.5
0.10
0.05
n, n_i
n_{Pu}
n_8
$t = 60$
n_{cr}
n_{Pu}
n
n_9
0
20
40
z
(b)
$t = 23$
$t = 200$
n_8
n_{cr}
n, n_i
n
n_{Pu}
n_9
0
20
z

FIG. 1.

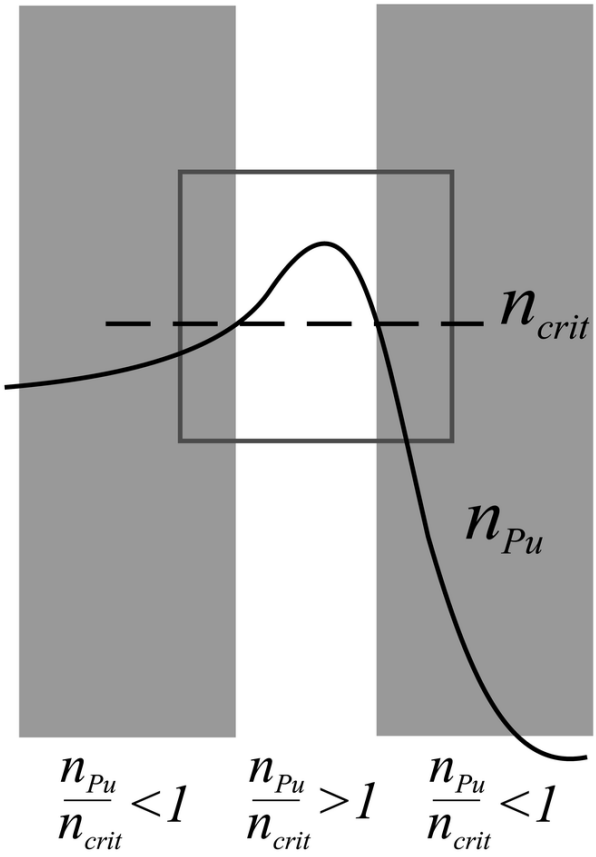

FIG. 2

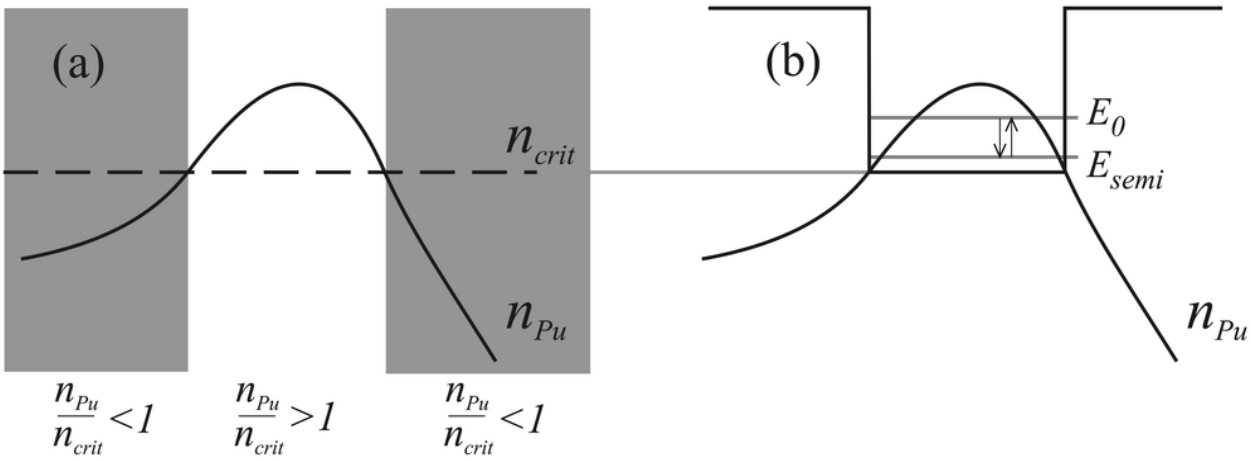
(a)
n_{crit}
n_{Pu}
$\frac{n_{Pu}}{n_{crit}} < 1$
$\frac{n_{Pu}}{n_{crit}} > 1$
$\frac{n_{Pu}}{n_{crit}} < 1$
(b)
E_0
E_{semi}
n_{Pu}

FIG. 3

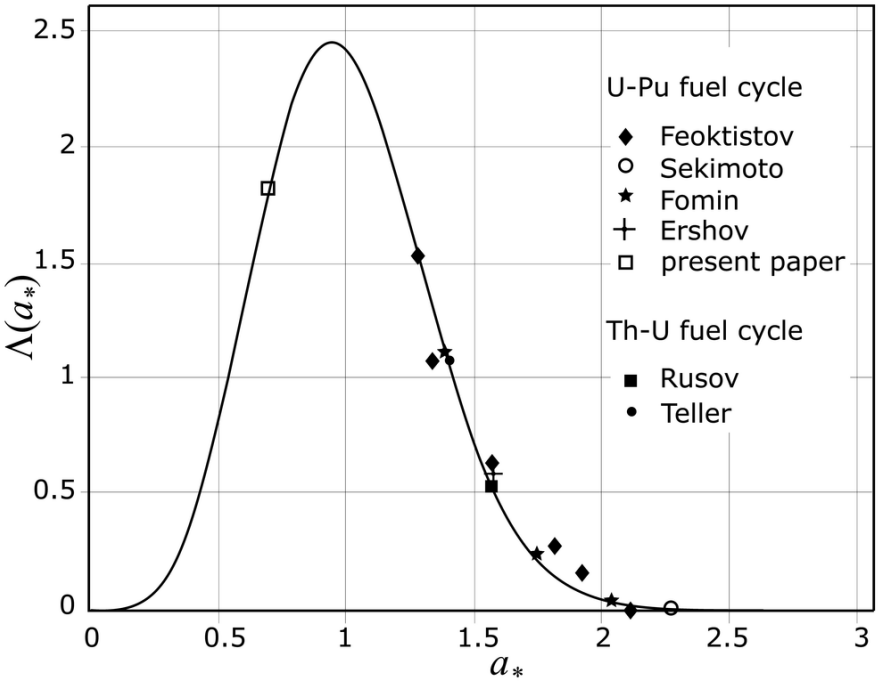
2.5
2
1.5
1
0.5
0
0
0.5
1
1.5
2
2.5
3
$\Lambda(a_*)$
a_*
U-Pu fuel cycle
Feoktistov
Sekimoto
Fomin
Ershov
present paper
Th-U fuel cycle
Rusov
Teller

FIG. 4

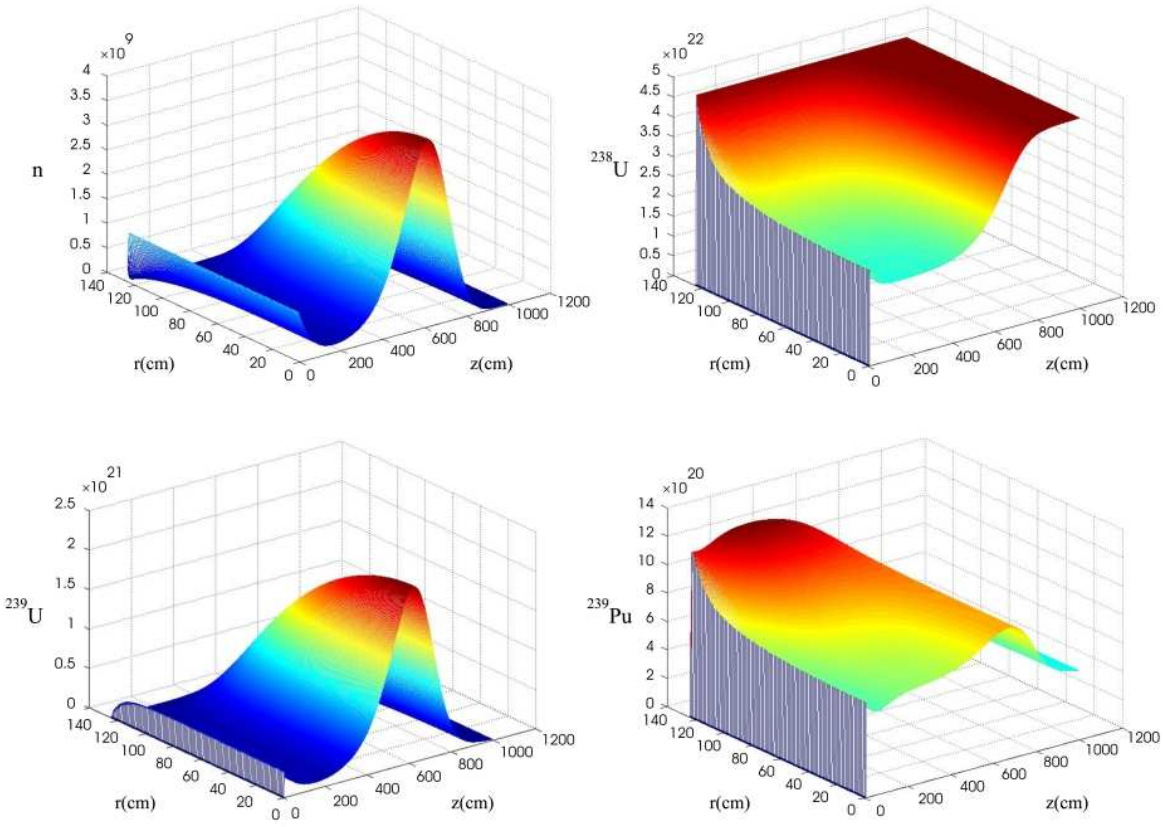
n
×10^9
r(cm)
z(cm)
238U
×10^22
r(cm)
z(cm)
239U
×10^21
r(cm)
z(cm)
239Pu
×10^20
r(cm)
z(cm)

FIG. 5

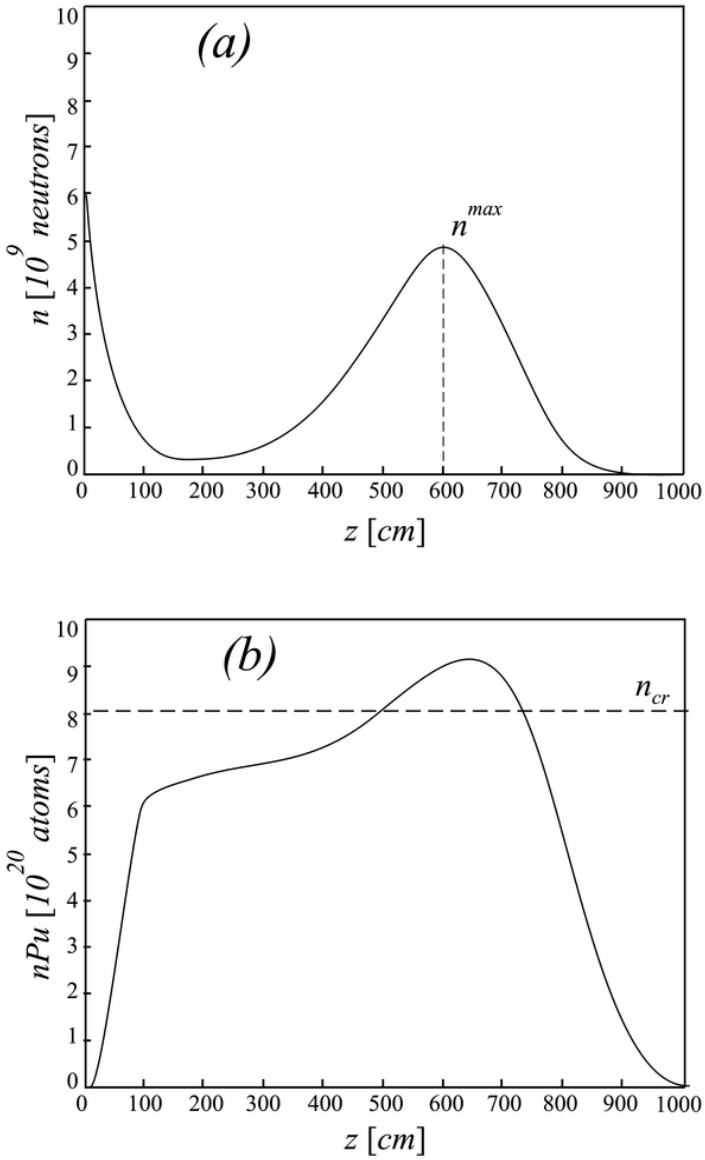

FIG. 6

CHAOTIC MODELING OF INTELLECT

Nikolay Serov [1]

In chromatism, the definitions are based on their classical (non-cognitive) interpretation in science. Thus for example, under 'intellect' (Latin: 'intellectus' – a sensation, perception, understanding) we mean the informative model of the personality. In chromatism, intellect is subdivided into definite "atomic" components in correspondence with its principal functions: biological (unconsciousness), psychological (subconsciousness) and social (consciousness). Each of these components of the intellect is characterized by the definite functions and formalized ontological plans of the system*: consciousness is a M-plan, subconsciousness is an Id-plan and unconsciousness is a S-plan.* As far as in the history of global culture each of the functional "atoms" in the intellect was archetypal linked with a definite color (*M* – white, *Id* – grey and *S* – black), we had called our model an archetypal model of intellect (AMI).

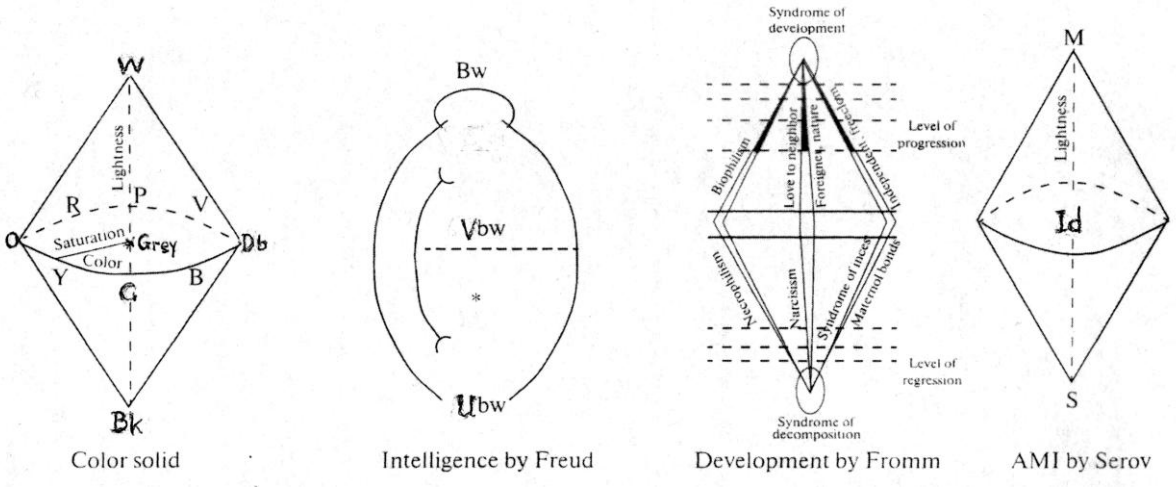

Fig. 1. Transition of the twentieth century concepts from the color solid to AMI.

Methodology of chromatism is based on ancient Greek notion 'chroma'. We shall represent the meanings of this notion: 1) Color image as something psychic, unobjectified, ideal, i.e. an *Id-plan of AMI*. 2) Tint as an object of outer space, being something physical and material relatively color and intellect. This is an *M-plan* of the "outer space – AMI" system.

[1] Faculty of Applied Psychology, St.Petersburg State Institute of Psychology & Social Work 199178-St.Petersburg (Russia) Corresponding author: nserov@gmail.com

3) Color designation objectified in a word is more material than a color image. This is an *M-plan of AMI*. 4) The pigmentation of a human body as something physiological, syntonic, i.e. *S-plan of AMI*. 5) Emotions as an informative-energetic correlation of the plans mentioned above. Objectively, this correlation manifests itself in such idioms as "to become red from shame", "to have a red face", "green with envy", "to become white as a sheet from fear" etc. These idioms show us in particular, the meaning of emotional relations between the psychic (color) and the physiological (the coloring of skin pigment), as between something ideal and material. Thus, the close link between given definitions and plans clearly show that neither the problem of color nor the problem of intellect can be solved independently by isolate scientific disciplines. That is why we have listed in short the possible stages in the intellect of processing color information about the outer environment from the point of view of chromatism. [1]

In the AMI-system these components are linked semantically with subdivision of individuals according to their gender (psychological sex) and, at the same time, with the definite colors that were canonized by world culture.[1] In accordance with such statement of the problem, it appeared to be necessary to experiment the link between gender distribution of "atomic" components in the AMI and preferred colors. From here came the principal task of the investigation: to verify the link between the ideal (a perception, a color concept) and the material (i.e. tests, objectivized in words, on one hand, and tints of stimulus samples as well as verbal color designations, on the other hand).

2. ONTOLOGICAL RELATIVISM OF THE COLOR CIRCLE AND INTELLECT

Similarly, one can imagine the reflection of colors in the color circle. As far as I know, Newton, Lambert, Young, Helmholtz, Maxwell, Munsell, Judd, and Wyszecki arranged the transition from red through green to blue clockwise. As a rule, these colors were stimuli. As for Goethe, Runge, Hegel, Schopenhauer, Hering, Kandinsky, Steiner, Ostwald, and Itten, all of them gave the same disposition of colors but in the opposite direction. They had dealt with perceptive colors.

Remarkably, that all over the world people calls the "red" those who share the "left" ideas (extremists, communists, etc). Hence, the world (not only of subconscious context, but entirely conscious text) uses percepts according to Goethe, i.e. unconscious image-percept rather than stimuli (where red in the color circle according to Newton, positioned to the right).

Psychology studies a human soul and spirit, i.e. in essence the ontologically ideal phenomenon. The functions of color concept are also ideal. [1; 2] That's why we suppose that color is an optimal instrument for studying intellect and its digital simulation. The dynamic functional model of a personality is based on the dynamic model of intellect (from Latin word 'intellectus' – 'sensation', 'perception', 'understanding').[1]

In chromatism the archetypal model of intellect (AMI) is subdivided into the following "atomic" functional components that are formalized in the plans of AMI (see Tabl.1). Consciousness (*M*-plan of AMI) deals with arbitrarily comprehended functions of social conditionality, verbal thinking, principles of formal logical processing of information and its understanding (in science, philosophy, etc). Subconsciousness (*Id*-plan of AMI) is characterized by unconscious and / or partially (e.g. arbitrary in the insight) conscious functions of cultural conditionality, image-logic operations and 'perception' (in art, creative activity, etc), as well as esthetic (non-pragmatic) perception of creative activity, games, in general, 'ideal'.[1] Unconsciousness (*S*-plan of AMI) included principally uncomprehended functions of natural conditionality, of 'sensation' (color phenomena in retina, nervous system, affects, etc) and genetic coding of information.

3. "FEMININE" AND "MASCULINE" LOGIC

To analyze 'gender' as spiritual (unlike sexual, bodily) dimorphism, it is necessary to give its definitions. 'Sex' is a physiological and juridical (passport) notion. 'Gender' is principally a psychological notion. According to our estimation, correlation between sex and gender quantitatively amounts to no less than 85 ±5% of individual, of both sexes. For instance, men and masculine women usually overestimate their knowledge, while women and feminine men underestimate one. Everything depends upon proportions between the intellect dominants (i.e. plans of AMI) because a human personality results from permanently changing phases of psychosexual development. That's why both feminine intellects on definite stages of its development pass through the ones where masculine components dominants, and a male intellect pass through stages of dominants feminine components. In chromatism they are simulated by definite plans of AMI and/or an AMI with gender opposition (*AMIGO*, see below) and definite colors, canonized by global culture.[1] [I ask readers to excuse me for the mistakes in tables 4 and 5 (ref.1) in which instead of gender (feminine and masculine) characteristics the sexual (male and female) ones for color canons were given.] So, representatively, all components of AMI are linked with chromatic functions of intellect and depend upon gender dominants. Nevertheless in publications on gender

psychology we may sometimes meet two diametrically contrary opinions about one and the same problem: logic of men and women either is being opposed or identified. But how are the things in reality?

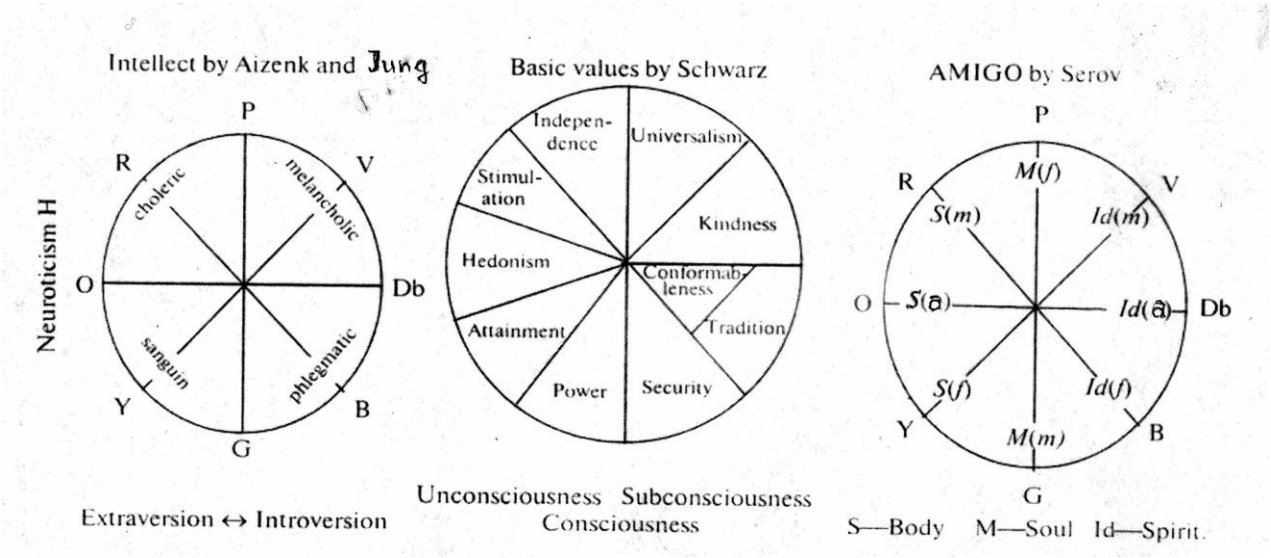

Fig. 2. Transition from the models of intelligence by Jung, Aizenk, Luscher and Schwartz to AMIGO [1].

The equation for AMI was obtained by three independent ways, but within the limits of the given report this equation follows from the Ostwald's achromatic equation:

$$Grey = White + Black. \tag{1}$$

From (1) it follows (see Table 1) that

$$I = M + A, \tag{2}$$

where $A = S / M\,d$ – total quantity of absorbed (bound, uncomprehended) information; M – total quantity of reflected (free, comprehended) information.

From here, equation (1) may be written for the AMI-plans as follows:

$$I = M + S/Md. \tag{3}$$

Here $I = Id / U$ – quantity of objective information about outer environment, where potential U is equal to the one of intellect d in optimal condition of adaptation (for polychrome color $Id \Rightarrow ch/\lambda_0$ and $I=iL_0$; $[i]=byte \cdot candle^{-1} \cdot m^2$; luminance $L_0=\varepsilon_\lambda (\lambda_2-\lambda_1)$; $[\varepsilon_\lambda]=candle \cdot m^{-2} \cdot nm^{-1}$, λ_1 and λ_2 – complementary wavelengths).

In chromatism the equation (3) links the plans of the outer and inner world. The solution of this equation for variable M gives two values: M_f (feminine legal consciousness) and M_m (masculine self-consciousness). The experience shows that M_m and M_f are really distinct for both men and women in 85±5 % cases. Strictly speaking, AMI-plans represent a

quantity of information that is processed on the levels of feminine and masculine components in AMI.

In Figure 3 the curves describe the dependence of comprehensible (M-plan) information upon color modelling components of the AMI. According to the legend, in the diagram we provide designations similar to the ones in the equation (2). We take the middle part of spectrum (green shades in M-plan) with linear development of logic M_f as being the

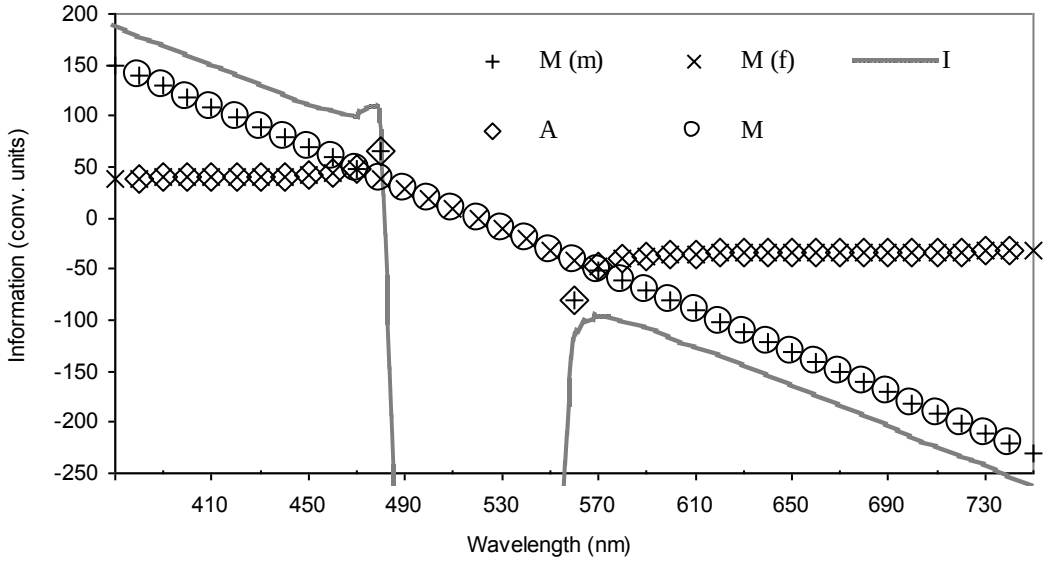

Figure 3: Estimation of gender function in AMI, obtained according to equation (3).

conventional standard for comprehending information I by M_f and M_m plans. Then, the interval from –50 to +50 cbyte (conventional information units) will be the standard for information perception.

First of all, it strikes our eyes that all over the spectrum area the curves of M_m-plan and objective information I develop parallels. It may be explained by the relatively high content of ferric ions in men's blood, which, consequently, have to be more empathic to change in information about the outer environment. At the same time, the curve of M_f-plan stays within the limits of conventional standard (0±50 cbyte) independently of information I about outer environment. From the diagram it follows that logics of M_f and M_m plans appear to be similar rather than opposite and mutually complement each other to obtain optimal quantity of "transparent" M-plan information: $M_f + M_m = I$. This is confirmed by the development of curve of M_f-plan that is similar to (M_f=A) all over the spectrum area except green, where it "reflects" (M_f=M) information I. M_m-plan "absorbs" information only in the green area (M_m=A), while in other parts of the area it "reflects" information (M_m=M). For all

this, the equation (2) keeps true. The gender characteristics were distinctly modeled by a color and demonstrated a polar nature on the diameters of a color circle: (red S_m – blue Id_f , purple M_f – green M_m; violet Id_m – yellow S_f , and deep-blue Id_a – orange S_a , where index 'a' is androgyny; 'f' is feminine and 'm' is masculine component in AMI [1]).

The reproduction of gender semantics in color canons during many thousands of world history was, in essence, the objectivism of subjective manifestation of the intellect (exceptions amount to less than 15% from total data base).

4. EXPERIMENTAL DATA

Figure 4 gives the preliminary results of experiments on visual choosing the stimulus-preferred colors (270 women and 58 men of 20-25 years of age). The given equations were obtained from equation (3) and represented in a legend where $C \approx I$ was a color concept. From Fig.2 we can see that within a warm area the necessity of *S*-plan *N(S)* dominated actually, within a cold one the necessity of *Id*-plan *N(Id)* did (as it followed from color canons [1]).

The experiments were held to confirm the atomic nature of AMI. The identification of atomic components in the AMI (that had been defined by completely different approaches) had to be found experimentally. Thus, on the one hand, choosing preferred colors in a visual test, as well as in a verbal one, could do it. On the other hand, the same results had to be obtained in answers to "transparent" test-question in verbal tests MMPI and AMI. In other words, ideally, all 4 tests had to enable each person under test to choose the same AMI- components. The preliminary results enable to think that AMI is really atomic, as far as colors of its "atoms" had been correlated (r=0.8±0.1) with relevant choice of color both in visual tests or verbal color designations, and in verbal question of the AMI-test, characterizing gender functions of each AMI-component. The experimental data obtained during 2001-2004 and given in Fig.2 showed that a contemporary keeps in himself the archetypal properties of our far ancestry.

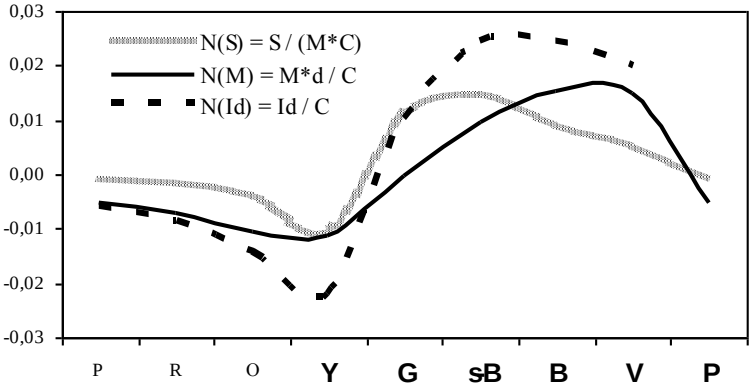

Figure 4: Experimental assessment of necessity for "atomic" AMI-components in choosing color stimuli. Abscissa axis is first letter of color designations; axis of ordinate is necessity (conventional units).

Table 3. The parameters of information in "atomic" model of intellect (AMI)

Type of information	**Semantic characteristics of information (plans of AMI)**	**Branch of science**	**Linkage of formulae**
Total I(OE) (flux I_0)	Objective information about outer environment (**OE**)	Physics: $\boldsymbol{\sigma = \alpha + \rho}$ Informatics: $\boldsymbol{A + M = I}$	$A = \alpha I_0$ $M = \rho I_0$
Free I_ρ (reflected, external)	Subjectively conscious, verbalized in OE, objectified in the past – (***M***-plan)	Psycholinguistics: $\mathbf{C_\lambda = C_\alpha + C_\rho}$	$C_\rho = M$ $C_\rho = \rho\, C_\lambda$ $C_\lambda \approx Id\,/U$
Image-concept (database AMI about OE)	Objectifying of information in uncomprehended image of OE for adaptation in the present – (***Id***-plan)	Chromatism: $\boldsymbol{I = M + S/Md}$	$M = S\,/\,Ad$ $I \approx i(\lambda_2 - \lambda_1)$ $Id = Md + S/M$
Bound I_α (absorbed, internal)	Subjectively unconscious , unobjectified in OE, demanded in the future – (***S***-plan)	Psychophysics: $\boldsymbol{\sigma\, \lambda_0 = \alpha\, \lambda_1 + \rho\, \lambda_2}$	$\alpha = C_\alpha / C_\lambda$ $\rho = 1 - \alpha$ $S = A\, Q(\lambda_0)$

CONCLUSION

In conclusion, by using the experimentally checked equations (1)-(3) we have got a chance for context dependent representing the information on all levels of digital coding. Taking into account heterogeneous data of multispectroscopy we may link the "archetypal" properties of color with objective parameters for digital processing of color information. The possibility is given for context dependant representation of information on all levels of digital coding. The equations for digital representation of a color concept are given as well. To my estimation the exceptions of the rule of archetypal properties of image-concept in color canons are no more than 15 % of all data obtained on color canons in various cultures.

The chromatic approaches to the information processing enabled to represent an archetype as a psychophysical formation that had been canonized by world cultures in the process of thousand of years and on the basis of which the archetypal model of intellect (AMI) of the atomic type was obtained. The link between the dominant character of "atomic" components in the AMI and choice of preferred colors was confirmed experimentally. Primary concordance with the experiment enabled to consider the established principles of AMI to be the basis for color simulation of gender aspects of a personality.

We have shown that "atomic" components in the AMI-system (*M*-, *Id*-, *S*-plans) are linked with relevant parameters of a color concept in psychophysics, chromatism, psycholinguistics, and informatics in tabl.3.Triad logic of a complex information system may be actually revealed only if we take into account the boundary that separates, and at the same time, combines complementary colors λ_2 and $\lambda_1$of the components, forming this system λ_0. The principles, established for the AMI, become the basis for digital representation of all stages for color information processing from spectral components of the outer environment to the forming of a color concept.

References

1. N.V. Serov, *The Ontology of Dimensionality for Anthropological Database Modeling* Automatic Documentation and Mathematical Linguistics, V.44, N.1, p.1–15, (2010).
2. L. Wittgenstein, *Remarks on colour.* (California Press, Berkeley, 1977).
3. Barbieri M. *The organic codes. An introduction to semantic biology.* (Cambridge University Press, Cambridge, UK, 2003).
4. N.V. Serov, *Electronic terms of molecules*, Optics & Spectroscopy, V.56, 3, p.240,-247. (1984).
5. *International lighting vocabulary*, in Publication CIE, 1, 1, № 17 (1970).
6. D.B. Judd, G. Wyszecki, *Color in business, science and industry.* (Wiley, N.Y., 1975).
7. N.V. Serov, *Attributes and functions of color space*, J. Optical Technology, V. 68, № 5, p. 349-352 (2001).
8. J. Liberman, *The effect of syntonic (colored light) stimulation on certain visual and cognitive functions*, J. Optometric Vision Development, V.17, p.2-11 (1986).
9. Y. Mijashita, *Neuronal correlation of pictorial short-term memory*, Nature, V.331, № 6151, pp.68-70 (1988).

10. N.V. Serov, *Data definition by color*, Automatic Documentation and Mathematical Linguistics, V.35, № 6, p.36-38 (2001).

Proceedings, 4th Chaotic Modeling and Simulation International Conference
31 May – 3 June 2011, Agios Nikolaos, Crete Greece

Nonlinear vibrations and chaos in electrostatic torsional actuators

R. Shabani†, S. Tariverdilo, G.Rezazadeh A.P. Agdam, and S. Mahjouri

Faculty of engineering, Urmia University, Urmia, Iran.

†E-mail: r.shabani@urmia.ac.ir

Abstract

Electrostatic torsional micro-mirrors have wide spread use in different industries for diverse purposes. This paper investigates the development of superharmonics and chaotic responses in electrostatic torsional micro-mirrors near pull-in condition. Appearance of nonlinear phenomena is investigated in models accounting for and disregarding coupling of torsional and flexural deflections. Analysis of the system response to step and harmonic excitation reveals the appearance of DC and AC symmetry breaking. Increasing the amplitude of harmonic excitation the response in the form of distinct superharmonics changes to a broad band response, where there is loss of periodicity and the response becomes chaotic. Accounting for flexural deflections in coupled model reduces the voltage thresholds corresponding to symmetry breaking and chaotic responses. It is also shown that damping has a regularizing effect and introduction of damping changes the chaotic undamped response into quasi-periodic one.

Keywords: Micro mirror, nonlinear vibrations, chaotic vibrations.

1. Introduction

Electrostatic torsional micro-mirrors are devices which are used for reflecting the light beams to specific directions. They are used in projection display systems, optical scanners for projection display, optical switches (In telecommunications), and optical cross-connects. For these applications, the performances of the torsional micro-mirrors depends on the mirror size, natural frequency, operating voltage, rotation angle, linearity range, and some surface specifications. Many investigations have been done on the analysis of the electrostatic torsional micro-mirrors. Static analysis of the mirrors was reported by Zhang *et al.* [1], where the pull-in conditions are extracted. Fischer *et al*. investigated the static and dynamic behavior of micro mirrors using finite element analysis and clarified the dependency of natural frequency on the squeeze film conditions [2]. Large deflection analysis of MEMS structures was examined by Chaterjee *et al.*, where beside the electrostatic nonlinearity the structural nonlinearity is also considered and dynamic pull-in conditions was studied [3]. The effects of intermolecular forces (Van der Waals and Casimir forces) on the static and dynamic responses of torsional actuators have been investigated by some researchers. Gusso *et al.* studied the effects of Casmir force on the response of micro mirrors [4]. Guo, and Zhao. considering the Van der Waals and Casimir forces, studied the effects of these forces on the static and dynamic behavior of electrostatic torsional micro and nanoelectromechanical actuators [5, 6]. In a separate study, they also considered the effect of Casmir and capillary forces on the stability of the micro-mirrors [7]. In the

analysis of micro mirrors in addition the torsional mode the bending mode may also be affects the response. The static coupling effects of bending and torsional modes of micromirrors have been studied by Huang *et al.* [8]. Rezazadeh *et al*. also investigated the effect of the coupling between bending and torsional modes on the static and dynamic behavior of micro mirrors [9, 10]. The main emphasis in the previous studies on the behavior of micro-mirrors is on the eigenfrequency analysis or developing the response of the system to step excitation [11] or mechanical shock. But the behavior of the system in nonlinear regime of the response are not clarified in details.
In this paper the emergence of nonlinear behavior in electrostatic torsional micro-mirrors are investigated with emphasis on the effect of bending deflection on the behavior of the system. Evidence of the nonlinear behavior for step and harmonic excitations appears when the amplitudes of the excitations exceed some specific thresholds. The behavior of the systemwith and without taking into account for bending deflection as excited by step and harmonic excitation are investigated

2. Mathematical modeling

A schematic 3D view of a torsional micro-mirror and its cross-sectional view are shown in Fig. 1, where the micro-mirror plate is suspended by two torsional micro- beams with length *l*, width *w*, and thickness *t*. The length and width of the micro-mirror plate are *L* and *a*, respectively, and *h* denotes the initial gap between the micro-mirror and electrode. The position and size of the electrodes are controlled by a_1 and a_2.

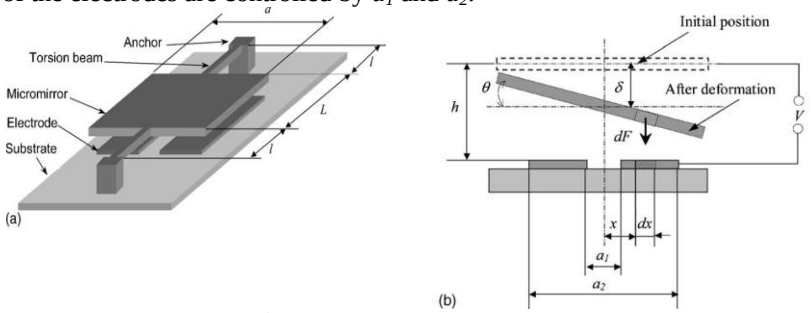

Fig. 1. Schematic diagram of torsional micro-mirror, a) 3-D isometric view, b) cross-sectional view [11].

In the micro-mirrors modeling it is customary to ignore the deflection of the micro-mirror plate, by assuming rigid micro-mirror plate. Ignoring the plate deformation, the micro-mirror becomes a system with two torsional and flexural degrees of freedom. When a potential voltage is applied between the micro-mirror and the electrodes, the micro-mirror rotates about its centerline (with angle of rotation θ) and also displaces in vertical directions (as denoted by δ). Assuming a proportional damping and also linear elastic restoring torque and bending forces for micro-mirror beams, the governing equations become.

$$m\ddot{\delta} + C_b\dot{\delta} + k_b\delta = F_e$$
$$I_t\ddot{\theta} + C_t\dot{\theta} + k_t\theta = T_e \quad (1)$$

Where *m* is the micro-mirror mass and I_t is the mass moment of inertia about the axis of rotation and C_b and C_t are the bending and torsional damping coefficients, respectively. The torsional and bending stiffness of the micro-

beams are denoted by k_t and k_b, respectively, and F_e and T_e are the electrostatic force and torque imposed to micro-mirror due to applied voltage. By introducing the following non dimensional parameters

$$Y = \frac{\delta}{h}, \varphi = \frac{a\theta}{2h}, \tau = \omega_0 t, \lambda_b = \frac{k_b}{m},\ {\omega_0}^2 = \frac{k_t}{I_t}\ , \alpha = \frac{a_1}{a}, \beta = \frac{a_2}{a}, R_1 = \frac{C_b}{m\omega_0}, R_2 = \frac{C_t}{I_t\omega_0}, \quad (2)$$

the governing equations of the system can be rewritten in non dimensional form as

$$\frac{d^2Y}{d\tau^2} + R_1\frac{dY}{d\tau} + \frac{\lambda_b}{{\omega_0}^2}Y = \frac{B_1V^2}{\varphi}\left[\frac{1}{1-Y-\beta\varphi} - \frac{1}{1-Y-\alpha\varphi}\right] \quad (3a)$$

$$\frac{d^2\phi}{d\tau^2} + R_2\frac{d\phi}{d\tau} + \varphi = \frac{B_2V^2}{\varphi^2}\left[\frac{1-Y}{1-Y-\beta\varphi} - \frac{1-Y}{1-Y-\alpha\varphi} + ln\left(\frac{1-Y-\beta\varphi}{1-Y-\alpha\varphi}\right)\right] \quad (3b)$$

where I and I_p are the cross-sectional and polar moment of the torsional micro-beams, respectively and ε is the permittivity of air and B_1 and B_2 are defined as following

$$B_1 = \frac{L\epsilon a}{4m{\omega_0}^2h^3}\ ; \quad B_2 = L\epsilon a^3/16I_th^3 \quad (4)$$

Expanding the right hand sides of Equation 3 in terms of nondimensionalized displacements gives rise to the appearance of these displacements with different powers. This means that the equation has a general form of Duffing equation. Therefore, it is anticipated that for excitation near the pull-in conditions, the forcing frequency multiplications (superharmonics) appears in the response, which is investigated in this paper.

3. Simulation results

The parameters of the micro-mirror used in the simulations are listed in Table 1. Using these parameters, frequencies of the torsional and vertical free vibration of the undeflected micro-mirror are calculated as 40 and 67 KHz, respectively.

Table 1. Parameters of the electrostatic torsional micro-mirror

Items	Parameters	Values
Material properties	Shear modulus, G (Gpa) Young's modulus, E (Gpa) Density (Kg/m3)	66 170.28 2,330
Micro-mirror	Width, *a* (μm) Length, *L* (μm)	100 100
Torsional beam	Length, *l* (μm) Width, *w* (μm) Thickness, t_h (μm)	65 2 1.5
Electrode	Width a_1 (μm) Width a_2 (μm) Gap *h* (μm)	6 84 2.75

To evaluate the effect of flexural deflections on the system response, two models are considered in the simulations. The first uncoupled model disregards coupling between flexural and torsional deflections, while second coupled model accounts for coupling between torsional and flexural deflections. Due to importance of the step and harmonic response of the

micro-mirrors in real world applications, in the following sections the response of the coupled and uncoupled micro-mirror models with and without damping to step and harmonic excitations is investigated.

3.1. Step response

When the micro-mirrors used as optical switches the transient response determined by settling time, overshoot and also pull-in voltage due to step excitations (stepped DC voltage) will be important. For uncoupled undamped case, the mirror has two equilibrium positions, a stable center one and an unstable saddle node. For DC step excitation voltages lower than 21 V the response is linear and the trajectories in the phase plane have symmetric forms (Figs. 2a). Increasing the voltage of the step excitation, the trajectories in the phase plane shows symmetry breaking for voltages between 21 and 23.22 V. For higher voltages a divergent response develops and the tilting angle increases abruptly until the mirror touches on the substrate. The voltage corresponding to the separatrix on the phase plane (trajectory crossing the saddle node) is called dynamic pull-in voltage, V_{DP}. Frequency spectrum of the response for different voltages (Fig. 2b) reveals the development of the multiply of natural frequency in the response for voltages near dynamic pull-in, which is an indication of the nonlinear oscillation.

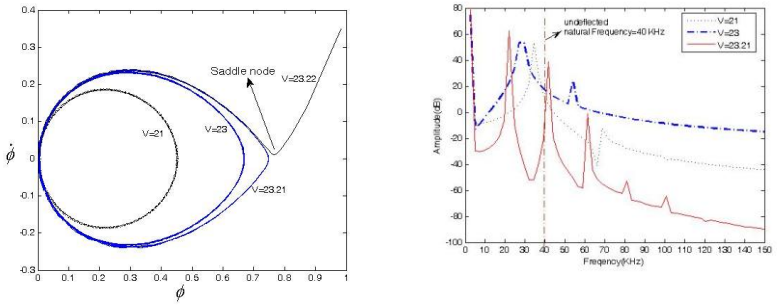

(a) (b)

Figure 2. Symmetry breaking and pull-in conditions in undamped step response of uncoupled model, a) phase plane, b) FFT plot.

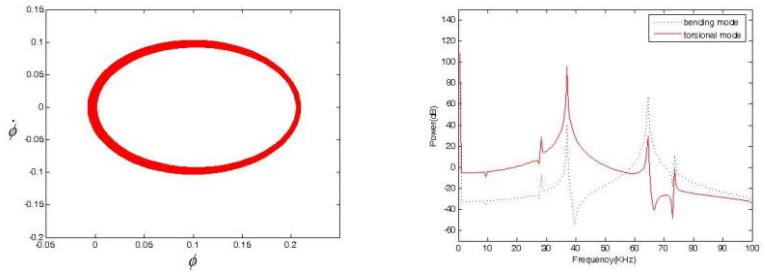

(a) (b)

Figure 3. Undamped response of uncoupled model due to step excitations of 15 volt, a) phase plane, b) FFT plot.

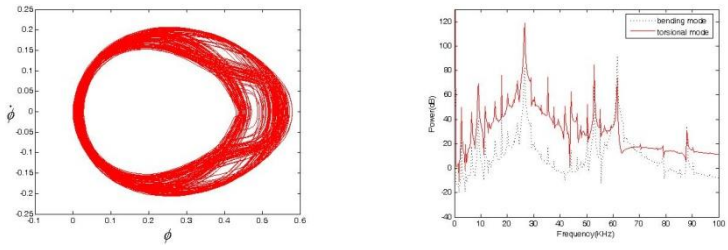

(a) (b)

Fig. 4. Undamped response of coupled model due to step excitations of 19.8 volt, a) phase plane of torsional mode, b) FFT plot of the torsional and bending modes.

Considering the response of coupled undamped model, there is a decrease in the threshold voltage corresponding to the symmetry breaking and at the same time the pull-in voltage decreases from 23.22 to 20 V. Fig. 3 depicts the step response of the coupled undamped model due to 15 V DC step excitation, where in spite of nearly symmetric response, FFT plot of the torsional and flexural responses reveals the emergence of superharmonics (Figs. 3a and 3b). By further increase of the excitation voltage to 19.8 V, in addition to symmetry breaking, there is loss of the periodicity in the response (Fig. 4a, b).

3.2. Harmonic excitation

For harmonic excitations the micro-mirror is excited with an AC voltage superimposed on a DC one. To study the nonlinear behavior, the DC excitation level is set near the pull-in voltage at 16 V.

Figs. 5 and 6 depict the response of the uncoupled model for harmonic excitations. In these simulations the damping ratio is set equal to 0.1 and forcing frequency is one tenth of the system undeflected torsional free vibration frequency. For small values of AC voltage the response is linear and the micro-mirror oscillates with the same frequency as the forcing frequency and ignoring the transient part of the response, the phase portrait has elliptic shape (Fig. 5a). However as AC voltage increases the response losses its symmetry and AC symmetry breaking occurs (Oval shape in Fig. 5b).

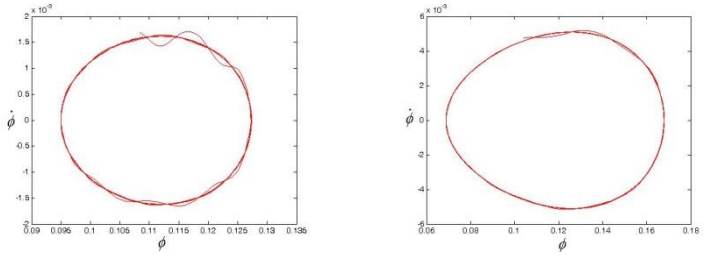

(a) (b)

Figure 5. Damped harmonic response of uncoupled model a)for AC voltage of 1 V, b) for AC voltage of 3 V

By further increase of AC voltage a cascade of period doubling bifurcations appears. Emergence of period doubling is shown in Figs. 6 where the amplitudes of harmonic excitations is 9 V. As discussed in the earlier section, the form of nonlinear excitation in Equation 3 leads to the appearance of different powers of rotational and translational displacements. This explains the appearance of superharmonics in the response.

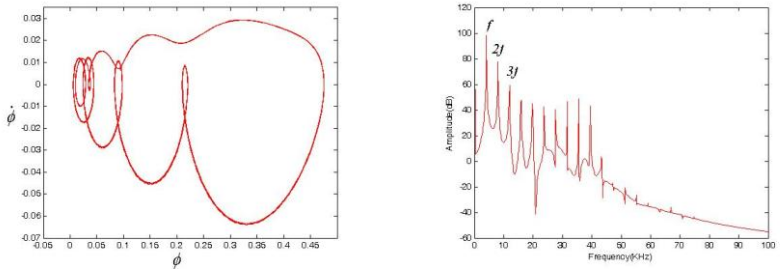

(a) (b)

Figure 6. Damped harmonic response of uncoupled model for AC voltage of 9 V, a) phase plane of torsional deflection, b) FFT plot of torsional deflection.

Increase of AC voltage results in the loss periodicity and appearance of quasi-periodic and chaotic responses. At harmonic excitation amplitude of 9.5 V, some evidence of loss of periodicity emerges and the response becomes quasi-periodic. The phase portrait and Poincare map are shown in Figs.7, which clearly show that the response is quasi-periodic.

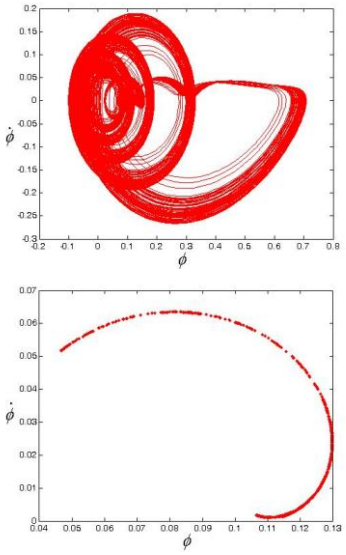

Figure 7. Damped harmonic response of torsional deflection of uncoupled model for AC voltage of 9.5 V, a) phase plane, b) Poincare map.

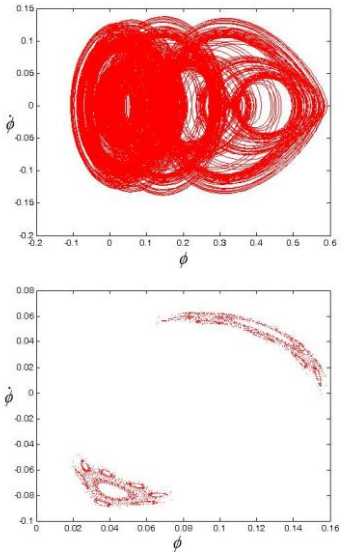

Figure 8. Undamped harmonic response of torsional deflection of uncoupled model for AC voltage of 9.102 V, a) phase plane, b) Poincare map.

Removing the damping from the system, which has a regularizing effect on the response, chaotic response emerges even at lower voltage at about 9.102 V, as is depicted in Fig. 8.
To develop the response of coupled model, again AC voltage superimposed on a DC voltage of 16 V and a damping ratio of 0.1 is used in the simulations. Increasing the AC amplitudes to 1.5 V the symmetry breaking is taking place which is not shown here. Further increase of the AC amplitude to 5 and 5.78 V, increases the number and strength of superharmonics and at the same time the response in the phase plane becomes increasingly complex. By further increasing the amplitude of excitation to 5.93 V, the Poincare map of the torsional response reveals the emergence of the quasi-periodic response, Fig. 9. Similar to the uncoupled case, in the coupled model the presence of the damping has a regularizing effect on the response and removing the damping from model, the quasi periodic response changes to chaotic ones (Fig. 10).

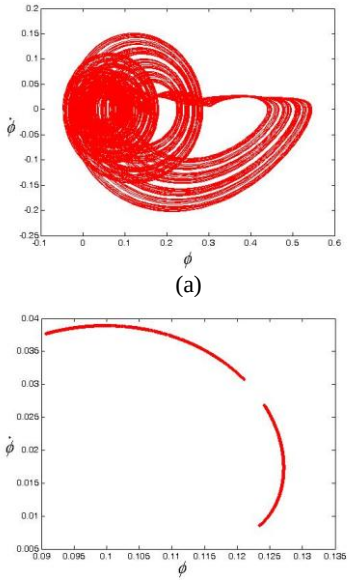

Figure 9. Damped harmonic response of of torsional deflection of coupled model with AC voltage of 5.79 V, a) phase plane, b) Poincare map.

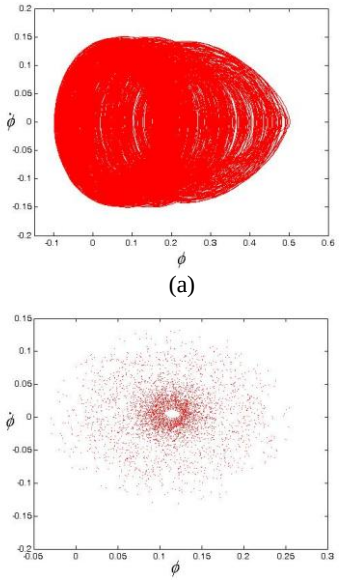

Figure 10. Undamped harmonic response of torsional deflection of coupled model for AC voltage of 4.93 V, a) phase plane, b) Poincare map.

5. Conclusion

Due to the structure of the electrostatic force, it is anticipated that the micro electromechanical systems such as micro-mirrors should have rich nonlinear dynamics near pull-in condition. It was shown that for voltages near pull in condition, DC symmetry breaking in step excitations and AC symmetry breaking in harmonic excitations occurs. Also for wide range of harmonic excitation amplitudes, decomposition of the response to its frequency

components reveals the existence of superharmonics. Further increase of excitation amplitude the response becomes quasi periodic or even chaotic. It is shown that damping regularizing the response turns the chaotic undamped response into quasi-periodic one.

References

1. X.M. Zhang, F.S. Chau, C. Quan, Y.L. Lam, A.Q. Liu, A study of the static characteristics of a torsional micromirror, *Sensors and Actuators A* 90 (2001), 73-81.
2. M. Fischer, M. Giousouf , J. Schaepperle, D. Eichner, M. Weinmann, W. von Munch, F. Assmus, Electrostatically deflectable polysilicon micromirrors– dynamic behaviour and comparison with the results from FEM modeling with ANSYS, *Sensors and Actuators A*, 67, (1998), 89-95.
3. S. Chaterjee, G. Pohit, A large deflection model for the pull-in analysis of electrostatically actuated microcantilever beams, *Journal of Sound and Vibration*, 322, (2009), 969–986.
4. A. Gusso, G.J. Delben, Influence of the Casimir force on the pull-in parameters of silicon based electrostatic torsional actuators, *Sensors and Actuators A* 135 (2007), 792–800.
5. Jian-Gang Guo and Ya-Pu Zhao, Influence of van der Waals and Casimir forces on electrostatic torsional actuators, *Journal of Microelectromechanical Systems*, 13(6), (2004), 1027-1035.
6. Jian-Gang Guo, Ya-Pu Zhao, Dynamic stability of electrostatic torsional actuators with van der Waals effect, *International Journal of Solids and Structures* 43 (2006), 675–685.
7. Jian-Gang Guo, Li-Jun Zhou, Ya-Pu Zhao , Instability analysis of torsional MEMS/NEMS actuators under capillary force, *Journal of Colloid and Interface Science* 331 (2009), 458–462.
8. J.-M. Huang, A.Q. Liu, Z.L. Deng, Q.X. Zhang, J. Ahn, A. Asundi, An approach to the coupling effect between torsion and bending for electrostatic torsional micromirrors, *Sensors and Actuators A* 115, (2004), 159–167.
9. Ghader Rezazadeh, Faraz Khatami, Ahmadali Tahmasebi, Investigation of the torsion and bending effects on static stability of electrostatic torsional micromirrors. *Microsyst Technol* , 13, (2007), 715–722.
10. Faraz Khatami , Ghader Rezazadeh, Dynamic response of a torsional micromirror to electrostatic force and mechanical shock, *Microsyst Technol* (2009) 15:535–545.
11. J.-M. Huang, A.Q. Liu, Z.L. Deng, Q.X. Zhang, A modeling and analysis of spring-shaped torsion micromirrors for low-voltage applications, *International Journal of Mechanical Sciences* 48 (2006) 650–661.

Simulation and Control of Highly Maneuverable Aircraft under Turbulent Atmosphere using Nonlinear Dynamics Inversion Technique

Sunil Sharma, A.K.Ghosh
Indian Institute of Technology Kanpur, Kanpur-208016, India
Email-ID : sunilsharmaiitk@gmail.com

Nomenclature

V	Velocity of flight in body frame
α	Angle of attack
β	Sideslip angle
μ	Velocity vector roll angle
γ	Flight path angle
φ,θ,Ψ	Body axis Roll,Pitch,Yaw angle respectively (Euler angles)
$\Omega=[p,q,r]$	Body axis Roll,Pitch,Yaw rate respectively (Angular velocities)
$\delta_a,\delta_e,\delta_r$	Aileron,Elevator,Rudder deflection respectively
T	Thrust command

Abstract : This paper presents a robust technique to design the flight controllers for the aircraft to fly under turbulent atmosphere as well as to perform maneuvers incorporating the whole highly nonlinear dynamics of the aircraft system.Aircrafts have a number of degrees of freedom (DOF) and so translational as well as rotational motion can be performed by the aircrafts in all those directions of freedom. Aircraft flight controller is required for the aircraft to undergo various flight conditions and to perform various types of maneuvers in a desired and controlled manner. In this study, completely nonlinear set of equations defining whole dynamics of the aircraft have been used for simulation and Nonlinear Dynamics Inversion (NDI) control technique has been used to design the controller of the flight vehicle. NDI control technique is a highly emerging time domain control methodology used to design the controllers for various types of highly nonlinear systems.
Keywords : Nonlinear dynamics inversion (NDI), Aircraft flight controller, Flight envelope.

1. Introduction :

In the field of aerospace vehicles, flight vehicle control law design methods have gained a lot of attention due to advancements in the theoretical concepts as well as exponential improvements in the hardware technologies over past decades. Any sort of flight vehicle designed i.e aircraft,rocket,missile is required to perform its intended task and alongwith that is an essential requirement for the vehicle to perform the task in a well controlled and desired manner and to implement that, there is requirement of a controller which would ensure that the

desired task is done in the controlled manner even if there is sudden turbulence caused by wind gusts. It is extremely important that these vehicles undergo any of the flight condition in a controlled manner. Several attempts have been made to design the controllers for all sort of flight vehicles. There are a number of control techniques to design controllers for nonlinear dynamics systems like aircrafts. In this study, NDI technique is discussed and implemented to design the controller of an aircraft. The advantage of preferring NDI control technique over other linear control methods is that the linear control methods linearize the nonlinear system about the equilibrium points to approximate it into a linear system and then design a control law, In this manner the approximated linearized equations can predict the actual system performance only in a very small flight envelope i.e. in a small range of operations and if the system goes beyond that range then these equations do not simulate the actual behavior of the system and so the linear controllers stay no more effective, whereas the NDI control technique does not linearize the system about any equilibrium point, rather it incorporates all the system nonlinearities while developing the control law and so NDI controllers stay quite efficient over a wide flight envelope.Thus NDI is a very efficient control technique to design controllers for the nonlinear systems.

In the field of control of aerospace vehicles, NDI control technique has gained a lot of attention and it has been applied to many of aircraft applications, such as F-16[1], F-18 HARV [2], F-117 [3] for designing the control law.

2. The Aircraft Model :

The modeled aircraft used in this study is McDonnell Douglas F-4 which is a highly maneuverable fighter aircraft. An attempt has been made to control the various flight conditions of the aircraft using NDI. The aircraft 6 DOF equations of motion are given by the following set of differential equations which explain the translational and rotational dynamics of the aircraft model[4,5].

$$\dot{V} = (f_x \cos\alpha \cos\beta + f_y \sin\beta + f_z \sin\alpha \cos\beta)/m$$

$$\dot{\alpha} = [(f_z \cos\alpha - f_x \sin\alpha)/(mV\cos\beta)] - p\cos\alpha \,\mathrm{Tan}\,\beta + q - r\sin\alpha \,\mathrm{Tan}\,\beta$$

$$\dot{\beta} = \left[\left(f_y \cos\beta - \sin\beta(f_x \cos\alpha + f_z \sin\alpha)\right)/(mV)\right] + p\sin\alpha - r\cos\alpha$$

$$\dot{\Omega} = [I]^{-1}[M - \Omega * ([I]\Omega)]$$

$$\begin{bmatrix}\dot{\varphi}\\ \dot{\theta}\\ \dot{\Psi}\end{bmatrix} = \begin{bmatrix}1 & \mathrm{Tan}_\theta \mathrm{Sin}_\varphi & \mathrm{Tan}_\theta \mathrm{Cos}_\varphi\\ 0 & \mathrm{Cos}_\varphi & -\mathrm{Sin}_\varphi\\ 0 & \mathrm{Sin}_\varphi \mathrm{Sec}_\theta & \mathrm{Cos}_\varphi \mathrm{Sec}_\theta\end{bmatrix}\begin{bmatrix}p\\ q\\ r\end{bmatrix}$$

$$\dot{\mu} = p_w + (q_w \mathrm{Sin}\mu \mathrm{Tan}\gamma) + (r_w \mathrm{Cos}\mu \mathrm{Tan}\gamma)$$

$$\dot{\gamma} = (q_w \mathrm{Cos}\mu) - (r_w \mathrm{Sin}\mu)$$

$$\begin{bmatrix}\dot{x}_e\\ \dot{y}_e\\ \dot{z}_e\end{bmatrix} = C_1(\varphi)C_2(\theta)C_3(\Psi)\begin{bmatrix}V\mathrm{Cos}_\alpha \mathrm{Cos}_\beta\\ V\mathrm{Sin}_\beta\\ V\mathrm{Sin}_\alpha \mathrm{Cos}_\beta\end{bmatrix}$$

where $p_w = (p\mathrm{Cos}\alpha + r\mathrm{Sin}\alpha)(\mathrm{Cos}\beta + \mathrm{Tan}\beta\mathrm{Sin}\beta) + \left(\frac{f_x \sin\alpha - f_z \cos\alpha}{mV}\right)\mathrm{Tan}\beta$

$$q_w = \left(\frac{f_x \sin\alpha - f_z \cos\alpha}{mV}\right)$$

$$r_w = \left[f_y \cos\beta - \sin\beta(f_x \cos\alpha + f_z \sin\alpha)\right]/(mV) \quad \text{--Eq.Set (1)}$$

Here f_x, f_y, f_z represent the net forces along X,Y,Z axes of the aircraft. Matrix [I] represent the moment of inertia matrix and M consists of the rotational moments about X,Y,Z axes of the aircraft and x_e, y_e, z_e represent the spatial position of the aircraft with respect to the earth axis system.

3. NDI Control Law :

In the implementation of NDI control law, the control commands are generated based upon the error signal generated from the desired state and current state received from the sensors via feedback path. In the NDI technique, generally a robust 2-scale separation method is used which allows the order of the controller to be smaller[6,7]. The NDI law used in this study uses time scale separation between slow variables and fast variables and correspondingly generates the control commands. Any aircraft system can be represented by the following nonlinear vector form dynamics equation

$$\dot{x} = f(x) + g(x)u \quad \text{--(2)}$$

x represents the vector representing state variables, $f(x)$ represent nonlinear state dynamic function and $g(x)$ represent the control distribution function.NDI control law inverts the dynamics equation and then replaces the inherent rate of change of state variable by the desired rate of change of that variable to generate the required command which is fed to the system. Inverting eq. (2) we get

$$u = g(x)^{-1}[\dot{x} - f(x)] \quad \text{--(3)}$$

Applying NDI control logic, above equation is converted into a form as

$$u_d = g(x)^{-1}[\dot{x}_d - f(x)] \quad \text{--(4)}$$

where,

$$\dot{x}_d = k(x_d - x) \quad \text{--(5)}$$

x_d in eq.(5) represents the vector consisting of the desired values of state variables and x represents the vector consisting of the measured values of corresponding state variables obtained via feedback path.k represents state gain matrix whose elements are design parameters of the controller and u_d represents the vector consisting of the control commands generated i.e. elevator, aileron, rudder deflections and thrust command which are to be fed to the aircraft system as control input.

4. Applicaton of NDI under various flight conditions :

The purpose of this study is to control the various parameters of the aircraft for different flight conditions like cruise flight, steady sideslip flight, co-ordinated turn, pull-up maneuver, velocity vector roll maneuver etc.

Table 1 shows all the flight conditions studied in this paper and shows the corresponding variables to be controlled in each flight condition so that the flight vehicle performs in the desired manner. For each case, NDI control law is implemented on the concerned set of governing nonlinear equations of the aircraft system and control commands corresponding to the desired states are generated.

Flight conditions	Control variables
Cruise flight	α,β,μ,γ
Steady sideslip flight	α,β,Ψ,γ
Co-ordinated turn	α,β,γ,Ψ̇
Pull-up maneuver	p,q,r,V
Velocity vector roll maneuver	α,β,γ,μ̇

Table 1.Various flight conditions and corresponding control variables

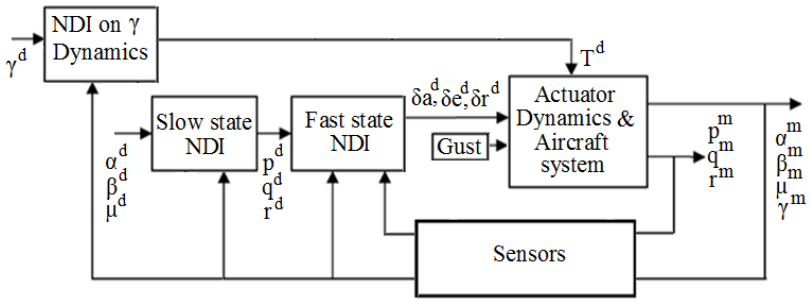

Figure1. NDI control approach for control variables α,β,μ,γ.

Figure1 explains the implementation of NDI control law for the cases in which control variables are α,β,μ,γ.The desired states are represented by(α^d,β^d,μ^d, γ^d). Similarly other variables can be controlled in the similar fashion for other cases. In present case, (α,β,μ,γ) act as slow state variables whereas (p,q,r) act as fast state variables.NDI is applied on slow state variables as well as fast state variables as explained in equations (2)-(5) and control surfaces deflection commands (δ_a^d,δ_e^d,δ_r^d) are generated. These command values are passed through the actuator dynamics system so as to ensure that the commands generated are well within the control surfaces deflection limits as well as within the maximum rate of deflection of control surfaces.Thrust command (T^d) is generated by applying NDI on γ dynamics equation in case of various flight conditions except pull-up and pull-down maneuvers as in these maneuvers, the thrust command is generated by applying NDI on dynamics equation of velocity.

5. Simulation, Control and Results :

The 6 DOF equations of motion of the aircraft explain its translational and rotational dynamics.The equations were simulated using numerical method Runge kutta-4 (RK-4) algorithm.For simulation,completely nonlinear set of aerodynamic data of McDonnell Douglas F-4 aircraft has been used [8].Results have been shown for different flight conditions as following.

Note : For all the following figures,the values of all the angles are in degrees, distances are in meters, time is in seconds, angular velocities (p,q,r) are in radian/sec, velocities are in meter/sec and acceleration is in meter/sec^2.

Case 1. **Cruise flight control under effect of wind gusts :**
In this case, Cruise flight is controlled under turbulent atmosphere as sudden gust comes and aircraft trim condition is disturbed and the controller has to control the aircraft and bring it back to the trim condition. As shown in figure 2, Aircraft is cruising at α= 4 deg and a sudden gust comes to disturb the trim condition of the aircraft and the controller acts to bring the aircraft back to the trim condition.

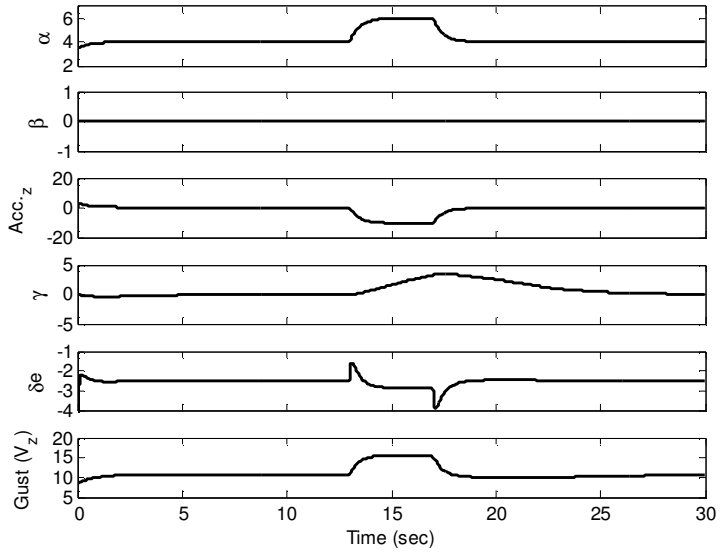

Figure 2. Cruise flight control under turbulent atmosphere

Case 2. **Steady sideslip flight under effect of wind gusts :**
In this case, aircraft is undergoing steady sideslip flight and suddenly a wind gust is introduced to disturb the aircraft states and the controller has to control and bring the aircraft states back to the desired values. As shown in figure 3, aircraft is flying at α = 4 deg, β = 2 deg and the aircraft is holding Ψ= -2 deg for proper steady sideslip and then a sudden gust is introduced but the aircraft controller still performs in the desired manner.

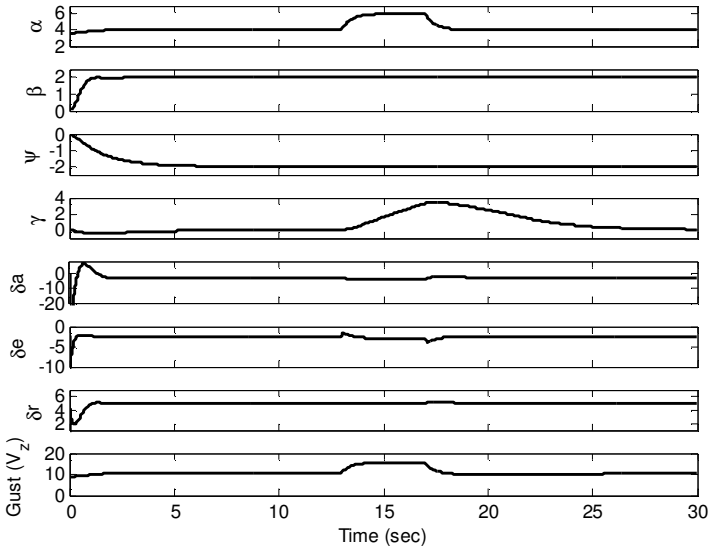

Figure 3. Steady sideslip flight control under turbulent atmosphere

Case 3. Steady co-ordinated turn :

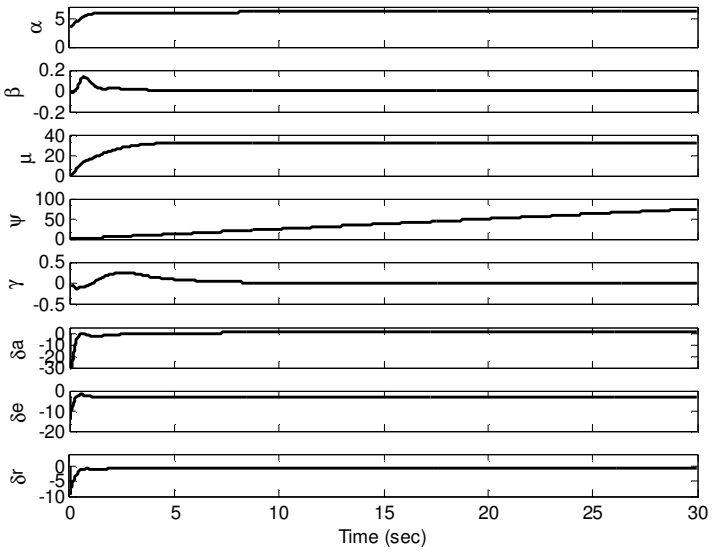

Figure 4. Aircraft states and control commands for co-ordinated turn

In case 3 as explained by figure 4, the aircraft has to undergo steady co-ordinated turn i.e. the sideslip angle should be zero during the turn. Here in this case, aircraft is turning at the rate of change of Ψ as 2.5 deg/sec at α= 6 deg.

Case 4. Pull-up maneuver :

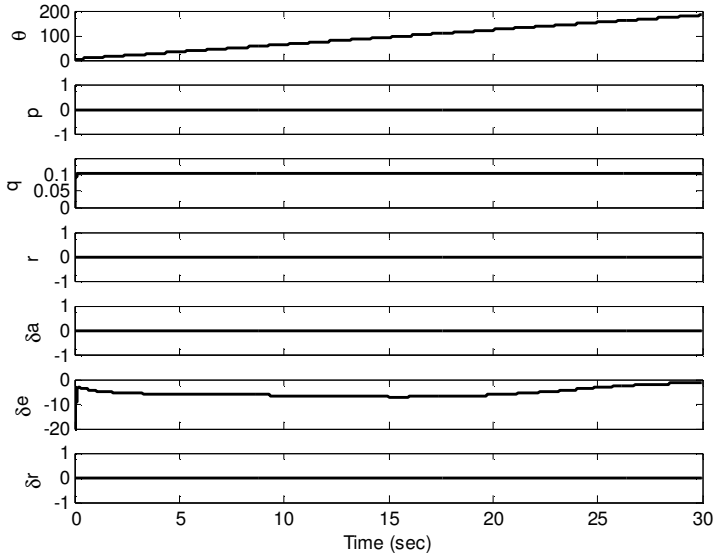

Figure 5(a). Aircraft states and control commands for pull-up maneuver

In this case, aircraft performs a continuous pull-up maneuver in vertical XZ plane. In this case, maneuver is done at pitch rate of 0.1 rad/sec as shown by figure 5(a). Figure 5(b) shows the trajectory in XZ plane during this flight condition.

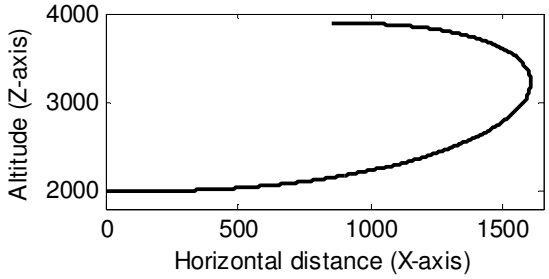

Figure 5(b). Aircraft trajectory in XZ plane during pull-up maneuver

Case 5. Velocity vector roll maneuver :
Aircraft performs a continuous roll maneuver about the velocity axis at high α. During it aircraft should not lose altitude. In this case, aircraft performs this maneuver at α=12 deg as shown in fig. 6.

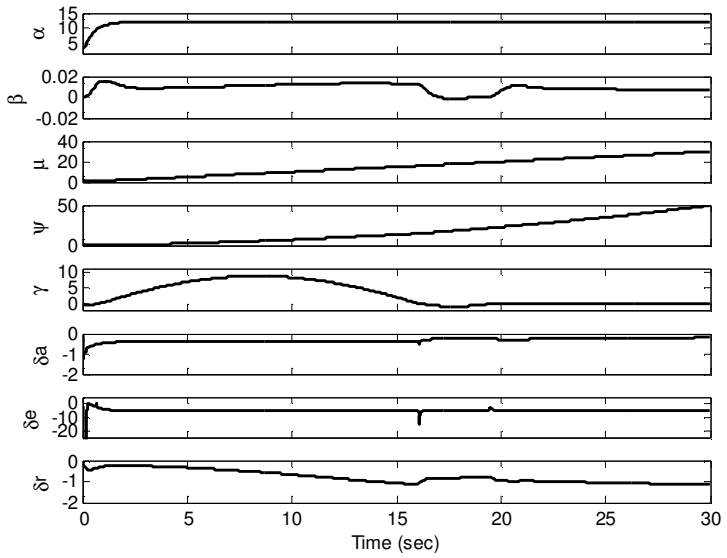

Figure 6. Velocity vector roll maneuver at α =12 degree

6. References :

1. Adams, R. J. ,Banda, S. S."Robust Flight Control Design Using Dynamic Inversion and Structured Singular Value Synthesis," IEEE Transactions on control systems technology,Vol.1,No. 2, NewYork,June 1993,pp 80-92.
2. Bugaski, D. J., Enns, D. F., and Elgersma, M. R., "A Dynamic Inversion Based Control with Application to the F-18 HARV," AIAA Paper 90-3407, Proceedings of the AIAA Guidance, Navigation, and Control Conference, Portland, OR, 1990, pp. 826-839.
3. Colgren, R., and Enns, D., "Dynamic Inversion Applied to the F-117A," AIAA Paper 97-3786, 1997.
4. Flight stability and automatic control,2nd edition,Robert C Nelson,Tata Mcgraw Hill.
5. Benjamin R. Carter, Time-optimization of high performance combat maneuvers-2005,Naval postgraduate school, Monterey,California
6. S. A. Snell, D. F. Enns, and W. L. Garrard Jr., "Nonlinear Inversion Flight Control for a Supermaneuverable Aircraft," Journal of Guidance, Control, and Dynamics, Vol. 15, No. 4, AIAA, 1992, pp. 976-984.
7. J. Reiner, G.J. Balas, W.J. Garrard, Flight control design using robust dynamic inversion and time-scale separation, Automatica 32 (11) (1996)1493–1504.
8. A Collection of Nonlinear Aircraft Simulations in MATLAB, NASA/TM-2003-212145.

Design of the software process model in accordance with standard of the chaos model

Narjes Shojaati[1] - Naser Nematbakhsh[2]

[1]Computer department
Isfahan University
Isfahan,Iran
E-mail:n.shojaati@eng.ui.ac.ir
[2]Computer department
Isfahan University
Isfahan,Iran
E-mail: nemat@eng.ui.ac.ir

Abstract: Software engineering is known as a problem solving activity and modeling. All the principles in software engineering are emphasized on the conditions for software producers are unpredictable because of the interactions and mutual relationships between all the factors involved in creating and those conditions never allow full control over this process. Since the emergence of software engineering processes, models and processes focus on reducing non-forecasting in the process model due to provide available software in a certain period with predicted cost, but it cannot be out of this complexity, and the simplicity would not lead by imposing a simple model to process model. The aim of this paper is design of a software process based on chaos theory.
In this article, software production process assumed as a nonlinear dynamic process, and hence it is located in the ordination complex systems. It would continue with using chaos techniques to analyze software production process and fractal structure of process models is presented.In particular, preparation of a model based on chaos theory can show close relationships between many of the facts contained in software development and reflect complex patterns that occur during the project, with a help of flexible and variable fractal structure.
Keywords: Software engineering, Chaos theory, Process model, Fractal , Problem

1. Introduction

The linear loop is not complete with solving a software problem. The complexity of software development causes chaos in project. Development is a continuum from the whole project down to each line of code and involves both human and technical issues on all levels[3].
Developers need to describe the structure between different parts of a software development process. They wants a flexible structure which reflects the intricate patterns that occur in real projects.
The problem definition can be very different such as a new program for solving an application or use the latest technology, or port a program to a new platform. Some of them are simple and some of them are complex.
During problem definition, developers choose a problem to solve it. The problem definition needs the ability of people to describe their problems and

solution-integration need the ability of development to find a solution. Developers must decide where the system should be in five and ten years[3].
Software project manager expects exact estimated processes. So clearly we need to improve the estimates and measurements in software engineering. However, so far few attempts form to identify and apply exactly the appropriate approach to software systems, while this action could influence in software costs.

2. Nonlinearity in software engineering

The study of nonlinear dynamical systems is called nonlinear science. Nonlinearity in software engineering is the rule rather than the exception. For a linear system, we can combine two solutions, and the result is also a solution for the system. The above property is called linearity, and it makes the linear systems mathematically tractable.
This is not true for nonlinear systems such as the process model . We cannot break up a software problem into little pieces, solve each piece separately and put them back together to make the complete solution.
Many nonlinear systems such as the process model are approximately linear for small perturbations about points of equilibrium, and if we consider that problems are linear, then we can solve all of them. In the other hand Nonlinear problems are seldom exactly solvable. Before the advent of computers, almost nothing could be said about the behavior of nonlinear systems.

3. Chaos in the process model

Before answering to the question of the applicability of chaos in software engineering, we must define the concept. How is chaos theory used exactly in software engineering? According to one definition of chaos, "Chaos theory is the qualitative study of unstable aperiodic behavior in deterministic nonlinear dynamical systems."[2] ,so with this definition, we can find the characteristics of chaos in software engineering.
First, that the system is dynamical, means that it changes over time. The software project scheduler are very fragile and sometimes the most pressure is applied to project staff.
Second, that the behavior of the system is aperiodic and unstable means that it does not repeat itself. Software industry was faced with the fact that the estimates do not have enough precision. None estimated models is generally superior than other models and experimental results are often contradictory in software engineering.
Third, although the chaotic behavior is complex, it can have simple causes.
Many software development organizations do not have real data about software costs, and more estimates are made by inadequate descriptions of user requirements.
Fourth, because the system is nonlinear, it is sensitive to initial conditions. The output of the software development process is not proportional to the input and the process model does not conform to the principle of additivity. The structure of a simple problem is different from the structure of a more complex problem.

In general, we cannot break complex problems into simpler sub problems. In the other word in software complex problem the whole is not equal to the sum of its parts. So cannot use this reductionist approach to deal with problems.
The software development has a partial decision-making problem, and risk assessment is difficult. All this shows the non-linear features in software engineering.
Fifth, because of the instability, aperiodicity, and sensitivity to initial conditions, the behavior of chaotic systems is not predictable even though it is deterministic.
Common software development process is a sequence of decision problems that attempts to convert a fuzzy set of expectations to requirements, specification, design and ultimately code and documentation. So it is not predictable, too. Even though it is deterministic.
A final feature of chaos, although not included in the above definition, is that of iteration or feedback, in which the output of the system is used as the input in the next calculation.
Usual cascade approach has been rejected in creating software to achieve its goals, because it is a method for resident and almost unchanged problems. This assumption is far from reality.

4. Fractal process model

For at least 200 years, the branch of mathematics , known as Analysis, is not only the richest of all the branches, but also by far the most useful for applications to quantitative science, from physics to engineering. Theoretical scientists became applied mathematicians. Software project manager expects exact estimated processes. So clearly we need to improve the estimates and measurements in software engineering.
Integrals, differential equations, series' expansions, integral representations of special functions are the tools that calculus has provided and that are capable of solving an amazing variety of problems in all areas of quantitative knowledge.
however,The mathematicians were telling us all along that smooth curves were the exception, not the rule[4].
Analysis is not the appropriate approach to software systems and chaos theory solves a wide variety of scientific and engineering problems, which do not respond to calculus.
The software development process provides a structure for problem solving. Common approach is suitable for simple problems, but it cannot solve any complex problem in software engineering.
To add the necessary complexity, the process model can combines with itself. Sequential design and parallel design are common mode.
Sequential design means the end of one complete problem solving cycle with the start of another. Parallel design is identified by many instances of start state, in other words problem solvers can solve problems in parallel[1],but none of them describe full connection between whole of a development beginning from problem definition until coding.

Fractal design structures are self-similar. It is chaos in space and fractal shows chaotic in space. There are many possible definitions of the word fractal. A very loose and general definition is this: a fractal is a geometric figure that does not become simpler when you analyze it into smaller and smaller parts. Which implies, of course, that it is not smooth. However, simple examples of fractals have been known to mathematicians for a long time[4].
Process model that is drawn in fractal mode, meaning that they do not become simpler when you examine them with an increasingly powerful microscope. Fractal design in the process model actually has a high degree of self-similarity when examined on finer scales.
As we said, the process model is a dynamical system because it is capable of changing with time. The process model such as a dynamical system consists of some "variables" and some "equations of motion" or "dynamical equations".
Developer can find variables in the process model. There are any things, which can vary with time. In other words, two similar process model with the same values of all the variables are in identical configurations now, and will evolve identically.
Time-chaos in the process model is the rule rather than the exception. The connection between time-chaos and space-chaos is very close.
We let time flow in process model base on chaos. As each area of the process model follows its trajectory, the process model itself moves and changes shape. During its evolution, slowly but surely the region will turn into a fractal. The fractal builds up as time progresses and becomes complete with an infinite time.

5. Conclusion

Chaos Theory solves a wide variety of engineering problems, which do not respond to calculus. Problem and the solution is thought as a component of the process model. Software problem cannot be broken up into little pieces and solved separately. They have to be dealt with in their full complexity. Chaos in the process model is the rule rather than the exception. To add the necessary complexity, we introduced fractal design in the process model.That was no reason for the lack of interest in these chaotic-looking phenomena at software engineering after known the fractal process model.

References

[1] J. G. Hall , and L. Rapanotti , Assurance-driven design in problem oriented engineering., *International Journal on Advances in Systems and Measurements*, 2(1), October, 2009.
[2] Jr.Vicente Valle, Chaos, Complexity and Deterrence, *National War College*, April, 2000.
[3] L. B. S. Raccoon . The chaos model and the chaos life cycle, *ACM SIGSOFT Software Engineering Notes, Volume 20, Number 1, Pages 55 to 66*, January 1995.
[4] M. Baranger, Chaos, Complexity, and Entropy A physics talk for non-physicists ,*Center for Theoretical Physics, Laboratory for Nuclear Science and Department of Physics, USA*,1997.

Proven complex dynamics of software engineering

Narjes Shojaati[1] - Naser Nematbakhsh[2]

[1]Computer department
Isfahan University
Isfahan,Iran
E-mail: n.shojaati@eng.ui.ac.ir
[2]Computer department
Isfahan University
Isfahan,Iran
E-mail: nemat@eng.ui.ac.ir

Abstract: Before making effort to analyze systems, we should identify the exact type of system and determine that we consider our system in which categories of systems. Rapid changes in technology are created the double problems in the field of planning and organizing the structure of manufacturing software engineering projects. Detailed industry estimates is impractical for preparing a software application. In such an environment, a new way of thinking is required.
Introduction of complex systems is discussed here as alternatives to plan and deal with these changes. Order in complex systems is not because a targeted behavior of the system elements or influence a central organization management. Regular patterns in this system are an example of Self-Organized. In this article, software engineering is proven as a nonlinear complex system and continues to review the components and features Self-Organized in software engineering.After demonstrating the software production process among the complex systems, we can use complexity theory and techniques relating to building complex systems for more accurate understanding of the process and prevented impact of inappropriate nonlinear to cost, function, relationship and program features.
Keywords: Software engineering, Complex system, Dynamic, Self-Organized Criticality, Process model, Life cycle.

1. Introduction

Patterns in complex systems are because communication between factor based on law on the very small levels of the system. These rules – adapt – under the influence of the experience and the learning abilities of the actors constituting the system [2] and alter the system characteristics as a consequence of development in the structure of complex systems. In other words, how can a regional map of the Earth, that is constantly changing, be useful? It should be noted, rejection long-term strategic plans do not mean rejection managing in a project. This is a common event in complex environments, and it is unpredictable. A large number of academics are engaged in research in complexity theory to help decision makers to improve its project management methods.
If we can prove that a system is nondeterministic nonlinear dynamic system, then this system will be complex. Linear systems are not complex. These systems have a set of very tight and stable rules and cannot adapt to the

environment. A complex system is a fully functional system that includes variable and dependent components. Unlike a perfectly regular linear system, components of a complex system do not have precisely defined communication ,or constant behavior or values and is not possible to explain the behavior of these components as well as conventional methods in linear systems. We cannot predict what happens in complex systems, but when it occurs, it is easy to identify patterns that system is based on. [8]
If we can consider the software development process as a complex system, then complexity theory and its quantitative techniques help us understand those processes and access to more accurate estimates.
In the article [7] the first stone is laid in the presence of chaos in software engineering.
Raccoon considers the presence of chaos in the production process and the software life cycle.
However, in [7] and also [5 , 6] are presented only theoretical matters and has not used the exact characteristics of chaos systems to prove this claim.

2. Complexity in Software Engineering

In 1994, as Gibbs said, despite 50 years experience in programming, the software industry is behind for years _perhaps decades _ from the needed rules to achieve the engineering requirements in the information age society.
Although software systems are faced extensive, but still production and development of software use the basic structure in software engineering. This has led researchers are using different approaches in dealing with the problem. Among them can be pointed to tools, methodology, the prototype and varies software processes.Inability to choose the exact way to solve software problems, indicating that Gibbs` opinion is still correct.
Demonstrating the complex dynamics in software engineering can be used from complexity theory and quantitative techniques related to complex systems for more accurate understanding of this area and prevented from the nonlinear inappropriate influence on cost and performance.
However, some of the articles are used characteristics of complex systems to identify such systems, but rules are stronger to correct identification of complex systems.
This article will continue to introduce and review the six major law of complex systems[1] in software engineering.

1-Complex systems contain many constituents interacting nonlinearly.
Nonlinearity is a necessary condition for complexity, and that almost all nonlinear systems whose phase space has three or more dimensions are chaotic in at least a part of that phase space. This does not mean that all chaotic systems are complex. Chaotic does happen with very few constituents; complexity does not.
Common software development process is a sequence of decision problems that attempts to convert a fuzzy set of expectations to be requirements, specification,

design and ultimately code and documentation.
Usual cascade approach was rejected to achieve its goals in creating software, because it is a method for resident and almost unchanged problems. This assumption is far from reality. Today, that process of modern software is based on creating a sample basis. These approaches indicate the fact that software development has a partial decision-making problem, and its risk assessment is difficult. This shows the non-linear features in software engineering.

2-The constituents of a complex system are interdependent.
Here is an example of interdependence. Remove a part of a system with non-complex components does not cause many difficult on the result. However, complex system does not allow us to do this, because of numerous communication between components.
Different systems in software engineering are placed together and occur the wide information flow between them. Many of these systems cannot be considered independent of the others, and if we removed the information flow, then data redundancy will grow with the system. Software engineering is therefore, including components with numerous dependence.

3- A complex system possesses a structure spanning several scales.
In this case, we can consider the human body as a complex system and its scale such as different organs and cells and bone .
Modeling a system starts with an initial process in software engineering. DFD that performing it, is called context diagram. This chart displays the whole input and output of a system. This chart can be seen all the foreign entities that interact with the system and data flow between these entities and the system.
The next level is identified that the main system process and high-level DFD are drawn. The DFD can be detailed to make the process, as well as they continue to display more details of the system in the lower levels.
The same structure of complex systems with different scales lead to one of the basic and new features of complex system , and it is the fourth feature.

4- A complex system is capable of emerging behavior.
Emergence happens when you switch the focus of attention from one scale to the coarser scale above it. A certain behavior, observed at a certain scale, is said to be emergent if it cannot be understood when you study, separately and one by one, every constituent of this scale, each of which may also be a complex system made up of finer scales. Thus the emerging behavior is a new phenomenon special to the scale considered, and it results from global interactions between the scale's constituents.
These features have been seen in use case related to software engineering. As the level to look into a process model, database and network can make new results that were different from the other levels. By combining similar or shared but incomplete low-level DFD operation can be understood major operation of systems. It is an example of this property in software engineering.

The combination of structure and emergence leads to the self-organization, which is what happens when an emerging behavior has the effect of changing the structure or creating a new structure. More detail about this property is discussed.

5- Complexity involves an interplay between chaos and non-chaos.
Many people have suggested that complexity occurs "at the edge of chaos", but no one has been able to make this totally clear. It is like a critical point in phase transitions. It is the point where the long-range correlations are most important. Perhaps complex systems manage to modify their environment to operate as much as possible at this edge-of-chaos place, which would also be the place where the self-organization is most likely to occur. It makes sense to expect the self-organization to happen when there are strong long-range correlations.
Use of parallel different processes is a way to obtain the best solutions in software environments.
Although some of these solutions will lead to fail, but some of them are very successful. This is a very effective method for developing software systems.
In this case, the software system is located in conditions between the full order - where flexibility of the system is limited and the ability is zero to identify and change to the new situation - and chaos - where the minimum structure exists in the system-.
Finally, there is one more property of complex systems that concerns all of us very closely, which makes it, especially interesting. In order to evolve and stay alive, in order to remain complex, all the complex systems need to obey the following rule:

6- Complexity involves an interplay between cooperation and competition.
Once again, this is an interplay between scales. The usual situation is that the competition on the scale n is nourished by cooperation on the finer scale below it (scale n+1).
This property can be easily seen in subsystems that designed for the original software system.
Although these subsystems are in a competitive mode, But at higher levels, they followed access to the main target.
Self-organization occurs when the emergence behavior leads to change the structure or create a new structure. Self-Organized Critically is the most important shared characteristics of complex systems.

3.Self-Organized Critically components in software engineering

Self-organization occurs when the emergence behavior leads to change the structure or create a new structure. Self-Organized Critically is the most important shared characteristics of complex systems. Table 1 shows components and their definition in software Engineering.

Table 1：Self-Organized Critically components and their definition in software engineering

SOC components	description
Power law and critical point	Size and structure distribution of the project. The critical point in the project is acceptance of the changes periodically.
Driving force	Changed on user requirements and demands Technology change Staff change Identify and create new solutions
Thresholds	Identified and predicted range of projects, Basic definitions of the project and Initial specified rules
Cascades	Change in a phase of the project and extend it to other parts

4. General characteristics of Self-Organized Critically in Software Engineering

SOC is the only known mechanism to produce the overall complexity. We show the most important characteristics of this mechanism in the software development process.

1-Relationship:
Components have more than one input and output on average. The perceived requirement starts creating problems for the software development process and software development process create different output with a software approach to solving these problems.

2-The converting status:
Approximately, it is equal to one. Increasing requirements cause to define problems that the reach of these problems led to a unique solution. A direct relationship is created between the numbers of problems and solutions by the software development process.

3-Learning ability:
Components have the learning ability from past experiences. Software development process can be given past experiences and create the optimal solution.

4-Parallel operation:

Components work parallel. These components exist to solve a problem or several problems. That is easily understandable to explain the software development process to solve problems in a parallel mode so it causes to improve speed and create the high adaptation ability.

5- change the interaction:
Components are able to change other components that interact with them. This change can be permanent or temporary. Problem and the solution is thought as a component of the relationship into the software development process, that could be causing transformations in each other.
At first, the problems are transferred into a series of solutions, but at validation phase, the definition of the problems may be revise. Assume a fixed environment is too restrictive for high-speed scenarios.
In software engineering are constantly changing the customer expectations and competitors`ability. Products will be assessed faster than expected and if they are unsuitable, they removed easily. There are some new means such as information technology, internet and global economy that help to shape this phenomenon.

6-feedback loops:
Outputs are returned to begin of the process in the feedback loop. The actual results of this operation will make the process correction. Creating positive feedback loops was discussed in the process model from years ago. It was more important when observed that adding manpower to backward project would cause the more delayed.
The presence of feedback loops can be seen in each stage of the software development process to redefine the problem or the solution. This feedback loop has a significant impact on performance of system.

7- Ability to Control:
There are many variables in the software problems and its solutions in the software development process. They cause to make requirement definition and convert it to the problem and the useable metric. The specific area is defined the overall image from the implementation process.
All variables must be controlled. However, controls should not cause to be changed, simply it keeps the system in the defined scope.

8-Attracted areas:
There are different ways to achieve an acceptable response in the software development process, so it shows creative freedom.
There are several problems, all of which eventually reach a specific solution that meets the system requirement. All of them show flexibility in the production process.

9-External borders:

Complete exact boundary is not imaginable between the problems creating and requirements and also offering solutions and product [3]. System boundaries are not completely closed and not completely open.

10- Performance:
The overall goal is construction of problem solving in the software development process. Even so, each one of problem solving has own means. Performance goals can be multiple. It will give a multi-dimensional aspect to the system.

11-Building blocks:
Problem and solution are clearly two-block in the software development process, but there are many other blocks such as problems assessment and evaluation with different aspects [4].
Subsystems could exist in different dimensions that make a fractal structure of the system.

12-The dominant properties:
You can consider a certain mode of the finding the problem and solve it for software development process with progress in the larger dimensions of time. Although this property is understandable in small size, but connected between components looks organized in the dimension broader.

13-Stability of the system:
Changed in requirements and existing technologies and creating the new solution cause unexpected side effects in the software development process over the time.
However, some of these conversions overturn into the software development process, but a group of them has a considerable impact on the problem definition and production process.

14-Decentralized control:
Centralized management and control is not in one part of the process. Each component requires separate management. Problem and solutions manage in the own area, although this does not cause to change the interactions between components.

15-Information flow:
Information and data flow exist increasingly in the software process that is from problem to the solution and vice versa.
The steady information flow changes the system mode from linear and definitive to nonlinear.

5. Conclusion

Attempt to estimate project schedule or activities terminate a series of partial non-exact estimates without regard to the type of software engineering dynamic. Clearly, the need is felt to improve the estimates and measurements in software engineering.
However, few effort assisted to identify exact systems in software engineering. In this article complex system was introduced as the best solution for complying with plenty of changes in software engineering.Software engineering and its scope is proven among the complex systems, so its rules can identify reliably direction to a useful software, and it causes a better understanding of problems and the factors that will lead the software engineering to create optimized software rather early move toward solutions.There are no fears of a complex nuclear in the software scope, direction to having paved reliable software.It is also an effective method to achieve competitive advantages in software engineering so software engineers find the superiority of information on software projects by using the complex theory.

References

[1] M. Baranger, Chaos, Complexity, and Entropy A physics talk for non-physicists ,*Center for Theoretical Physics, Laboratory for Nuclear Science and Department of Physics*, USA,1997.
[2] J.H. Holland , hidden order, how adaptation builds complexity, *Perseus Books,* Cambridge, Massachusetts. 1995.
[3] B. Kitchenham, The certainty of uncertainty. FESMA,1998.
[4] P. Kokol , R.Crespo, and A. Cardoso, Assessing software structure by entropy and information density, *ACM SIGSOFT Software Engineering Notes. Volume 29, Number 2*, March 2004.
[5] L. B. S.Raccoon , The chaos strategy, *ACM SIGSOFT Software Engineering Notes, Volume 20, Number 5*, December 1995, Pages 40 to 47.
[6] L. B. S. Raccoon. The complexity gap, *ACM SIGSOFT Software Engineering Notes, Volume 20, Number* 3, July 1995.
[7] L. B. S. Raccoon . The chaos model and the chaos life cycle, *ACM SIGSOFT Software Engineering Notes, Volume 20, Number 1*, January 1995.
[8] W. B. Rouse , Complex Engineered, Organizational and Natural Systems. *Wiley InterScience, Systems Engineering, Volume. 10, Number. 3*, 2007.

Proceedings, 4th Chaotic Modeling and Simulation International Conference
31 May – 3 June 2011, Agios Nikolaos, Crete Greece

About Principles of creating of the structured particles mechanics

Vyacheslav M. Somsikov
Institute of ionosphere, Alma-Ata, 480020, Kazakhstan
E-mail: vmsoms@rambler.ru

Abstract. The principles of creation of the mechanics of structured particles are considered. The explanation how this mechanics leads to the account of dissipative forces is offered. The explanation of a motion equation for the system consisting from the potentially interacting material points is submitted. It is discussed why the motions of the system determine by two type of symmetry: symmetry of the system and symmetry of space and how it leads to two types of energy and forces accordingly. It is shown how the mechanics of the structured particles leads to thermodynamics, statistical physics and kinetics.

Keywords: **Dynamics, irreversibility, Hamilton formalism, classical mechanics, entropy.**

Introduction. The Newton's motion equation is gained on the basis of the model bodies in the form of the material points (MP) and solid bodies. Such idealization of models of real bodies leads us to the second law of Newton. According to this law, the acceleration of MP is proportional to the potential force which acts on it [1, 2]. The work of this force is equal to their integral along the way. The energy conservation law of MP from here follows. In connection with this law the dynamics of MP is determined by two types of energy: the kinetic energy and potential energy. Along trajectory of MP the sum of these types of energy is constant. The MP motion is reversible. It is follows from the Newton's second law and potentiality of forces.

All bodies in the nature have a structure. Therefore they have the internal energy which is caused by relative motion of the body's elements. Therefore the works of the external forces change not only the body's motion energy but the internal energy also. However the Newton's motion equation, which has been constructed on the basis of models of structureless bodies, does not include the terms responsible for the change an internal energy. In practice they are taken into account by addition to the Newton's motion equation of the empirical force of a friction.

The work of the frictional forces defines the dissipative part of motion energy which goes to the body's internal energy and dissipated in the environment [2]. The friction coefficient is taken from the experiment. Thus, the rigorous description of the dynamics of bodies in the frame of classical mechanics is absent. It is due to the simplification of the bodies models. Therefore **for description of a motion of real bodies, the MP should be replaced on a structural particle and the motion equation for the structural particles should be obtained**.

The great diversity of structures does not allow analyzing all types of energy dissipation. But we can select such relatively simple models that allow understanding the nature of dissipation in the framework of the laws of classical mechanics. It is a system of potentially interacting material points.

The problem of description of the dissipative forces in the frame of the classical mechanics is similar to the problem of irreversibility. This problem was formulated by Boltzmann. All attempts to solve it without the use of statistical laws were till now unsuccessful. The generally accepted explanations of the irreversibility of today are based on probabilistic laws contradicting the determinism of classical mechanics [3]. Nevertheless, the explanation of irreversibility without attraction of probabilistically laws, if particles possess by the structure, can be offered [4, 5].

To find an approach to solving the irreversibility problem in the framework of the laws of classical mechanics we studied in the beginning the dynamics of hard disks. As a result, it was found that the system, consisting of two interacting of disks subsystems, moves to equilibrium [4]. It has been shown that this is due to the transformation of energy of relative motion of subsystems into the motion energy of disks relative to the centre of masses (**CM**) of the corresponding subsystem. The same mechanism of equilibration takes place for the structured particles (**SP**) where *SP is equilibrium system consisting from a big enough number of potentially interacting MP*.

Mechanic of SP can be constructed at following restrictions [6]: 1). Everyone MP is belonging to its SP during all process. 2). SP is in equilibrium during all time. The first restriction eliminates inessential complications related to the necessity to reconsider of SP structure due to transitions MP between them. The second restriction is equivalent to the requirement of weak interacting which accepted in thermodynamics.

The aim of this paper is to show how the mechanics of SP can be constructed on the bases of a Newton's laws for MP. For this purpose the nature of the restrictions of classical mechanics is analyzed. The explanation of the necessity of the systems dynamics description on the basis of two types of symmetry: the symmetry of the system and the symmetry of the space are submitted. How from SP mechanics to come to thermodynamics, statistical physics and kinetics and how to introduce the concept of entropy into the classic mechanics are explained.

THE SYSTEM OF TWO MP. The basic principles for construct of the SP mechanics as well as the method of its construction can be illustrated on the example of system of two MP. The task of two MP is solved by transition to a coordinate system of CM [7]. In this case, the variables are separated. The nature of such separation of variables is connected with the emergence of a new quality of a system that is absent for MP. It is internal energy caused by the relative motions of system elements. The energy of two MP in laboratory coordinates of system (**LS**) has the form:

$$E = m(v_1^2 + v_2^2)/2 + U(r_{12}) + U^{env}(r_1) + U^{env}(r_2) = const\,, \qquad (1)$$

where $U(r_{12})$ is a potential energy of MP interaction; $U^{env}(r_1), U^{env}(r_2)$ are potential energies for MP in an external field of forces; r_1, r_2 -coordinates of MP; $r_{12}=(r_1-r_2)$, v_1, v_2 are the velocities of MP.

The motion of each MP is caused by two independent types of forces: forces of interaction MP and external forces. In the LS coordinate system the task is nonlinear because the motion of one MP depends from the motion of the other MP. Thus in the LS coordinates of system the MP motion are interdependent. Therefore the LS system is unacceptable for the description of dynamics of system. New variables are set as follows: $R_2=(r_1+r_2)/2$, $V_2=\dot{R}_2$ are coordinates and velocities for CM, $v_{12}=\dot{r}_{12}$. In these variables the system's energy is:

$$E=\{MV_2^2/2\}+\{mv_{12}^2/4+U(r_{12})\}+U^{env}(R_2,r_{12}) \quad (2)$$

Here $MV_2^2/2$ is a kinetic energy of CM system's motion. The energy $mv_{12}^2/4+U(r_{12})$ is a *internal energy* of system determined by forces of interaction MP and their relative motion; $v_{12}=\dot{r}_{12}$; $U^{env}(R_2,r_{12})$-is a potential energy of system in an external field. $M=2m$. Differentiating the energy (2) with respect to time, we get:

$$MV_2\dot{V}_2+mv_{12}\dot{v}_{12}/2+F_{12}v_{12}+F_{R_2}^{env}V_2+F_{r_{12}}^{env}v_{12}=0, \quad (3)$$

where $F_{12}=\partial U(r_{12})/\partial r_{12}$, $F_{R_2}^{env}=\partial\left[U^{env}(R_2,r_{12})\right]/\partial R_2$, $F_{r_{12}}^{env}=\partial\left[U^{env}(R_2,r_{12})\right]/\partial r_{12}$.

If there is no external force field, the last two terms in eq. (3) are zero. Variables are separated and eq. (3) is integrable. If the external field exist but does not depend from r_{12} then last term in the eq. (3) is equal to zero and its breaks up on two independent equations:

$$MV_2\dot{V}_2+F_{R_2}^{env}V_2=D, \quad (4) \qquad 2mv_{12}\dot{v}_{12}+F_{12}v_{12}=-D. \quad (5)$$

Here the eq. (4) describes the motion of the CM system in an external field of force; the eq. (5) describes the relative motion MP which does not depend on exterior forces; D is a constant which we take equal to zero. It means that when the external forces are homogeneous the internal energy can't change. Thus, in the first and second cases the motion of two MP is determined by the Newton's third law. In general case the exterior forces can change both the energy of system motion and internal energy.

Thus, on the example of the two-body system has shown that the energy of the system is split into two independent types by transition to the CM coordinates system. It is the internal energy which depends on the relative velocities of MP and the forces of their interaction. And it is the energy of the system motion in the field of external forces which depends on the coordinates of the CM and its velocity. We can see that by summarizing of the motion equation for LS, we exclude internal forces, leaving only the external forces. As a result we come to the system's motion equation in space. By subtracting these equations, we exclude the external forces and come to the equation for the relative motion of MP in the interaction field of forces. I.e. the system's motion, unlike the MP motion, is determined by two invariants: the energy of its motion and internal energy.

All bodies consist of microparticles or molecules. Therefore they can be represented in the form of the SP whose position is determined by its CM. As shown on example of two MP, the motion of each MP should be determined in relative to the CM. Coordinates and velocities of the MP relative to the CM systems we will call *micro variables*, the coordinates and velocity of the CM systems we will call as *macro variables*. Since internal and external forces are independent, then these variables are also independent. Hence the two spaces variables in relevant micro and macro variables, also independent. I.e. the new variables divide the space of the generalized co-ordinates and velocities on two independent subspaces. One subspace is determined by the internal symmetries of the system, and the second subspace is determined by the symmetry of the outer space [8]. Thus the systems dynamics is defined by two types of symmetry: symmetry of the system which defined by distribution of its elements and character of their interactions, and symmetry of space in which the system moves. Hence, the energy of the system will be the sum of two invariants of motion: internal energy and the energy of motion of the system as a whole.

Since the energy, unlike the forces, is the additive function of dynamic parameters of the MP, the mechanics of SP conveniently builds basing on the energy function. Below we will obtain the expression for the energy of the system consisting from potentially interacting MP which will be written down in micro and macro dynamic variables.

ENERGY OF THE MP SYSTEM. Let us take a system from N of potentially interacting a unit mass MP. The potentials in each point of space are additive. Therefore, the force acting on a given MP is equal to the sum of forces acting on it from all others MP and from the external forces. The forces between everyone two MP are determined by distance between them. Thus, the kinetic energy of system T_N can be represented as the sum of the kinetic energies of the MP. So, $T_N=\sum_{i=1}^{N}mv_i^2/2$. Potential energy is equal to the sum of potential energies of all MP in the field of the external forces and potential energies of MP pair interactions among themselves which is $U_N(r_{ij})=\sum_{i=1}^{N-1}\sum_{j=i+1}^{N}U_{ij}(r_{ij})$, where $i,j=1,2,3...N$ are the number of MP, v_i – is a velocity of i-element; $v_{ij}=\dot{r}_{ij}$. Hence, full energy of system is equal to $E_N=T_N+U_N+U^{env}=const$. It is obvious that kinetic energy of system includes the

energy of its motion in the field of external forces, T_N^{tr} and kinetic energy of relative motion, T_N^{ins} caused by interactions MP among themselves. I.e., $T_N = T_N^{tr} + T_N^{ins}$. We will write down the velocities of everyone MP in the form of the sum: $v_i = V_N + \tilde{v}_i$ where $V_N = \dot{R}_N$, $R_N = (\sum_{i=1}^N r_i)/N$, $\sum_{i=1}^N \tilde{v}_i = 0$. Momentum of the system P_N is the sum of the moment of all MP. I.e., $P_N = \sum_{i=1}^N m_i v_i = M_N V_N$. Thus, the relationship between the momentum P_N and body is the same as between the momentum of one MP with the weight M_N. I.e., the system can be considered as a point with the coordinates of the CM that moves with velocity equal to the sum of the velocities of all MP. Therefore the dynamics of the system, unless you consider changing its internal energy, is determined by Newton's equation of motion for MP with a mass equal to M_N. Hence it is clear that in a CM coordinate system the momentum of the system is equal to zero and $T_N = \sum_{i=1}^N m v_i^2/2 = M_N V_N^2/2 + \sum_{i=1}^N m\tilde{v}_i^2/2$. It means that unlike one MP, the total kinetic energy of motionless system is equal to the sum kinetic energies of MP determined by their velocities relative to the CM. I.e., one part of kinetic energy of system is connected with motion of the MP relative to the CM, and the second part is connected with the motion of the system CM. Hence, the velocity of system is determined by the velocity of its CM whose position is defined by a radius-vector R_N.

Thus, the system's energy consists of the kinetic energy of the MP motion relative to the CM and the potential energy of their interaction. The sum of this energy called *the internal energy* of the system. Then the energy can be written as a sum of internal energy plus the system's energy in the field of external forces. I.e.:

$$E_N = T_N^{tr} + E_N^{ins} + U^{env}, \tag{6}$$

where $E_N^{ins} = T_N^{ins} + U_N$ is internal energy, $T_N^{ins} = \sum_{i=1}^N m\tilde{v}_i^2/2$ is a kinetic part of internal energy, U_N is a potential part of internal energy, determined by the interactions of MP.

Quadratic function of the kinetic energy can be expressed through a quadratic function in which arguments are the velocities of the MP in relative to the CM and the velocity of the CM system. This conclusion is follow from the equality: $N\sum_{i=1}^N v_i^2 = (\sum_{i=1}^N v_i)^2 + \sum_{i=1}^{N-1}\sum_{j=i+1}^N v_{ij}^2$. So we have: $T_N = [M_N V_N^2 + (m/N)\sum_{i=1}^{N-1}\sum_{j=i+1}^N v_{ij}^2]/2$ (a). The first term in (a) is the kinetic energy of the CM motion. The second term is the kinetic part of the internal energy determined by the relative velocities of MP. Let's transform the energy T_N by replacement: $v_i = V_N + \tilde{v}_i$, where $\tilde{v}_i$ is a MP velocities relative to the CM. As $\sum_{i=1}^N \tilde{v}_i = 0$, then: $T_N = M_N V_N^2/2 + \sum_{i=1}^N m\tilde{v}_i^2/2$. Using (a) we will find: $\sum_{i=1}^N m\tilde{v}_i^2/2 = (1/2N)\sum_{i=1}^{N-1}\sum_{j=i+1}^N m v_{ij}^2$. Therefore $T_N^{ins} = \sum_{i=1}^N m\tilde{v}_i^2/2 = (m/N\ \sum_{i=1}^{N-1}\sum_{j=i+1}^N v_{ij}^2)/2$.

Thus, the law of energy conservation for the system can be formulated as follows: **the sum of the system's kinetic energy of motion, its internal energy and of the potential energy in the external field of forces always is a constant along the trajectory of the CM.** The difference of the energy conservation laws for the system and for MP leads to a qualitative distinction for their motions. Indeed, the trajectory MP is defined by transformation of potential energy of an external field only into the kinetic energy of its motion. But the trajectory of system is defined by transformation of potential energy of an external field both to its kinetic energy and to internal energy. Thus, the natural variables that define these types of energy are macro and micro variables.

THE SYSTEM'S MOTION EQUATION. There are basic differences of dynamics of the systems, possessing structure and the sizes, from dynamics of MP. The motion of MP is uniquely determined by the point in space. But SP motion is determined by the area of space occupied with it and CM position. Therefore for unequivocal definition of dynamics of system it is necessary to know, both change of its kinetic energy of the system motion and change of internal energy as energy of an external field goes on change of these two types of energy. The system's motion depends from its sizes if the spatial heterogeneity of external forces is exist.

Another fundamental difference between the dynamics of MP and the dynamics of the system base on the fact that for one MP the principle of superposition of forces is valid, while for the different MP it is not so. Indeed, the change of the internal energy has a place when the sum of internal forces is equal to zero. Therefore if to summarize the equations of motion for each MP, we will lose the terms which determine the change of the internal energy. But the system's motion is determined by the change of two types of energy: the system's motion energy and internal energy. Therefore the motion equation should be submitted in the variables that determine the motion of its CM and motion of the MP relative to the CM.

Differentiating eq. (6) over time we obtain [5, 6]:

$$V_N M_N \dot{V}_N + \dot{E}_N^{ins} = -V_N F^{env} - \Phi^{env}, \tag{7}$$

where $F^{env} = \sum_{i=1}^N F_i^{env}(R_N, \tilde{r}_i)$, $\dot{E}_N^{ins} = T_N^{ins}(\tilde{v}_i) + U_N^{ins}(\tilde{r}_i) = \sum_{i=1}^N \tilde{v}_i(m\dot{\tilde{v}}_i + F(\tilde{r}_i)_i)$, $r_i = R_N + \tilde{r}_i$, $v_i = V_N + \tilde{v}_i$, $F_i^{env} = \partial U^{env}/\partial \tilde{r}_i$, $\Phi^{env} = \sum_{i=1}^N \tilde{v}_i F_i^{env}(R_N, \tilde{r}_i)$, $\tilde{v}_i, \tilde{r}_i$, are the velocities and coordinates of MP relative to the CM, V_N, R_N are the velocity and coordinates of the CM. The eq. (7) is equation of system's energy balance. In the left-hand side the first term

$T_N^{tr} = V_N M_N \dot{V}_N$ is a change of system's kinetic energy. The second term is a change of system's internal energy, defined in the coordinates and velocities of MPs relative to the CM. The right-hand side defines the work of external forces that change the energy of the system. Here the first term defines the change of the T_N^{tr}. The second term defines the change of the E_N^{ins}.

Now let us take the external forces which scale of heterogeneity is commensurable with the systems scales. In this case we can write: $F^{env} = F^{env}(R + \tilde{r}_i)$ where R is a distance to the CM. If $R >> \tilde{r}_i$, than the force F^{env} is expanded in a small parameter. Retaining in the expansion of the zero and first order, we write: $F_i^{env} = F^{env}\big|_{R_0} + (\nabla \cdot F_i^{env})\big|_{R_0} \tilde{r}_i = F_{i0}^{env} + (\nabla \cdot F^{env})_{i0} \tilde{r}_i$. Because $\sum_{i=1}^N \tilde{v}_i = \sum_{i=1}^N \tilde{r}_i = 0$ and $\sum_{i=1}^N F_{i0}^{env} = N F_{i0}^{env} = F_0^{env}$, we will have:

$$V_N (M_N \dot{V}_N + F_0^{env}) + \sum_{i=1}^N m \tilde{v}_i (\dot{\tilde{v}}_i + F(\tilde{r}_i)_i) \approx - (\nabla \cdot F^{env})_{i0} \sum_{i=1}^N \tilde{v}_i \, \tilde{r}_i \quad , \tag{8}$$

The work of the potentially part of force, F_0^{env}, change the system's motion energy. The term in the right-hand side has a first order of smallness as the condition $R >> \tilde{r}_i$ does not mean smallness of the $\dot{\tilde{r}}_i = \tilde{v}_i$. This term is proportional of the gradient of external force and determines the work on change of internal energy. Its variation can't be expressed by the integral of the gradient of any scalar function on the way. It is because the change of internal energy is a sum of work of external forces on motion of MP, while the sum of these forces is zero. But these forces can be expressed through the effectiveness of the change in internal energy. This can be done so.

Multiplying (7) on V_N and dividing result on V_N^2, we obtain the system's motion equation:

$$M_N \dot{V}_N = -F_0^{env} - \alpha_N V_N , \tag{9}$$

where $\alpha_N = (\Phi^{env} + \dot{E}_N^{ins}) / V_N^2$.

The second term in the right-hand side defines a non-potential part of forces whose work changes the internal energy. If the external field of force is homogeneous or when the forces between MP are much more of the external forces, this term is equal to zero and the eq. (9) becomes the Newton's motion equation.

Thus, to obtain the motion equation for the structured body, it is necessary to execute consistently the following operations. Firstly, it is necessary to present a body as a system of microparticles. By transition to micro and macro parameters we present the system's energy as a sum of the motion energy and an internal energy. From here we obtain the equation of energy streams for these types of energy. From here we will come to a system's motion equation which takes into account non-potential force changing its internal energy. It is important to note that the **eqs. (6-9) strictly follow from Newton's laws for MP. Therefore, all properties of the dynamics of such systems, which follow from these equations, are determined only by these laws.**

SYSTEMS OF SP. The above equations are valid for the general case of any systems of potentially interacting MP in the external field of forces. In general case due to the nonlinearities they are not integrable. But integration is possible if the system represents as a set of equilibrium SP. The equilibrium of SP means that it can be split on the rather large equilibrium subsystems which are motionless relative to each other. Therefore the SP internal energy is the sum of the internal energies of subsystems. I.e. the collective processes of energy, momentum and mass flows into SP are absent. Therefore at feeble enough action on SP not breaking equilibrium, its motion will be determined by the change of the motion energy and an internal energy.

In the approach of the local equilibrium approximation any nonequilibrium system can be represented by a set of SP which has a relative motion to each other. In the thermodynamic limit at enough weak interactions, each of the SP during the entire process can be regarded as equilibrium [9]. Then the dynamics of nonequilibrium systems can be described by the eq. (9). Let us the system consists of two SP: L and K. Let us L is a number of MP in L-SP, a K is a number MP in K-SP, i.e. $L + K = N$. Let us CM for two SP motionless, i.e. $LV_L + KV_K = 0$, where V_L and V_K velocities of two SP relative CM of the system. Differentiating energy of system on time we will obtain: $\sum_{i=1}^N v_i \dot{v}_i + \sum_{i=1}^{N-1} \sum_{j=i+1}^N F_{ij} v_{ij} = 0$, where $F_{ij} = \partial U / \partial r_{ij}$. For finding the equation for L-SP, we gather at the left hand side only the terms defining the change of kinetic and potential energy of interaction of L-SP elements among themselves. All other terms we displaced into the right hand side and combined the groups of terms in such a way that each group contained of the terms with identical velocities. In accordance with Newton equation, the groups which contain terms with velocities of the elements from K-SP are equal to zero. As a result the right hand side of the equation will contain only the terms which determine the interaction of the elements L-SP with the elements K-SP. Thus we will have: $\sum_{i_L}^L v_{i_L} \dot{v}_{i_L} + \sum_{i_L=1}^{L-1} \sum_{j_L=i_L+1}^L F_{i_L j_L} v_{i_L j_L} = \sum_{i_L=1}^L \sum_{j_K=1}^K F_{i_L j_K} v_{j_K}$, where double indexes are entered for a designation of an accessory of a particle to corresponding subsystem. If we will make replacement $v_{i_L} = \tilde{v}_{i_L} + V_L$, where $\tilde{v}_{i_L}$ is a velocity of i_L particle in relative to CM of L-SP then we obtain the equation for L-SP. The equation for K-SP can be obtained in the same way. As a result we will have: [6, 11]:

$$V_L M_L \dot{V}_L + \dot{E}_L^{ins} = -\Phi_L - V_L \Psi, \quad (10) \qquad V_K M_K \dot{V}_K + \dot{E}_K^{ins} = \Phi_K + V_K \Psi, \quad (11)$$

where $\Psi = \sum_{i_L=1}^{L} F_{i_L}^K$, $\Phi_L = \sum_{i_L=1}^{L} \tilde{v}_{i_L} F_{i_L}^K$, $\Phi_K = \sum_{i_K}^{K} \tilde{v}_{j_K} F_{j_K}^L$, $F_{i_L}^K = \sum_{j_K=1}^{K} F_{i_L j_k}$, $F_{j_K}^L = \sum_{i_L=1}^{L} F_{i_L j_k}$,

$\dot{E}_L^{ins} = \sum_{i_L=1}^{L-1} \sum_{j_L=i_L+1}^{L} \tilde{v}_{i_L j_L} [m\dot{\tilde{v}}_{i_L j_L} / L + F_{i_L j_L}]$, $\dot{E}_K^{ins} = \sum_{i_K=1}^{K-1} \sum_{j_K=i_K+1}^{K} \tilde{v}_{i_K j_K} [m\dot{\tilde{v}}_{i_K j_K} / K + F_{i_K j_K}]$, $M_L = mL$, $M_K = mK$.

The eqs. (13, 14) are the equations of energy exchange. The potential force, Ψ, defines motion of the CM of SP. The non-potential forces which determined by the terms Φ_L and Φ_K, will transform the motion energy of SP into the internal energy as a result of chaotic motion of elements one SP in the field of the forces of another SP. They are dependent on velocities and can't be expressed through the gradient from any scalar function. These forces are equivalents to dissipative forces. The SP motion equations corresponding to the equations (10, 11) can be written as [6]:

$$M_L \dot{\vec{V}}_L = -\vec{\Psi} - \alpha_L \vec{V}_L, \quad (12) \qquad M_K \dot{\vec{V}}_K = \vec{\Psi} + \alpha_K \vec{V}_K, \quad (13)$$

where $\alpha_L = (\dot{E}_L^{ins} + \Phi_L) / V_L^2$; $\alpha_K = (\Phi_K - \dot{E}_K^{ins}) / V_K^2$

The eqs. (12, 13) are written down for SP which are considered equilibrium during all process of interaction. In this case we can neglect by the energy, momentum and mass flows in SP. Due to equilibrium of SP its internal energy can't be transformed into SP motion energy. This follows from the law of conservation of momentum, according to which neither any internal MPs motions can change of SP velocity. From here we come to a conclusion about **irreversibility** of SP dynamics. Therefore, coefficients α_L, α_K are friction coefficients.

Dynamics of non-equilibrium systems is determined by the eqs. (12, 13). Consequently the Lagrange Hamilton and Liouville equations for the systems, whose elements are the SP, will also be determined by these equations. It is well known that the Hamilton principle for MP derived from differential D'Alambert principle using Newton's equation [2]. For this purpose the time integral of virtual work δw^e done by effective forces is equated to zero. Integration over time is carried out provided that external forces possess a power function. It means that the canonical principle of Hamilton is valid only for cases when $\sum F_i \delta R_i = -\delta V$ (b), where $i-$ is a particle number, and F_i - is a force acting on this particle. But for interacting SP the condition of conservation of forces is not fulfilled because of the presence of a non-potential component. Therefore in the equations of Lagrange, Hamilton and Liouville for systems from SP, the terms caused by non-potentiality of collective forces are appeared. The Liouville equation for SP is written as [4, 6]:

$$df / dt = -f \sum_{L=1}^{R} \partial F_L / \partial V_L \quad (14)$$

Here $f-$ is a distribution function for a set of SP, F_L is a dissipative force, V_L is the velocity of $L-$SP.

The state of this system can be defined in the phase space which consists of $6R-1$ coordinates and momentums of SP, where R is a number of SP. Location of each SP is given by three coordinates and their moments. Let us call this space us S-space for SP in order to distinguish it from the usual phase space for MP. The S-space unlike usual phase space is compressible though total energy of all MP is a constant. It is caused by transformation of the motion energy of SP into their internal energy. The SP internal energy can't be transformed into the SP energy of motion as SP momentum can't change due to the motion of its MP. Therefore S-space is compressible because the internal energy will increase until the relative motion of SP will not disappear.

It is necessary to redefine the geometrical concept of an interval [2] for systems whose elements are the SP. Indeed, we have shown that the dynamics of the SP is determined by two types of symmetry: the internal symmetry and the symmetry of the space. Therefore the motion of the system is determined by two types of energy: kinetic energy of the SP and its internal energy. Each of these types of energy has its own type of forces. This is reflected in the fact that the geometry of motion of the SP, in contrast to the geometry of motion of the MP, is the sum of the squares of the two intervals, that can be written as [2, 7]: $d\bar{s}^2 = ds_{tr}^2 + ds_{ins}^2$. Here ds_{tr}^2 is a square of an interval corresponding to SP motion energy, ds_{ins}^2 - is a square of the interval corresponding to SP internal energy.

Thus, the square of the interval of a nonequilibrium system splits into the sum of the squares of the two independent intervals. The first one corresponds to the system motion while the second corresponds to its internal energy. These intervals are orthogonal since they satisfy the Pythagorean Theorem.

MECHANICS OF SP AND THERMODYNAMICS. Difficulties of substantiation of the empirical laws of thermodynamics based on fundamental laws of physics are connected with the reversibility of the Newton's motion equations. The reversibility is due to its constructing on the bases of unstructured body's models. Acceptance in attention of structure leads to occurrence of non-potential component of the collective forces of body's interaction changing their internal energy. For SP this energy can only increase due to the energy of its motion. It is equivalent to irreversibility of the SP dynamics. Let us explain this conclusion.

The presence of reversible dynamics for SP would mean that its internal energy is capable to pass into motion energy. In turn this would mean the possibility of increasing momentum of SP at the expense of its internal energy. But this contradicts the law of conservation of momentum. Indeed, for each of the equilibrium subsystems into which splits SP the sum of the velocities of MP in subsystems and sum of their interaction forces are equal to zero. But for SP momentum appearing it is necessary that at least in one of subsystems the requirement of equality to zero of the

sum of forces has been disrupted. It is impossible because according to a law of momentum conservation any of subsystems cannot acquire a relative velocity or due to internal MP motion or forces from unmovable subsystems. I.e. internal energy of the SP can't transform into the energy of its motion. It is equivalent to irreversibility. From the mathematical point of view this conclusion follows from the fact that microparameters determining the MP motion are not dependent on the macro parameters that determine the SP motion energy. This mechanism of irreversibility is deterministic because its follows from the Newton's laws. There is a fundamental difference between deterministic and probabilistic mechanisms. For deterministic mechanism the "coarse-grain" hypothesis isn't required.

Let us explain how can connect the mechanics SP and thermodynamics [5, 6]. In thermodynamics the work of external forces breaks up on two parts. One part is related to the reversible work. Another part of energy goes into heating system. According to it the basic equation of thermodynamics looks like: $dE = dQ - Pd\mathrm{Y}$. Here E is the energy of a system; Q is the thermal energy; P is the pressure; Y is the volume. As we deal with equilibrium systems, then $dQ = TdS$, where T - temperature, S - entropy. According to the eq. (7), coming into the system energy can be divided on two part. There are energy of relative motion of the SP and its internal energy. It was showed [5] that in thermodynamics to the change of the SP energy of relative motion there corresponds the value of $Pd\mathrm{Y}$, and to change of SPs internal energy there corresponds value, TdS. Thus, we will come to the basic thermodynamic equation if in the equation (7) to carry out standard transition to thermodynamic parameters [5, 9, 10].

Let us take the system consisting from «R» numbers of SP. Each SP consists from N_L number of MP and $N_L >> 1$, where $L = 1,2,3...R$, $N = \sum_{L=1}^{R} N_L$ - full number MP in system. Then the share of energy, which goes on internal energy increasing, is determined by the expression [5, 6]:

$$\Delta S = \sum_{L=1}^{R} \left\{ N_L \sum_{k=1}^{N_L} [\int \sum_s F_{ks}^L v_k dt] / E_L \right\} \qquad (15)$$

Here E_L is the kinetic energy of L-SP; s - is a number of the external elements which interact with elements k belonging to the L-SP; F_{ks}^L is a force, acted on k-element; v_k -is a velocity of the k element.

The eq. (15) can be viewed as entropy definition. This definition of entropy corresponds to Clausius definition [9, 10]. Difference consists only that this entropy follows from analytical expression for the change of an internal energy obtained by us on the basis of Newton's laws. From the eq. (15), it is possible to obtain the value of the entropy production and obtain the conditions which necessary for sustain the non-equilibrium system in the stationary state [6].

Mechanics of SP leads to statistical physics and kinetics. Indeed, the velocities of SP are determined by average values of velocities of MP. The sum of the MP velocities relative to the CM is equal to zero. Thus the internal energy is equivalent to the rms fluctuation of the MP velocities relative to the system's velocity. This means that the dynamics of the SP is expressed through the first and second moments of the motion [9].

CONCLUSION. The key idea of expansion of the Newtonian mechanics allowing to include the dissipative forces into description, consists in replacements of MP on SP. External simplicity of this idea does not mean its obviousness. Indeed **the dynamical characteristics of the system do not follow directly from simple plurality of dynamical characteristics of elements.** This is evident from the fact that the structure of the system determines not only its motion but also the collective forces of interactions. In connection with the construction of the mechanics of the SP requires knowledge of the principles of synthesis of the properties of systems based on the properties of its elements [11]. The first question is how to find the SP motion equation on the basis of Newton's laws without attracted of some statistical hypotheses.

It became clear as a result of studying of dynamics of two MP systems that SP mechanics must to be built in space of micro and macro variables. In these variables the energy of SP breaks up on the energy of its motion and an internal energy. The SP motion energy is expressed through macro-parameters - co-ordinates and velocities of CM. Its change is connected with the work of the external force acted on the CM of SP. The internal energy is expressed through micro-parameters. The increasing of internal energy is provided by the work of the external forces which change the relative motion of MP. The internal and external forces are independent. Therefore the SP motion energy and internal energy are independent also. Independence internal and external forces tell us about presence **two types of symmetry. It is symmetry of space and symmetry of system**. According to these types of symmetries the system's energy breaks up on two invariants: the SP motion energy and SP internal energy.

The major factor causing difference of SP dynamics from MP dynamics is a structure and an internal energy. Taking SP as a system's elements we, thereby, have supplied this elements with a new properties – structure and an internal energy. The change of an internal energy provided by the work of collective forces is a cause's difference of SP dynamics from dynamics of MP.

Newton's laws were obtained for models structureless bodies. To use them to determine the equation of motion of real bodies with the structure, we took a model of SP, consisting of potentially interacting MP. Using the Newton's law for MP, we find the equation of motion of such a SP, taking into account changes in its internal energy. This was done by using the expression for the energy of the SP by shifting to the variables that characterize its dynamics. Derivation of the SP motion equation is carried out so. We write the SP energy through independent macro and micro-variables. In these variables, it splits into SP's energy of motion and the internal energy. Differentiating this energy in

time, we obtain the equation for the flux of the motion energy and internal energy. From here we come to the SP's motion equation. Dissipative forces are defined through the relation of this work to the SP's motion energy.

Irreversibility is a new property of the SP dynamics. The mechanism of irreversibility is related to the transformation of SP motion energy into the internal energy and the inability of the inverse transformation due to momentum conservation law. Because the SP motion equation obtained on the basis of Newton's laws, the irreversibility of the dynamics of the SP is deterministic. If we neglect the change in internal energy, the motion of the SP will be determined by Newton's motion equation.

There are both similarities and differences between accepted today a probabilistic explanations of irreversibility [3] and our explanations. In the basis of probabilistic mechanism of irreversibility is a fact of randomization of trajectories of Hamiltonian systems in phase space due to the exponential instability and the hypothesis of "coarse-grain" of the phase space. In the deterministic mechanism of irreversibility both the exponentially instability and mixing in phase space determine the efficiency of transformation of the motion energy into the internal energy. But the irreversibility follows from the momentum conservation law and the non-potentiality of the forces which transform the energy of motion into the internal energy. The hypothesis about «coarse-grain» of the phase space is not required. In accordance with a deterministic mechanism of irreversibility in classical mechanics the concept of entropy is appeared. This entropy corresponds to the empirical entropy offered by Clausius and is consistent with the mathematical form of its probabilistic definition proposed by Boltzmann.

References.

1. Newton I. Mathematical principles of natural Philosophy. New York, 1846.
2. Lanczos C. The variation principles of mechanics. University of Toronto press. 1962.
3. Loskutov Yu.A. Charm of chaos // UPS. V.150. № 12. P. 1305-1329. 2010.
4. Somsikov V.M. Equilibration of a hard-disks system// IJBC. Vol. 14. N. 11-p. 4027-4033. 2004.
5. Somsikov V.M. Thermodynamics and classical mechanics// Journ. of Phys. Conference series. 23. p. 7-16. 2005.
6. Somsikov V.M. The restrictions of classical mechanics in the description of dynamics of nonequilibrium systems and the way to get rid of them. New Adv. in Physics. Vol. 2. No 2. September. p. 125-140. 2008.
7. Goldstein G. Classical mechanics. M. 1975.
8. Lubarsky G. Ya. Group theory and its application to the physics. M. 1958.
9. Rumer Yu. B, Ryvkin M. Sh, Thermodynamics. Stat. Physics and Kinematics. M. 1977.
10. Landau L.D., Lifshits Ye. M. Statistical Physics. M.1976.
11. Somsikov V.M. What gives the solution of irreversibility problem of. PEOS. V.11. No.1. P. 4-20. 2009

Proceedings, 4th Chaotic Modeling and Simulation International Conference
31 May – 3 June 2011, Agios Nikolaos, Crete Greece

Nonlinear Vibrations and Chaos in Floating Roofs

S. Tariverdilo, R. Shabani, F. Gahramanian, and S. Mahjouri

Faculty of engineering, Urmia University, Urmia, Iran.
E-mail: r.shabani@urmia.ac.ir

Abstract
Hamilton's variational principle is used to derive the nonlinear response of floating roofs of cylindrical liquid storage tanks due to harmonic base excitations. The contained liquid is assumed incompressible and inviscid. The variational principle accounts for nonlinearity caused by large deflections of the floating roofs. Derived nonlinear ordinary differential equations has cubic nonlinear stiffness terms similar to Duffing equation. Due to small damping of the fluids, storage tanks are subjected to the resonance in the case of coincidence of natural frequency with excitation one. It is shown that accounting for large deflections of the roof plate, reduces the height of sloshing induced surface waves. Evaluating the response of nonlinear model for increasing amplitude of harmonic excitations, gives rise to the appearance of sub and super harmonics in the response. Further increase of excitation amplitude increases the contribution of sub and superharmonics in the response and for some excitation amplitudes the response become chaotic. Fractal structure of the Poincare maps is the evidence of the chaotic responses.
Keywords: Floating roof, variational principle, large deflection, sloshing.

1. Introduction

Floating roofs are used in the petroleum industries for storage of liquid hydrocarbons in atmospheric storage tanks. Noting that serious damages in floating roofs due to large deflections could be attributed to the sloshing of the contained liquid [1], it will be essential to take into account for interaction between floating roof and supporting liquid in the nonlinear analysis of the system for base excitation.

Many investigations have been done on the dynamic response and sloshing behavior of the storage tanks. Assuming small surface waves, and using potential theory Jacobsen [2] and Senda and Nakagawa [3] studied the sloshing effects in cylindrical storage tanks. Nakagawa [4] and Yamamoto [5] considering the interaction between rigid massless floating roof and contained liquid studied the sloshing effects in the storage tanks. Sakai *et al*. [6] employing the linear potential theory and using the variational principle derived the free vibration properties of the system and compared the results with the experiment. Matsui [7] developed an analytical solution for the response of cylindrical storage tanks with floating roofs under seismic excitations.Due to small amount of damping in these models large amplitude oscillation is anticipated for near resonance excitation. This indicates that accounting for different sources of nonlinearity in the model. Different researcher considered different source of nonlinearity in their

investigations. In an static analysis and considering the large deflections of the floating roof, the authors studied the importance of the flexural and membrane stiffnesses on the stress analysis of deck plate [8]. Frandsen [9] carried out extensive investigations on the nonlinear sloshing behavior of rectangular storage tanks without roof for vertical, horizontal and combined excitations. Cho and Lee investigated the hydrodynamic characteristics of large amplitude sloshing response of storage tanks with baffles using nonlinear finite element method [10]. In this study, using the Hamilton's variational principle for large deflection analysis of the floating roofs and contained liquid, the sloshing response of the floating roof under harmonic excitation is investigated. Weighted residual method is adopted to minimize the error in the integral solution of the coupled field. It is shown that the resulting equations are similar to the Duffing equation with cubic nonlinearities. The discritized Duffing type equations solved numerically for harmonic base excitations with different acceleration amplitudes and frequencies. By sweeping the excitation amplitudes, the bifurcation diagrams are plotted at different frequencies near the resonance conditions. Presence of sub and super harmonics and chaotic vibrations are examined using Poincare maps and frequency spectrums.

2. The Variational principle

Figure 1 depicts a typical liquid storage tank with single deck floating roof and the cylindrical coordinate used in the analysis. Simultaneous application of the Hamilton's variational principles on the deck plate and the liquid facilitates the problem of imposing the compatibility of deformation between the floating roof and the supporting liquid.

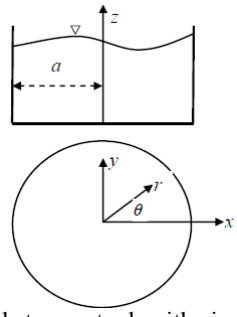

Figure 1. Typical liquid storage tank with single deck floating roof.

The extended Hamilton's principle for coupled fluid-structure system considering only the conservative forces reads

$$\delta \int_{t_i}^{t_f} (T - U + F) dt = 0 \tag{1}$$

where T, U and F are the kinetic energy and strain energy of the deck plate and fluid Lagrangian, respectively. For incompressible and inviscid fluid it is possible to treat fluid flow using potential function. Assuming no separation between fluid and deck plate, the fluid Lagrangian will be

$$F = \int_{S_d} \rho[-\frac{1}{2}(\frac{\partial \Phi}{\partial z})\Phi + \frac{\partial w}{\partial t}\Phi - \frac{g}{2}w^2]dS \tag{2}$$

where S_d is the deck plate area (deck plate-fluid interface), w is the plate deflection and Φ is the velocity potential function. Considering the large deflection theory and assuming that the in-plane displacements are infinitesimal and ignoring associated nonlinear terms in strain-displacement relation, the strain-displacement relation can be expressed as

$$\varepsilon_r = \frac{\partial u_r}{\partial r} + \frac{1}{2}(\frac{\partial w}{\partial r})^2 \;;\; \varepsilon_\theta = \frac{1}{r}\frac{\partial u_\theta}{\partial \theta} + \frac{u_r}{r} + \frac{1}{2}\left(\frac{1}{r}\frac{\partial w}{\partial \theta}\right)^2$$
$$\varepsilon_{r\theta} = \frac{1}{r}\frac{\partial u_r}{\partial \theta} + \frac{\partial u_\theta}{\partial r} - \frac{u_\theta}{r} + \frac{1}{r}\frac{\partial w}{\partial r}\frac{\partial w}{\partial \theta} \tag{3}$$

where ε denotes the deck plate strains and u_r, u_θ and w are radial, tangential and flexural displacements of the deck plate. Decomposing the displacements into flexural and membrane components, we have

$$u_r = u_r^0 - z\frac{\partial w}{\partial r} \;;\; u_\theta = -z\frac{1}{r}\frac{\partial w}{\partial \theta} \tag{4}$$

Where it is assumed that the mid plane displacement in peripheral direction is negligible in comparison with flexural and radial displacements. The variation in the strain energy of the deck plate can be obtained by integrating on the deck plate volume

$$\int_{t_i}^{t_f} \delta U dt = \int_V (\sigma_{rr}\delta\varepsilon_{rr} + \sigma_{\theta\theta}\delta\varepsilon_{\theta\theta} + \sigma_{r\theta}\delta\varepsilon_{r\theta})dV \tag{5}$$

Defining time dependent generalized coordinates of B_i and C_i, we decompose the flexural and radial displacements in terms of interpolation functions ξ_i and η_i as

$$w = \sum_{i=1}^{I} B_i(t)\xi_i(r,\theta) \;\;;\;\; u_r^0 = \sum_{i=1}^{I} C_i(t)\eta_i(r,\theta) \tag{6}$$

Now the with substitutions of Eq. 6 in to Eq. 5 the variation of strain energy can be rewritten as

$$\int_{t_i}^{t_f} \delta U dt = \sum_{i=1}^{I} \left(\sum_{j=1}^{I} H_{ij} C_j + \sum_{l=1}^{I} \sum_{k=1}^{I} \Gamma_{lki} B_l B_k \right) \delta C_i + \sum_{i=1}^{I} \left(\sum_{j=1}^{I} Q_{ij} B_i + \sum_{l=1}^{I} \sum_{k=1}^{I} \sum_{m=1}^{I} \chi_{lkmi} B_l B_k B_m \right) \delta B_i \quad (7)$$

Where H, Γ, Q and χ are the coefficients, which can be calculated using numerical integrations methods. The kinetic energy of deck plate is

$$T = \frac{1}{2} \int_{s_d} m \dot{w}^2 dS_d \quad (8)$$

Where m denotes the unit mass of the deck plate. Rewriting the deck plate deflection in terms of interpolation functions and evaluating the variation of kinetic energy we arrive at

$$\int_{t_i}^{t_f} \delta T dt = -m \int_{S_d} \sum_{i=1}^{I} \sum_{j=1}^{I} \ddot{B}_j(t) \delta B_i(t) \xi_i \xi_j dS_d \quad (9)$$

This can be expressed as

$$\int_{t_i}^{t_f} \delta T dt = \sum_{i=1}^{I} P_{ij} \ddot{B}_j \delta B_i \quad ; \quad (10)$$

Where P is two-dimensional coefficient, which can be calculated.On the other hand the potential function in the fluid Lagrangian, should satisfy the Laplace equation subject to the following boundary conditions

$$\left. \frac{\partial \Phi}{\partial z} \right|_{z=H} = \dot{w} \ \ on \ S_d \ ; \ \left. \frac{\partial \Phi}{\partial z} \right|_{z=0} = 0 \ \ on \ S_b \ ; \ \left. \frac{\partial \Phi}{\partial r} \right|_{r=a} = \dot{\bar{X}} \cos\theta \ on \ S_w \quad (11)$$

where $\dot{\bar{X}}$ is the velocity of base excitation and S_d, S_b and S_w are deck plate-fluid interface, tank bottom surface and tank wall surface, respectively. Solving the Laplace equation subject to the second and third boundary conditions gives the potential function as

$$\Phi = \left[r\dot{\bar{X}} + \sum_{k=1}^{K} A_k(t) \frac{J_1(\frac{\varepsilon_k}{a} r) \cosh(\frac{\varepsilon_k}{a} z)}{J_1(\varepsilon_k) \cosh(\frac{\varepsilon_k}{a} H)} \right] \cos\theta \quad (12)$$

where J_1 is the Bessel function of the first kind of order one, A_k is time dependent modal amplitude and ε_k is the root of $J'(\varepsilon_k) = 0$. Evaluating the variation in the Lagrangian of the contained liquid yields the following compact form.

$$\int_{t0}^{tf} \delta L_f \, dt = \sum_{k=1}^{K} [-\sum_{l=1}^{\infty} \rho\pi S_{lk} A_l + \sum_{i=1}^{\infty} \rho\pi T_{ik} \dot{B}_i]\delta A_k$$
$$+ \sum_{i=1}^{I} [-\sum_{j=1}^{\infty} \rho g U_{ij} B_j - \rho F_i \ddot{\bar{X}} - \sum_{k=1}^{\infty} \rho T_{ik} \dot{A}_k]\delta B_i \quad (13)$$

where *S, U, F* and *T* the confidents with integral forms. After evaluation of the first variation of different terms and substituting in Equation 1, we conclude first variations of an integral form equation. Then by Setting equal to zero the coefficient of δA and δC, it is possible to evaluate **A** and **C** in terms of **B** as follows

$$A_k = \sum_{l=1}^{K} [S_{lk}]^{-1} \sum_{i=1}^{I} T_{ik} \ddot{B}_i$$
$$C_i = \sum_{j=1}^{J} -[H_{ij}]^{-1} \sum_{l=1}^{I} \sum_{k=1}^{I} \Gamma_{lkj} B_l B_k = \sum_{l=1}^{I} \sum_{k=1}^{I} \Psi_{lki} B_l B_k \quad (14)$$

Now equating the coefficients of δB_i to zero and substituting expressions for **A** and **C** from Equations 14, the governing nonlinear differential equation for the generalized coordinate **B** becomes

$$(\mathbf{P} + \rho_f \mathbf{T}\mathbf{S}^{-1}\mathbf{T}^t)\ddot{\mathbf{B}} + (\mathbf{Q} + \rho_f g\mathbf{U})\mathbf{B} + \boldsymbol{\chi}\mathbf{B}^3 = \rho_f \mathbf{F}\ddot{\bar{X}} \quad (15)$$

This is the equation of flexural vibration of the deck plate accounting for the large deflections in the deck plate and at the same time considering the fluid-structure interaction. Accounting for fluid-structure interaction leads to additional mass and stiffness matrixes simulating fluid's added mass and added stiffness.

Considering the large deflections of deck plate gives rise to the cubic stiffness term in Equation 16. Due to similarity between this equation and Duffing equation, emergence of rich dynamics including quasi-periodic and or chaotic responses are expected. Due to small amount of damping in the fluid, near resonance excitation could result in violent response. In this case, the nonlinear stiffness term could have a suppressing effect reducing the sloshing induced wave elevation. Considering the form of excitation (Equation 12c) and using the shape functions of deck plate in air, following interpolation functions for flexural and radial deflections are used

$$\xi_i(r,\theta) = [\alpha_i J_1(k_i r) + \beta_i I_1(k_i r)]\cos(\theta)$$
$$\eta_i(r,\theta) = \sin(\lambda_i \frac{r}{a})\cos(\theta) \quad (16)$$

where I_1 denotes the modified Bessel function of the first kind of order one and k_i and λ_is are wave numbers. The wave number and the ratio of the amplitudes α_i

and β_i can be determined from the requirement of free-edge natural boundary conditions (including zero shear and moment) on the deck plates edge.

3. Numerical simulations and results

The numerical simulation investigates the sloshing response of a liquid storage tank with floating roof to harmonic excitations of different amplitudes and frequencies. Table 1 gives the tank parameters used in the simulations. Damping in the system is considered using a stiffness-proportional Rayleigh damping with damping ratio of 0.5% at systems first natural frequency.

Table 1. The values of parameters used in the analysis.

Parameter	Value
Tank Radius (m)	4
Tank Height (m)	3
Mass density of the deck plate (kg/m^2)	77
Mass density of contained liquid (kg/m^3)	850
Poisson's ratio of deck plate	0.3
Deck plate thickness (m)	0.01
Module of elasticity of deck plate (N/m^2)	2.1×10^9

In the following the appearance of quasi-periodic and chaotic response due to presence of the nonlinear term in Equation 15 is investigated.Due to presence of the cubic nonlinearity in this equation and its similarity with Duffing equation, appearance of strange response is expected. To study the nonlinear behavior of the system the phase plane, Poincare map and frequency spectrum of the responses are employed. To evaluate the emergence of the nonlinear effects due to large deflection of deck plate, the strange responses are studied near the resonance conditions.

Figure 2 depicts the phase plane and Poincare map of the response for excitation frequency 0.6 Hz and ground acceleration amplitude 2.84 m/s^2 . Interesting point in this figure is the emergence of subharmonics in the response. In contrast to the linear case where the Poincare map, includes a fixed point, in nonlinear cases the presence of the subharmonics results in the emergence of multiple points in the Poincare map.

By increasing the excitation amplitude to 5.26 m/s^2, the simulation results are shown in Figure 3 where the appearance of the horse show like structure of the Poincare map is the evidence of the chaotic motions. To show period doubling bifurcation for increasing level of ground acceleration, in Figure 4 the bifurcation diagram for excitation frequency of 0.6 Hz is plotted. This figure shows that for some ranges of excitation amplitudes, subharmonics are emerged and for some other amplitude, the response becomes chaotic.

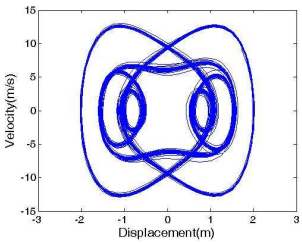

(a)

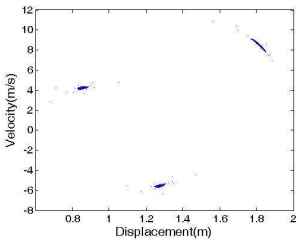

(b)

Figure 2. Response of nonlinear model for ground motion acceleration amplitude of 2.84 m/s^2 and excitation frequency of 0.6 Hz, a) phase plane, b) Poincare map, c) spectrum.

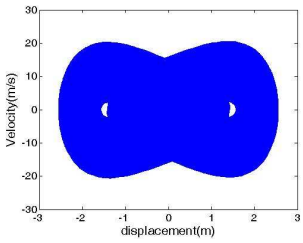

(a)

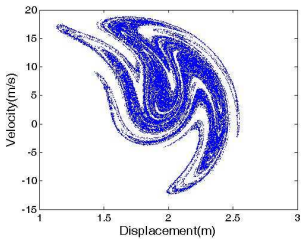

(b)

Figure 3. Response of nonlinear model for ground motion acceleration amplitude of 5.26 m/s^2 and excitation frequency of 0.6 Hz, a) phase plane, b) Poincare map (50000 points), c) spectrum.

To study the effect of frequency variation near the resonance condition (where the nonlinear term has significant effects) the bifurcation diagram is also plotted for excitation frequency of 0.5 Hz, in Figure 5. Increasing the excitation amplitude, different type of the responses emerges, representing period doubling rout to chaos.

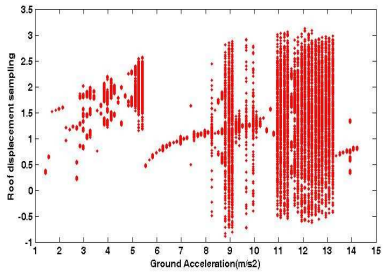

Figure 4. Bifurcation diagram of the roof edge displacement for increasing ground accelerations and excitation frequency of 0.6 Hz.

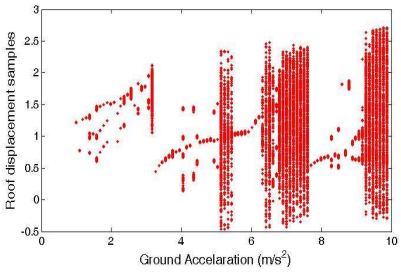

Figure 5. Bifurcation diagram of the roof edge displacement for increasing ground accelerations and excitation frequency of 0.5 Hz.

4. Conclusion

Using Hamiltonian variational principle the governing equations for sloshing response of floating roofs accounting for large deflection of deck plate are derived. Similarity is found between nonlinearity of derived equation and those of Duffing equation. It is shown that this nonlinearity has suppressing effect for near resonance excitation and could substantially reduce the wave height. Investigating the response for near resonance excitations results in appearance of sub and super harmonics in the response and further increase of the excitation amplitude leads to chaotic response. Phase plane diagram and fractal like structure of the strange attractors in Poincare map are used to clarify the chaotic responses.

References

[1] Hatayama, K., Zama, S., Nishi, H., Yamada, M., Hirokawa, M., and Inoue, R., The damages of oil storage tanks during the 2003 Tokachi-oki earthquake and the long period ground motions, *Proceedings of the JSCE-AIJ Joint Symposium on Huge Subduction Earthquakes—Wide Area Strong Ground Motion Prediction*, (2005),7–18.

[2] Jacobsen, L. S., Impulsive hydrodynamics of fluid inside a cylindrical tank and of fluid surrounding a cylindrical pier, *Bulletin of the Seismology Society of America*, **39**(3), (1949), 189–202.

[3] Senda, K., and Nakagawa, K., On the vibration of an elevated water tank I, *Technol. Rep. Osaka Univ.,* 4(117), (1954), 247–264.

[4] Nakagawa, K., On the Vibration of an elevated water tank II, *Technol. Rep. Osaka Univ*., 5(170), (1955), 317–336.

[5] Yamamoto, Y.,The liquid sloshing and the impulsive pressures of oil storage tanks due to earthquakes, *Journal of High Pressure Institute of Japan*, 3(1), (1965), 1965, 2–8.

[6] Sakai, F., Nishimura, M., and Ogawa, H., (1984), Sloshing behavior of floating-roof oil storage tanks, Computers and Structures, 19(2), 183–192.

[7] Matsui T., Sloshing in a cylindrical liquid storage tank with a floating roof under seismic excitation, *Journal of Pressure Vessel Technology*, 129, (2007), 557-566.

[8] R. Shabani, S. Tariverdilo, H. Salarieh, G. Rezazadeh, (2010), Importance of the flexural and membrane stiffnesses in large deflection analysis of floating roofs, *Applied mathematical modeling,* 34(9), 2426-2436.

[9] Jannette B. Frandsen, Sloshing motions in excited tanks, *Journal of Computational Physics,* 196, (2004), 53–87.

[10] J.R. Cho, H.W. Lee, Numerical study on liquid sloshing in baffled tank by nonlinear finite element method, *Computer Methods in Applied Mechanics and Engineering*, 193, (2004), 2581–2598.

Proceedings, 4th Chaotic Modeling and Simulation International Conference
31 May – 3 June 2011, Agios Nikolaos, Crete Greece

Adaptive Backstepping Neural Network Control for Mechanical Pumps

Kyriakos G. Vamvoudakis, Manolis A. Christodoulou

Abstract: In this paper, an Adaptive Backstepping Neural Network control approach is used for a class of affine nonlinear systems which describe the pump model in the strict feedback form. The close loop signals are semi globally uniformly ultimately bounded and the output of the system is proven to follow a desired trajectory. Simulation results are presented to show the effectiveness of the approach proposed in order to control the pump output.

1. Introduction

Recent technological developments have forced control engineers to deal with extremely complex systems that include uncertain and possibly unknown nonlinearities, operating in highly uncertain environments. Man has two principal objectives in the scientific study of his environment: he wants to understand and to control. The two goals reinforce each other, since deeper understanding permits firmer control, and, on the other hand, systematic application of scientific theories inevitably generates new problems which require further investigation, and so on.

Adaptive control [1], [10] is a powerful tool that deals with modeling uncertainties in nonlinear (and linear) systems by on line tuning of parameters. Very important research activities include on-line identification [11], [13] and pattern recognition inside the feedback control loop. Nonlinear control includes two basic forms of systems, the feedforward systems and the feedback systems.

The strict feedback systems can be controlled using the well known backstepping [1], [4], [15] technique. The purpose of backstepping is the recursive design of a controller for the system by selecting appropriate virtual controllers. Separate virtual controllers are used in order to stabilize every equation of the system. In every step we select appropriate update laws. The strict feedforward systems can be controlled using the forwarding technique that is something like backstepping but in reverse order. Other cases of systems that can be converted to the previous forms are part of a larger class of systems that are called interlaced systems as described by [17], and [18]. In these systems we combine backstepping and forwarding techniques together in order to recursively design feedback control laws. Interlaced systems are not in feedback form, nor in feedforward form. These systems have a specific methodology that differs from

K. G. Vamvoudakis is with the Automation and Robotics Research Institute, The University of Texas at Arlington, 7300 Jack Newell Blvd. S., Ft. Worth, TX 76118, *e-mail*: kyriakos@arri.uta.edu;

M.A Christodoulou is with the Department of Electronic and Computer Engineering,Technical University of Crete, Chania, Crete, GREECE 73100 GR, *email:* manolis@ece.tuc.gr and Dipartimento di Automatica et Informatica, Politecnico di Torino, Piemonte, Torino, ITALIA, 10128 IT, *email:* Manolis@polito.it

backstepping and forwarding. We don't start from the top equation, neither from the bottom.

Other special cases of systems are part of other forms that we call mixed interlaced and we introduce their study in the present paper. The methodology is based on classical interlaced systems and is developed by the authors. We want to make the systems solvable by one of the well known backstepping and forwarding methods. This can be reached after some specific steps that convert the system into a known form. We start from the middle equation and we continue with the top. The previous method is based on classical interlaced forms that are introduced by [17] and [18] and can be extended to more complicated systems.

A lot of researchers developed a series of results that generalized and explained the basic idea of nonlinear control. Teel [19] in his dissertation introduced the idea of nested saturations with careful selection of their parameters to achieve robustness for nonlinear controllers. After Teel [19], [17] proposed a new solution to the problem of forwarding that is based on a different Lyapunov solution.

In this paper we control a pump which is a fifth order nonlinear model, but for simplification purposes we use a third order reduced model that exists in the literature. The pump has inherent structural uncertainties with high degrees of uncertainty, thus we are forced to use our non-linear adaptive control techniques.

2. Problem Analysis

A. System Pump Description

Consider a Pump model found in the literature [20] which is presented by the following well known scheme. (The various variables are explained later in the paper. Here we give the basic figure)

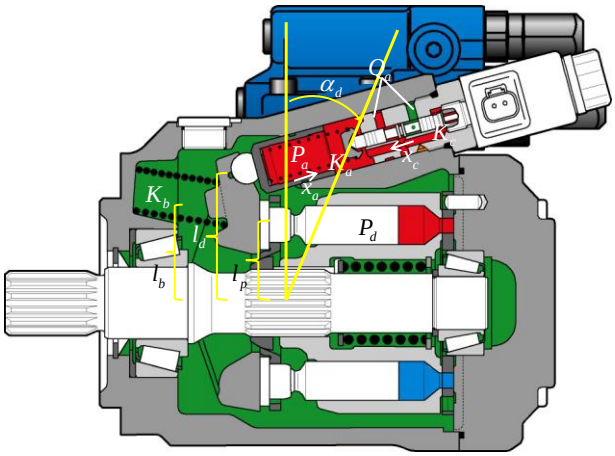

Fig1: Schematic representation of a general Pump mechanical design

Assume we have second order dynamics

$$\dot{x}_c = v_c$$
$$\dot{v}_c = \frac{1}{m_c}\left(-x_c\left(K_c + K_a\right) - K_a l_d \tan\left(\alpha_d\right) - f_c v_c + \phi_s i_s\right) \quad (1)$$

Where x_c is the piston linear displacement, a quantity that can always be measured.

Consider certain volume within the hydraulic actuator $V_a\left(\alpha_d\right) = V_{a0} - S_a l_d \tan\left(\alpha_d\right)$; the dynamics of pressure within the control actuator are:

$$\Delta\dot{P}_a\left(t\right) = \frac{\beta_{oil}}{V_a\left(\alpha_d\right)}\left[-Q_a\left(x_c\right) + \frac{l_d S_a}{\cos^2\left(\alpha_d\right)}\omega_d\right], \quad (2)$$

where the actuator ingoing/outgoing flow is

$$Q_a\left(x_c\right) = \begin{cases} -\mu_{a,in} f\left(x_c\right)\operatorname{sgn}\left(P_d - P_a\right)\sqrt{\left|\Delta P_d - \Delta P_a\right|} & x_c < 0 \\ \mu_{a,out} f\left(x_c\right)\operatorname{sgn}\left(P_a - P_i\right)\sqrt{\left|\Delta P_a - \underline{P_i}\right|} & x_c > 0 \end{cases} \quad (3)$$

Remark 1: The outgoing actuator flow has been assumed to be positive, i.e., $x_c > 0 \Leftrightarrow Q_a > 0$.

Remark 2: The valve stroke is modelled as

$$f\left(x_c\right) = a_1\left|x_c\right| + a_2 x_c^2. \quad (4)$$

The dynamic behaviour of the disc is governed by the following torque equations:

$$\dot{\alpha}_d = \omega_d$$
$$\dot{\omega}_d = \frac{1}{J\left(\alpha_d\right)}\Big[-K_T\left(\omega, \alpha_d\right)\tan\left(\alpha_d\right) - f_c\left(\alpha_d\right)\omega_d^2 - \quad (5)$$
$$f_d\left(\alpha_d, \Delta P_d\right)\omega_d - l_d K_a x_c\left(\alpha_d\right) - l_d S_a \Delta P_a - f_p\left(\alpha_d\right)\Delta P_d\Big]$$

with

$$
\begin{aligned}
&f_p(\alpha_d) = \frac{NA_p l_p}{2\pi \cos^2(\alpha_d)}\gamma_0;\\
&f_d(\alpha_d, P_d) = \frac{NC_p l_p^2}{2\cos^4(\alpha_d)} + K_d(P_d)\\
&f_c(\alpha_d) = \frac{NM_p l_p^2}{\cos^4(\alpha_d)}\tan(\alpha_d);\\
&K_T(\omega, \alpha_d) = l_d^2 K_a + K_b l_b^2 - \frac{NM_p l_p^2 \omega^2}{2\cos^2(\alpha_d)}\\
&J(\alpha_d) = J_d + \frac{NM_p l_p^2}{2\cos^4(\alpha_d)}
\end{aligned}
\tag{6}
$$

The output flow of the pump is given by:

$$
\begin{aligned}
&Q_p = K_p(\omega) l_d \tan(\alpha_d), \quad x_c > 0\\
&Q_p = K_p(\omega) l_d \tan(\alpha_d) - Q_a(x_c), \quad x_c < 0
\end{aligned}
\tag{7}
$$

The mechanical link between the disc and the actuator is provided by the following equation (assuming that the angle is small, we linearize the tangent)

$$
x_a = l_d \tan(\alpha_d) \approx l_d \alpha_d ,
\tag{8}
$$

Under all the above assumptions the fifth order nonlinear model for the pump is given by:

$$
\begin{aligned}
&\dot{x}_c = v_c\\
&\dot{v}_c = \frac{1}{m_c}\left(-x_c(K_c + K_a) - K_a x_a - f_c v_c + \phi_s i_s\right)\\
&\dot{x}_a = v_a\\
&\dot{v}_a = \frac{1}{J}\left[-K_T x_a - f_c x_a v_a^2 - f_d v_a - l_d^2 K_a x_c - l_d^2 S_a \Delta P_a - f_p \Delta P_d\right]\\
&\Delta\dot{P}_a(t) = \frac{\beta_{oil}}{V_{a0} - S_a x_a}\left[-Q_a(x_c) + S_a v_a\right];
\end{aligned}
\tag{9}
$$

with

$$f_p = \frac{NA_p l_p l_d \gamma_0}{2\pi}; \qquad f_d\left(\Delta P_d\right) = \frac{NC_p l_p^2}{2} + K_d\left(\Delta P_d\right)$$
$$f_c = \frac{NM_p l_p^2}{l_d^2}; \qquad K_T\left(\omega\right) = l_d^2 K_a + K_b l_b^2 - \frac{NM_p l_p^2 \omega^2}{2}; \tag{10}$$
$$J = J_d + \frac{NM_p l_p^2}{2}$$

Assuming negligible valve dynamics we may get a reduced third order model as follows:

$$\dot{x}_a = v_a$$
$$\dot{v}_a = \frac{1}{J}\left[-K_T x_a - f_c x_a v_a^2 - f_d v_a - l_d^2 K_a x_c - l_d^2 S_a \Delta P_a - f_p \Delta P_d\right] \tag{11}$$
$$\Delta\dot{P}_a\left(t\right) = \frac{\beta_{oil}}{V_{a0} - S_a x_a}\left[-Q_a\left(x_c\right) + S_a v_a\right];$$

and

$$x_c = \frac{\phi_s i_s - K_a x_a}{K_c + K_a} = b_s i_s - b_a x_a \tag{12}$$

The pump is commanded assuming action on the actuator flow, and then we get:

$$\dot{x}_a = v_a$$
$$\dot{v}_a = \frac{1}{J}\left[-K_T x_a - f_c x_a v_a^2 - f_d v_a - l_d^2 S_a \Delta P_a - f_p \Delta P_d\right] \tag{13}$$
$$\Delta\dot{P}_a\left(t\right) = \frac{\beta_{oil}}{V_{a0} - S_a x_a}\left[-Q_a\left(x_c\right) + S_a v_a\right];$$

and $x_c = b_s i_s$.

Equation (11) can be expressed in (or transformed to) the following nonlinear state space form:

$$\dot{x}_i = f_i(\bar{x}_i) + g_i(\bar{x}_i) x_{i+1}, 1 \le i \le n-1$$
$$\dot{x}_i = f_i(\bar{x}_i) + g_n(\bar{x}_n) u \ , n \ge 2 \tag{14}$$
$$y = x_1$$

where $\bar{x}_i = [x_1, x_2, ...x_i]^T \in R^i, i = 1,...n, u \in R, y \in R$ are state variables, input and output respectively. More accurately for the pump model (11) we have $f_1(x_1) = 0$,

$$g_1(x_1)=1,\ f_2(\bar{x}_2)=\frac{1}{J}\left(-K_T x_a - f_c x_a v_a^2 - f_d v_a\right),$$

$$g_2(\bar{x}_2)=\frac{1}{J}\left(-l_d^2 S_a \Delta P_a - f_p \Delta P_d\right),\ f_3(\bar{x}_3)=\frac{\beta_{oil}}{V_{a0}-S_a x_a} S_a v_a,$$

$$g_3(\bar{x}_3)=-Q_a\left(b_s\right)\frac{\beta_{oil}}{V_{a0}-S_a x_a}.$$

Our purpose is to construct a specific adaptive Neural Network controller (the proof is omitted due to space) such that:

i) all the signals in the close loop remain semi globally ultimately bounded

ii) the output signal y follows a desired trajectory signal y_d, with bounded derivatives up to $(m+1)th$ order.

In order to approximate some unknown nonlinearities we use Neural Networks [2], [3], [5], [9], [16]. This approximation is guaranteed within some compact sets Ω.

Since $g_i(.)$, $i=1,...n$ are smooth functions, they are therefore bounded within some compact set. According to the previous we can make two assumptions.

Assumption 1: The signs of $g_i(.)$ are bounded for example there exist constants $g_{i1}(.)\geq g_{i0}(.)>0$ such that, $g_{i1}(.)\geq\left|g_{i1}(.)\right|\geq\left|g_{i0}(.)\right|$, $\forall\bar{x}_n\in\Omega\subset R^n$.

Assumption 2: There exist constants $g_{id}(.)>0$ such that $g_i(.)\leq g_{id}(.)\ \forall\bar{x}_n\in\Omega\subset R^n$.

B. RBF Neural Networks

Dynamical Neural Networks are well established tools used in the control of nonlinear and complex systems. We use RBF Neural Networks [6] in order to approximate the nonlinear functions of our systems [14], [15]. The idea behind this is described fully at [2], [3], [7], [8], [9], [15]. The RBF NN we use are of the general form $F(.)=\theta^{\mathrm{T}}\xi(.)$, where $\theta\in R^p$ is a vector of regulated weights and $\xi(.)$ a vector of RBF's. It has been shown that given a smooth function $\mathrm{F}:\Omega\to R$, where Ω is a compact subset of R^m (m is an appropriate integer) and $\varepsilon>0$, there exists an RBF vector $\xi:\mathrm{R}^{\mathrm{m}}\to R^p$ and a weight vector $\theta^*\in R^p$ such that $\left|\mathrm{F}(\mathrm{x})-\theta^{*\mathrm{T}}\xi(\mathrm{x})\right|\leq\varepsilon\ \forall x\in\Omega$. Here ε is called the network reconstruction error. The optimal weight vector is chosen as an appropriate value that minimizes the reconstruction error over Ω.

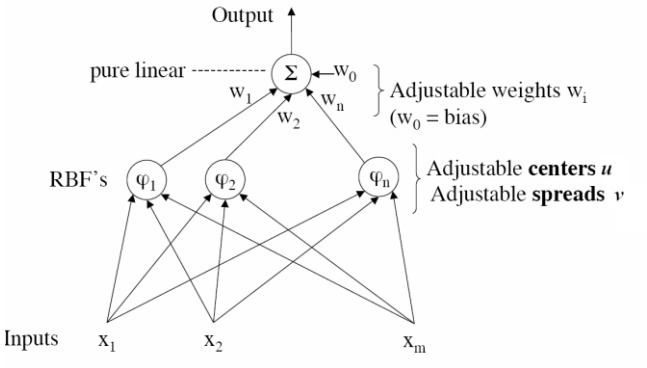

Fig2: Schematic representation of RMF Neural Networks

C. Controller Design

In [15], a desired feedback control law was initially proposed for system (13) and Neural Networks are used to parameterize the desired feedback control law. Finally adaptation laws are used to tune the weights of neural networks for closed loop stability. In our paper we use the controller designed by Kaynak et al. [4]. The design procedure is described in 3 steps because in the pump model above we have 3 states. Each backstepping stage results in a new virtual control design obtained from the preceding design stages. When the procedure ends, the feedback design for the control input is obtained, which achieves the original design objective.

Step1: In this step we want to make the error between x_1 and $x_{1d}\ (= y_d)$ as small as possible.

The previous is described by the following equation:

$$e_1 = x_1 - x_{1d} \tag{15}$$

We take the derivative of e_1. After that we have:

$$\dot{e}_1 = \dot{x}_1 - \dot{x}_{1d} \Rightarrow \dot{e}_1 = f_1(x_1) + g_1(x_1)x_2 - \dot{x}_{1d} \tag{16}$$

by using x_2 as the virtual control input. The previous equation can be changed by multiplication and division with $g_1(x_1)$ to the following form:

$$\dot{e}_1 = g_1(x_1)[g_1^{-1}(x_1) f_1(x_1) + x_2 - g_1^{-1}(x_1)\dot{x}_{1d}] \tag{17}$$

We choose the virtual controller as:

$$x_{2d} = x_2 = -g_1^{-1}(x_1) f_1(x_1) + g_1^{-1}(x_1)\dot{x}_{1d} - k_1 e_1 \tag{18}$$

where k_1 is a positive constant. In order to approximate the unknown nonlinearities (functions $f_1(x_1)$ and $g_1(x_1)$) we use RBF Neural Networks. A Neural Network based virtual controller is used as follows:

$$x_{2d} = -\theta_1^{\mathrm{T}}\xi_1(x_1) + \delta_1^{\mathrm{T}} n_1(x_1)\dot{x}_{1d} - k_1 e_1 \tag{19}$$

where we have substituted the unknown nonlinearities $g_1(x_1)^{-1} f_1(x_1)$ and $g_1(x_1)^{-1}$ with the RBF Neural Networks $\theta_1^{\mathrm{T}}\xi_1(x_1)$ and $\delta_1^{\mathrm{T}} n_1(x_1)$ respectively based on Lyapunov stability [2].

We take the following adaptation laws (σ-modification) in order to avoid large values of the weights:

$$\begin{aligned}\dot{\theta}_1 &= \Gamma_{11}[e_1\xi_1(x_1) - \sigma_1\theta_1] \\ \dot{\delta}_1 &= \Gamma_{12}[-e_1 n_1(x_1)\dot{x}_{1d} - \gamma_1\delta_1]\end{aligned} \tag{20}$$

with σ_1, γ_1 small and positive constants and $\Gamma_{11} = \Gamma_{11}^{\mathrm{T}} > 0$, $\Gamma_{12} = \Gamma_{12}^{\mathrm{T}} > 0$ are the adaptive gain matrices.

Step 2: In this step we make the error between x_2 and x_{2d} as small as possible. The previous is described by the following equation:

$$e_2 = x_2 - x_{2d} \tag{21}$$

We take the derivative of e_2. After that we have:

$$\begin{aligned}\dot{e}_2 &= \dot{x}_2 - \dot{x}_{2d} = f_2(\bar{x}_2) + g_2(\bar{x}_2)x_3 - \dot{x}_{2d} \\ &= g_2(\bar{x}_2)[g_2(\bar{x}_2)^{-1} f_2(\bar{x}_2) + x_3 - g_2(\bar{x}_2)^{-1}\dot{x}_{2d}]\end{aligned} \tag{22}$$

By taking the x_{3d} as a virtual control input and by substituting the unknown nonlinearities $g_2(\bar{x}_2)^{-1} f_2(\bar{x}_2)$ and $g_2(\bar{x}_2)^{-1}$ with the RBF Neural Networks $\theta_2^{\mathrm{T}}\xi_2(\bar{x}_2)$ and $\delta_2^{\mathrm{T}} n_2(\bar{x}_2)$ respectively based on Lyapunov stability [2], we have:

$$x_{3d} = -e_1 - \theta_2^{\mathrm{T}}\xi_2(\bar{x}_2) + \delta_2^{\mathrm{T}} n_2(\bar{x}_2)\dot{x}_{2d} - k_2 e_2 \tag{23}$$

We take the following adaptation laws (σ-modification) in order to avoid large values of the weights:

$$\dot{\theta}_2 = \Gamma_{21}[e_2\xi_2(\bar{x}_2) - \sigma_2\theta_2]$$

$$\dot{\delta}_2 = \Gamma_{22}[-e_2 n_2(\bar{x}_2)\dot{x}_{2d} - \gamma_2 \delta_2] \tag{24}$$

with σ_2, γ_2 small and positive constants and $\Gamma_{21} = \Gamma_{21}^{\mathrm{T}} > 0, \Gamma_{22} = \Gamma_{22}^{\mathrm{T}} > 0$ are the adaptive gain matrices.

Step 3 (Final): In this step we make the error between x_3 and x_{3d} as small as possible.

The previous is described by the following equation:

$$e_3 = x_3 - x_{3d} \tag{25}$$

We take the derivative of e_3. After that we have:

$$\begin{aligned} \dot{e}_3 &= \dot{x}_3 - \dot{x}_{3d} = f_3(\bar{x}_3) + g_3(\bar{x}_3)u - \dot{x}_{3d} \\ &= g_3(\bar{x}_3)[g_3(\bar{x}_3)^{-1} f_3(\bar{x}_3) + u - g_3(\bar{x}_3)^{-1}\dot{x}_{3d}] \end{aligned} \tag{26}$$

Where u is the control input and by substituting the unknown nonlinearities $g_3(\bar{x}_3)^{-1} f_3(\bar{x}_3)$ and $g_3(\bar{x}_3)^{-1}$ with the RBF Neural Networks $\theta_3^{\mathrm{T}}\xi_3(\bar{x}_3)$ and $\delta_3^{\mathrm{T}} n_3(\bar{x}_3)$ respectively, we have:

$$u = -e_2 - \theta_3^{\mathrm{T}}\xi_3(\bar{x}_3) + \delta_3^{\mathrm{T}} n_3(\bar{x}_3)\dot{x}_{3d} - k_3 e_3 \tag{27}$$

We take the following adaptation laws (σ-modification) in order to avoid large values of the weights:

$$\begin{aligned} \dot{\theta}_3 &= \Gamma_{31}[e_3\xi_3(\bar{x}_3) - \sigma_3\theta_3] \\ \dot{\delta}_3 &= \Gamma_{32}[-e_3 n_3(\bar{x}_3)\dot{x}_{3d} - \gamma_3\delta_3] \end{aligned} \tag{28}$$

with σ_3, γ_3 small and positive constants and $\Gamma_{31} = \Gamma_{31}^{\mathrm{T}} > 0, \Gamma_{32} = \Gamma_{32}^{\mathrm{T}} > 0$ are the adaptive gain matrices.

3. Simulation

In order to show the effectiveness and apply the above approach a simulation is presented for the pump model:

$$\dot{x}_1 = x_2$$
$$\dot{x}_2 = -\phi_a x_1 - f_a\left(x_1, x_2\right)x_2 - a_a x_3$$
$$\dot{x}_3 = \chi_a\left(x_1\right)\left[x_2 - q_a\left(x_3\right)u\right]$$
$$y = x_1$$

where x_1, x_2, x_3 and y are states and output of the system respectively. The initial conditions are $x_0 = [x_{10},\ x_{20},\ x_{30}]^T = [0.3,\ 0.2,\ 0.1]^T$ and the desired output signal of the system is $y_d = (atan\left(10*\left(t-10\right)\right)/\pi) + 0.5$. These selections are not based on any experiments in the lab.

We make the assumption that all the basis function of the NNs [12] have the form $G(\bar{x}_i) = \exp[-\frac{(\bar{x}_i - u_i)^T(\bar{x}_i - u_i)}{v_i^2}]$ (as described in [6]) where $u_i = \left[u_{i1},\ u_{i2},\ \ldots,\ u_{ij}\right]^T$ are the centers of the receptive field and v_i are the widths of the Gaussian function.

The Neural Networks $\theta_1^T\xi_1(x_1)$ and $\delta_1^T\eta_1(x_1)$ have 5 nodes with centres u_j evenly spaced in [-6, 6] and widths $v_j = 1$, $\theta_2^T\xi_2(\bar{x}_2)$ and $\delta_2^T\eta_2(\bar{x}_2)$ have 25 nodes with centres u_j evenly spaced in [-6, 6] x [-6, 6] and widths $v_j=1$ and $\theta_3^T\xi_3(\bar{x}_3)$, $\delta_3^T\eta_3(\bar{x}_3)$ have 125 nodes with centers u_j evenly spaced in [-6, 6] x [-6, 6] x [-6, 6] and widths v_j=1. We select the design parameters of the above controller as $k_1 = k_2 = 3.5$, $\Gamma_1 = \Gamma_2 = diag\{2\}$, $\sigma_1 = \sigma_2 = \gamma_1 = \gamma_2 = 0.2$. The initial weights θ_1, θ_2, θ_3 are arbitrarily taken in [-1.2, 1.2] and δ_1, δ_2, δ_3 in [0, 1.2].

Figs. 3-8 show the simulation results of applying the controller for tracking the desired signal y_d. From figure 3 we can see that good tracking performance is obtained. Figure 4 shows the trajectory of the controller. Figure 5 shows the phase plane of the system. Figure 6 shows the error e_1, Figure 7 shows the error e_2 and finally Figure 8 shows the error e_3.

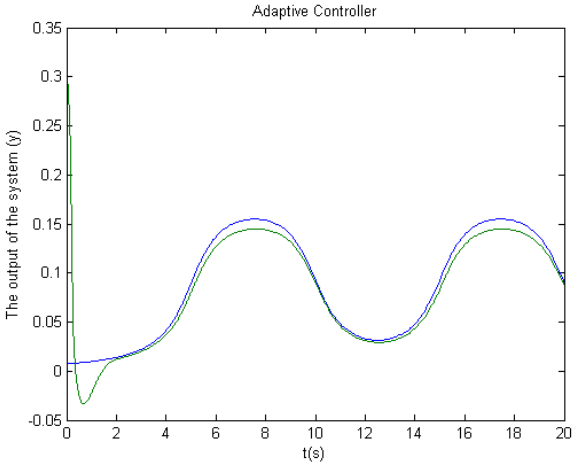

Fig. 3: The output of the system under adaptive controller.

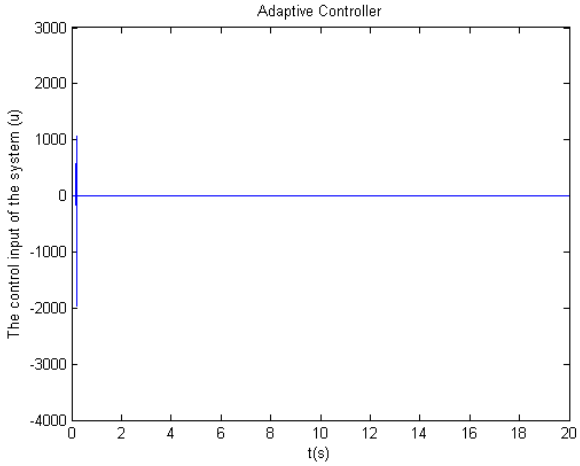

Fig. 4: The trajectory of the adaptive controller.

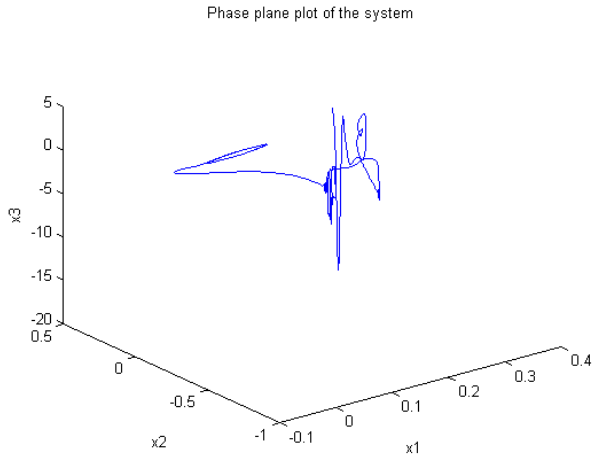

Fig. 5: The phase plane plot of the system.

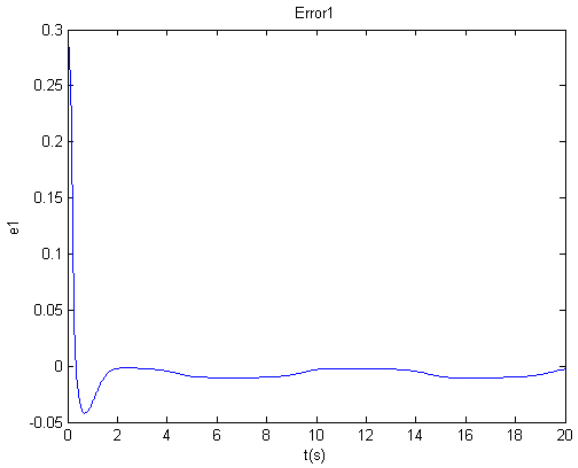

Fig. 6: Error e_1.

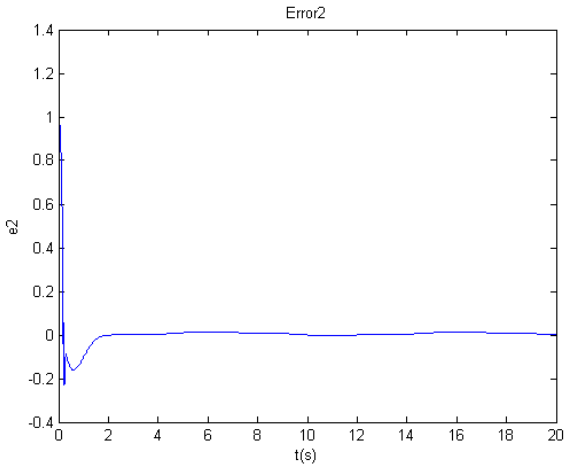

Fig. 7: Error e_2.

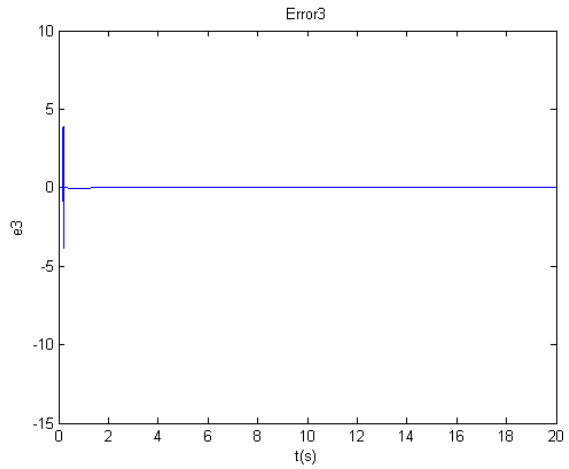

Fig. 8: Error e_3.

4. Conclusion

In this paper, we apply a backstepping controller scheme to control the output of the pump model to reach a specific pressure behavior without knowing the dynamics. The tracking error is bounded and is established on the basis of the Lyapunov approach. Simulation results show the effectiveness of this algorithm in controlling the mechanical pump. Future research will be focused on implementing this algorithm in the real experimental model.

References

[1] M. Krstic, I. Kanellakopoulos, and P. V. Kokotovic, Nonlinear and Adaptive Control Design, New York: Wiley, 1995.

[2] F. L. Lewis, S. Jagannathan, and A. Yesildirek, Neural Network Control of Robot Manipulators and Nonlinear Systems, Taylor & Francis, 1999.

[3] G.A. Rovithakis, and M.A. Christodoulou, Adaptive Control with Recurrent high-order Neural Networks, Springer Verlag, New York, USA, 2000.

[4] Yahui Li, Sheng Qiang, Xianyi Zhuang, and Okyay Kaynak, "Robust and Adaptive Backstepping Control for Nonlinear Systems Using RBF Neural Networks," *IEEE Trans. Neural Netowrks*, vol 15, pp 693-701, 2004.

[5] S. S.Shuzhi, S.S. Ge, and C.Wang, "Direct adaptive NN control of a class of nonlinear systems," *IEEE Trans. Neural Networks*, vol . 13, no. 1, pp. 214-221, 2002.

[6] R. M. Sanner and J. E. Slotine, "Gaussian networks for direct adaptive control," *IEEE Trans. Neural Networks*, vol. 3, pp. 837-863, Nov. 1992.

[7] G.A. Rovithakis, and M.A. Christodoulou, "Adaptive Control of Unknown Plants Using Dynamical Neural Networks," *IEEE Trans. Systems, Man, and Cybernetics*, Vol. 24, No. 3, Mar. 1994, pp. 400-412.

[8] Luis J. Ricalde, and Edgar N. Sanchez, "Inverse Optimal Design for Trajectory Tracking with Input Saturations via Adaptive Recurrent Neural Control," in Proc. of the 42nd IEEE Conference on Decision and Control, December 2003.

[9] S. Haykin, Neural Networks: A comprehensive Foundation, 2nd ed. Upper Saddle River, NJ: Prentice-Hall, 1999.

[10] P. A. Ioannou and J. Sun, Robust Adaptive Control, Englewood Cliggs, NJ: Prentice-Hall, 1993.

[11] K. S. Narendra and K. Parthasarathy, "Identification and control of dynamical systems using neural networks," *IEEE Trans. Neural Networks*, vol. 1, no. 1, pp. 4-27, 1990.

[12] B. Igelnik and Y-H. Pao, "Stochastic choice of basis functions in adaptive function approximation and the functional-link net", *IEEE Trans. Neural Networks*, vol. 6, no. 6, pp. 1320-1329, November 1995.

[13] M. M. Polycarpou and P. A. Ioannou, "Identification and Control Using Neural Network Models: Design and Stability Analysis," Dept. Elect. Eng. Syst., Univ. Southern California, Los Angeles, Tech. Rep. 91-09-01, 1991.

[14] G. A. Rovithakis, "Tracking Control of multi-inputs affine nonlinear dynamical systems with unknown nonlinearities using dynamical neural networks, "*IEEE Trans. Syst., Man, Cybern.*, vol. 29, pp. 447-451, 1999.

[15] T. Zhang, S. S. Ge, and C. C. Hang, "Adaptive neural control for strict feedback nonlinear systems using backstepping," *Automatica*, vol. 36, pp. 1835-1846, 2000.

[16] Kyriakos G. Vamvoudakis, Manolis A. Christodoulou, "Adaptive Backstepping Control for MAPK Cascade Models Using RBF Neural Networks," Proc. Mediterranean Conf. Control & Automation, Athens, Greece, June 2007.

[17] P. V. Kokotovic, R. Sepulchre and M. Jankovic, Constructive Nonlinear Control. New York: Springer Verlag, 1997.

[18] M. Krstic, "Feedback Linearizability and Explicit Integrator Forwarding Controllers for Classes of Feedforward Systems," *IEEE Trans. on Automatic Control*, vol. 49, pp. 1668-1682, 2004.

[19] A. R. Teel, "Feedback stabilization: Nonlinear solutions to inherently nonlinear problems," Ph.D., Univ. California, Berkeley, CA, 1992.

[20] E. Canuto, S. Malan, Wilber Acuna, "Pump modelling", Technical Report, Politecnico di Torino, 2009.

Proceedings, 4th Chaotic Modeling and Simulation International Conference
31 May – 3 June 2011, Agios Nikolaos, Crete Greece

Adaptive Control of Mixed-Interlaced forms

Kyriakos G. Vamvoudakis, Manolis A. Christodoulou

Abstract: In this paper we combine forwarding and backstepping techniques to stabilize mixed interlaced systems. All the signals in the close loop remain semiglobally ultimately bounded the output signal y follows a desired trajectory signal y_d, with bounded derivatives up to m^{th} order. We also present simulation examples that prove the adaptation of mixed interlaced forms, using a backstepping controller.

1. Introduction

Recent technological developments have forced control engineers to deal with extremely complex systems that include uncertain and possibly unknown nonlinearities, operating in highly uncertain environments. Man has two principal objectives in the scientific study of his environment: he wants to understand and to control. The two goals reinforce each other, since deeper understanding permits firmer control, and, on the other hand, systematic application of scientific theories inevitably generates new problems which require further investigation, and so on. Nonlinear control includes two basic forms of systems, the feedforward systems and the feedback systems.

The strict feedback systems can be controlled using the well known backstepping technique. The purpose of backstepping is the recursive design of a controller for the system by selecting appropriate virtual controllers. Separate virtual controllers are used in order to stabilize every equation of the system. In every step we select appropriate update laws. The strict feedforward systems can be controlled using the forwarding technique that is something like backstepping but in reverse order. Other cases of systems that can be converted to the previous forms are part of a larger class of systems that are called interlaced systems as described by [9], and [3]. In these systems we combine backstepping and forwarding techniques together in order to recursively design feedback control laws. Interlaced systems are not in feedback form, nor in feedforward form. These systems have a specific methodology that differs from backstepping and forwarding. We don't start from the top equation, neither from the bottom.

Other special cases of systems are part of other forms that we call mixed interlaced and we introduce their study in the present paper. The methodology is based on classical interlaced systems and is developed by the authors. We want to make the systems solvable by one of the well known backstepping and forwarding methods. This can be reached after some specific steps that convert the system into a known form. We start from the middle equation and we continue with the top. The previous method is based on classical interlaced forms

K. G. Vamvoudakis is with the Automation and Robotics Research Institute, The University of Texas at Arlington, 7300 Jack Newell Blvd. S., Ft. Worth, TX 76118, e-mail: kyriakos@arri.uta.edu;

M.A Christodoulou is with the Department of Electronic and Computer Engineering,Technical University of Crete, Chania, Crete, GREECE 73100 GR, *email:* manolis@ece.tuc.gr

that are introduced by [9] and [3] and can be extended to more complicated systems.

A lot of researchers developed a series of results that generalized and explained the basic idea of nonlinear control. Teel [10] in his dissertation introduced the idea of nested saturations with careful selection of their parameters to achieve robustness for nonlinear controllers. After Teel , Sepulchre, Jankovic and Kokotovic [9] proposed a new solution to the problem of forwarding that is based on a different Lyapunov solution.

The paper consists of four sections including the current one. The next section introduces the meanings of Adaptive Control, Backstepping and Forwarding techniques. In Section 3, the main body of this paper, the mixed interlaced forms are analyzed. Finally section 4 draws some concluding remarks.

2. Background in Adaptive Control

The history of adaptive control began from the early 1950's. With the passing of the years a lot of papers and books have been published. These research activities have proposed solutions for basic problems and for broader classes of systems. Especially the interest for nonlinear adaptive control began from the mid-1980's. A lot of great scientists, such as Kokotovic et al [2], Lewis et al [4], Ioannou and Sun [7], Christodoulou and Rovithakis [5] have studied adaptive control and its applications extensively.

Adaptive control is a powerful tool that deals with modeling uncertainties in nonlinear (and linear) systems by on line tuning of parameters. Very important research activities include on-line identification and pattern recognition inside the feedback control loop.

Through time, adaptive control has existed big development (Sepulchre et al [9]) in order to control plants with unknown dynamics that appear linearly. Adaptive control is based on Lyapunov design.

In order to make it clear, a short example will be reported. Let us consider the nonlinear plant:

$$\dot{x} = u + \theta x^2 \tag{1}$$

And select the control law as:

$$u = -qx - \hat{\theta} x^2 \tag{2}$$

which, if the estimated θ ($\hat{\theta}$) is equal to real θ such that $\hat{\theta} \equiv \theta$, then the result is a close loop system of the form:

$$\dot{x} = -qx \tag{3}$$

The filtered version of the signals x is:

$$x_f = \frac{1}{s+1} x^2 \tag{4}$$

The prediction error *e* is:

$$e = x - \hat{x} = (\theta - \hat{\theta})x_f = \hat{\theta}x_f \tag{5}$$

We use the commonly normalized update law:

$$\dot{\hat{\theta}} = -\frac{\gamma}{1+x_f{}^2}x_f{}^2\tilde{\theta} \tag{6}$$

The previous update law is linear. It can be proved that $\tilde{\theta}$ does not converge to zero faster than exponentially and the easiest case is:

$$\tilde{\theta} = e^{-\gamma t}\tilde{\theta}(0) \tag{7}$$

Finally the close loop system has the following form:

$$\dot{x} = -x + \tilde{\theta}x^2 \tag{8}$$

where for simplicity *q* substituted with 1 and by substituting $\tilde{\theta}$ from the previous equation is obtained:

$$\dot{x} = -x + e^{-t}\tilde{\theta}(0)x^2 \tag{9}$$

where for simplicity γ substituted with 1.
It is easy to see that the explicit solution of the previous is determined by the following equation:

$$x = \frac{2x(0)}{x(0)\tilde{\theta}(0)e^{-t} + [2 - x(0)\tilde{\theta}(0)]e^{-t}} \tag{10}$$

From the previous it is clear that if $x(0)\tilde{\theta}(0) < 2$ then it is obvious that *x* converge to zero as $t \to \infty$. At the case that $x(0)\tilde{\theta}(0) > 2$, at the time:

$$t_{esc} = \frac{1}{2}\ln\frac{x(0)\tilde{\theta}(0)}{x(0)\tilde{\theta}(0) - 2}$$

the difference of the two terms of the exponential in the denominator becomes zero, that is:

$$|x(t)| \to \infty \text{ as } t \to t_{esc}$$

The previous model is unstable (x goes to infinity at t_{esc}) and Lyapunov design models must be specified in order to achieve stabilization.
Let choose the following Lyapunov function:

$$V = \frac{1}{2}x^2 + \frac{1}{2}(\hat{\theta} - \theta)^2 \tag{11}$$

The derivative of the Lyapunov function for our nonlinear plant is:

$$\dot{V} = x(u + \theta x^2) + (\hat{\theta} - \theta)^2 \dot{\hat{\theta}}$$

In order to find a control and an update law we must specify:

$$\dot{V} \le -x^2 \Rightarrow x(u + \theta x^2) + (\hat{\theta} - \theta)^2 \dot{\hat{\theta}} \le -x^2 \tag{12}$$

From the previous equation in order to remove the unknown θ we use the update law:

$$\dot{\hat{\theta}} = x^3$$

And the control law is:

$$u = -x - \hat{\theta}x^2$$

Both control law and update law yield $\dot{V} \le -x^2$ such that stability maintains in opposition to the previous approach without Lyapunov.

Adaptive control in most cases has tracking error that converges to zero.

i) Adaptive Backstepping Design

Backstepping ([1], [2], [4], [7]) is a recursive design for systems of the form:

$$\begin{aligned}
\dot{x}_1 &= x_2 + \varphi_1^{\mathrm{T}}(x_1, x_2)\theta \\
\dot{x}_2 &= x_3 + \varphi_2^{\mathrm{T}}(x_1, x_2, x_3)\theta \\
\dot{x}_3 &= u \ + \varphi_3^{\mathrm{T}}(x_1, x_2, x_3)\theta
\end{aligned}$$

with state $x=[x_1^T, x_2^T, x_3^T]$ and control input u. The value θ is a p *x 1* vector which is constant and unknown. The function φ_1 depends only to x_1, x_2 function φ_2, φ_3 depends only to x_1, x_2, x_3.

The purpose of backstepping is the recursive design of a controller for the previous system by selecting appropriate virtual controllers. The virtual controller

for the first equation of the system is x_2 and is used to stabilize the first equations, the virtual controller for the middle equation is x_3 and is used to stabilize the first two equations, and finally the controller for the last is u. We use separate virtual controllers in order to stabilize every equation of the system. In every step we select appropriate update laws.

In classical backstepping, the output is selected as the state x_1 and the purpose of adaptive control is to make this state to follow a desired trajectory x_{1d}.

Adaptive backstepping design is a Lyapunov based design [4]. The previous procedure can be applied only to systems that have (or transformed to) the previous form (strict feedback).

ii) Adaptive Forwarding Design

Forwarding ([9]) is something like backstepping but for strict feedforward systems. Let us introduce forwarding technique with an example such as:

$$\dot{x}_1 = x_2 + {x_3}^2 + x_2 u$$
$$\dot{x}_2 = x_3 - {x_3}^2 u$$
$$\dot{x}_3 = u$$

In the previous example we do not have feedback paths.
Firstly we stabilize the last equation ($\dot{x}_3 = u$). We take the following Lyapunov function:
$V_3 = \frac{1}{2}{x_3}^2$ and a feedback to stabilize the system is $u = -x_3$. With the previous we augment $\dot{x}_3 = -x_3$ by the middle equation, and write our system in the cascade form:

$$\dot{x}_2 = \varphi_2(x_3)$$
$$\dot{x}_3 = -x_3$$

where $\varphi_2(x_3) = x_3 - {x_3}^3$ is the interconnection term. $\dot{x}_2 = 0$ is stable and $\dot{x}_3 = -x_3$ is GAS and LES. The next step is to construct Lyapunov function V_2 for the augmented system when V_3 is given.
After some specific steps we reach the following control law:

$$u = -x_3 - (x_2 + x_3 + \frac{{x_3}^3}{3})(1 + {x_3}^2) \qquad (13)$$

3. Mixed Interlaced Forms

a. Introduction and Linearization Method

To begin with we consider the following third order mixed interlaced system and via an example we will introduce mixed interlaced forms [12]:

$$\begin{aligned}\dot{x}_1 &= -\beta_3 x_1 + a_{32}(c_3 - x_1)x_2 + a_{31}(c_3 - x_1)x_3 \\ \dot{x}_2 &= -\beta_2 x_2 + a_{23}(c_2 - x_2)x_1 + a_{21}(c_2 - x_2)x_3 \\ \dot{x}_3 &= -\beta_1 x_3 + (c_1 - x_3)u(t)\end{aligned} \qquad (14)$$

The previous system is not in feedback nor is it in feedforward form because of specific terms such as x_1x_2, x_1x_3, x_2x_3. The Jacobi linearization of the previous system is a chain of integrators.

Instead from starting on top, we start from the middle equation and treat x_3 as virtual control and we want $\dot{x}_2 = -x_2$ for stability. There exists a Lyapunov function of the form $V_1 = \frac{1}{2}{x_2}^2$ and a stabilizing feedback is $x_3 = \frac{-\beta_2 x_2 + a_{23}c_2 x_1 - a_{23}x_2 x_1 + x_2}{a_{21}x_2 - a_{21}c_2}$ which is $x_3=a(x_1,x_2)$. We employ one step of backstepping to stabilize the middle equation augmented by the top equation of our system:

$$\begin{aligned}\dot{x}_1 &= -\beta_3 x_1 + a_{32}(c_3 - x_1)x_2 + \\ &+ a_{31}(c_3 - x_1)\left(\frac{-\beta_2 x_2 + a_{23}c_2 x_1 - a_{23}x_2 x_1 + x_2}{a_{21}x_2 - a_{21}c_2}\right) + \\ &+ a_{31}(c_3 - x_1)v \\ \dot{x}_2 &= -x_2 + v\end{aligned} \qquad (15)$$

where the control x_3 has been augmented to $x_3=a(x_1,x_2)+v$. With v=0, the equilibrium $(x_1,x_2)=(0, 0)$ is globally stable and forwarding yields the following Lyapunov function:

$$\begin{aligned}V_2 &= V_1 + \lim \tilde{x}_1(s) \\ &= \frac{1}{2}{x_2}^2 + \frac{1}{2}{\xi_1}^2, \\ \xi_1 &= x_1 + x_2 - \frac{1}{2}{x_2}^2 - \frac{1}{3}{x_2}^3\end{aligned} \qquad (16)$$

The feedback law: $v = -(1-x_2^{\,2})\xi_1$ maintains the system globally stable and the augmented control is

$$\begin{aligned} x_3 = a_1(x_1, x_2) \;\; + v &= \frac{-\beta_2 x_2 + a_{23}c_2 x_1 - a_{23}x_2 x_1 + x_2}{a_{21}x_2 - a_{21}c_2} \\ -(1-x_2^{\,2})\xi_1 \;\; &= a_2(x_1, x_2, \xi_1) \end{aligned} \qquad (17)$$

In order to stabilize our system we apply the backstepping technique.

b. Mixed Interlaced Forms, Adaptive Control and Simulations

Adaptive Control of dynamical systems has been an active area of research since the 1960's. The system is described by the following figure:

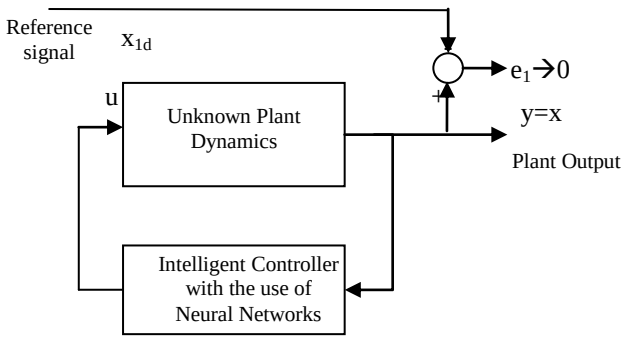

Because we have 3 states our controller design is described with Kaynak et al [1] controller in 3 steps.

Step1: In this step we want to make the error between x_1 and $x_{1d}\,(=y_d)$ as small as possible.

The previous is described by the following equation:

$$e_1 = x_1 - x_{1d} \qquad (18)$$

We take the derivative of e_1. After that we have:

$$\dot{e}_1 = \dot{x}_1 - \dot{x}_{1d} \Rightarrow \dot{e}_1 = f_1(x_1) + g_1(x_1)x_2 - \dot{x}_{1d} \qquad (19)$$

by using x_2 as the virtual control input. The previous equation can be changed by multiplication and division with $g_1(x_1)$ to the following form:

$$\dot{e}_1 = g_1(x_1)[g_1^{-1}(x_1) f_1(x_1) + x_2 - g_1^{-1}(x_1)\dot{x}_{1d}] \quad (20)$$

We choose the virtual controller as:

$$x_{2d} = x_2 = -g_1^{-1}(x_1) f_1(x_1) + g_1^{-1}(x_1)\dot{x}_{1d} - k_1 e_1 \quad (21)$$

where k_1 is a positive constant. In order to approximate the unknown nonlinearities (functions $f_1(x_1)$ and $g_1(x_1)$) we use RBF Neural Networks ([11]). A Neural Network based virtual controller is used as follows:

$$x_{2d} = -\theta_1^{\mathrm{T}}\xi_1(x_1) + \delta_1^{\mathrm{T}} n_1(x_1)\dot{x}_{1d} - k_1 e_1 \quad (22)$$

where we have substituted the unknown nonlinearities $g_1(x_1)^{-1}f_1(x_1)$ and $g_1(x_1)^{-1}$ with the RBF Neural Networks $\theta_1^{\mathrm{T}}\xi_1(x_1)$ and $\delta_1^{\mathrm{T}} n_1(x_1)$ respectively based on Lyapunov stability ([6], [8]).

We take the following adaptation laws (σ-modification) in order to avoid large values of the weights:

$$\dot{\theta}_1 = \Gamma_{11}[e_1\xi_1(x_1) - \sigma_1\theta_1] \quad (23)$$

$$\dot{\delta}_1 = \Gamma_{12}[-e_1 n_1(x_1)\dot{x}_{1d} - \gamma_1\delta_1] \quad (24)$$

with σ_1, γ_1 small and positive constants and $\Gamma_{11}=\Gamma_{11}^{T}>0$, $\Gamma_{12}=\Gamma_{12}^{T}>0$ are the adaptive gain matrices.

Step 2: In this step we make the error between x_2 and x_{2d} as small as possible. The previous is described by the following equation:

$$e_2 = x_2 - x_{2d} \quad (25)$$

We take the derivative of e_2. After that we have:

$$\begin{aligned}\dot{e}_2 &= \dot{x}_2 - \dot{x}_{2d} = f_2(\bar{x}_2) + g_2(\bar{x}_2)x_3 - \dot{x}_{2d} \\ &= g_2(\bar{x}_2)[g_2(\bar{x}_2)^{-1} f_2(\bar{x}_2) + x_3 - g_2(\bar{x}_2)^{-1}\dot{x}_{2d}]\end{aligned} \quad (26)$$

By taking the x_{3d} as a virtual control input and by substituting the unknown nonlinearities $g_2(\bar{x}_2)^{-1} f_2(\bar{x}_2)$ and $g_2(\bar{x}_2)^{-1}$ with the RBF Neural Networks $\theta_2^{\mathrm{T}}\xi_2(\bar{x}_2)$ and $\delta_2^{\mathrm{T}} n_2(\bar{x}_2)$ respectively based on Lyapunov stability ([6], [8]), we have:

$$x_{3d} = -e_1 - \theta_2^{\mathrm{T}}\xi_2(\bar{x}_2) + \delta_2^{\mathrm{T}} n_2(\bar{x}_2)\dot{x}_{2d} - k_2 e_2 \qquad (27)$$

We take the following adaptation laws (σ-modification) in order to avoid large values of the weights:

$$\begin{aligned}\dot{\theta}_2 &= \Gamma_{21}[e_2\xi_2(\bar{x}_2) - \sigma_2\theta_2] \\ \dot{\delta}_2 &= \Gamma_{22}[-e_2 n_2(\bar{x}_2)\dot{x}_{2d} - \gamma_2\delta_2]\end{aligned} \qquad (28)$$

with σ_2, γ_2 small and positive constants and $\Gamma_{21}=\Gamma_{21}^{T}>0$, $\Gamma_{22}=\Gamma_{22}^{T}>0$ are the adaptive gain matrices.

Step 3(Final): In this step we make the error between x_3 and x_{3d} as small as possible.
The previous is described by the following equation:

$$e_3 = x_3 - x_{3d} \qquad (29)$$

We take the derivative of e_3. After that we have:

$$\begin{aligned}\dot{e}_3 &= \dot{x}_3 - \dot{x}_{3d} = f_3(\bar{x}_3) + g_3(\bar{x}_3)u - \dot{x}_{3d} \\ &= g_3(\bar{x}_3)[g_3(\bar{x}_3)^{-1} f_3(\bar{x}_3) + u - g_3(\bar{x}_3)^{-1}\dot{x}_{3d}]\end{aligned} \qquad (30)$$

Where u is the control input and by substituting the unknown nonlinearities $g_3(\bar{x}_3)^{-1} f_3(\bar{x}_3)$ and $g_3(\bar{x}_3)^{-1}$ with the RBF Neural Networks $\theta_3^{\mathrm{T}}\xi_3(\bar{x}_3)$ and $\delta_3^{\mathrm{T}} n_3(\bar{x}_3)$ respectively, we have:

$$u = -e_2 - \theta_3^{\mathrm{T}}\xi_3(\bar{x}_3) + \delta_3^{\mathrm{T}} n_3(\bar{x}_3)\dot{x}_{3d} - k_3 e_3 \qquad (31)$$

We take the following adaptation laws (σ-modification) in order to avoid large values of the weights:

$$\dot{\theta}_3 = \Gamma_{31}[e_3\xi_3(\bar{x}_3) - \sigma_3\theta_3]$$
$$\dot{\delta}_3 = \Gamma_{32}[-e_3 n_3(\bar{x}_3)\dot{x}_{3d} - \gamma_3\delta_3] \qquad (32)$$

with σ_3, γ_3 small and positive constants and $\Gamma_{31}=\Gamma_{31}^T>0$, $\Gamma_{32}=\Gamma_{32}^T>0$ are the adaptive gain matrices.

In order to prove the stabilization of mixed interlaced systems we apply the previous described by [1] and we perform the following simulations:

We make the assumption that $c_1>>x_1$, $c_2>>x_2$, $c_3>>x_3$ and $a_{21}=a_{32}=\beta_1=\beta_2=\beta_3=1$, $c_1=9.99$, $c_2=6.66$, $c_3=3.33$. Also we want our desired output to be $y_d=sin(t)$.

Figs. 1-6 show the simulation results of applying the controller for tracking the desired signal y_d. From figure 1 we can see that good tracking performance is obtained. Figure 2 shows the trajectory of the controller. Figure 3 shows the phase plane of the system. Figure 4 shows the error e_1, Figure 5 shows the error e_2 and finally Figure 6 shows the error e_3.

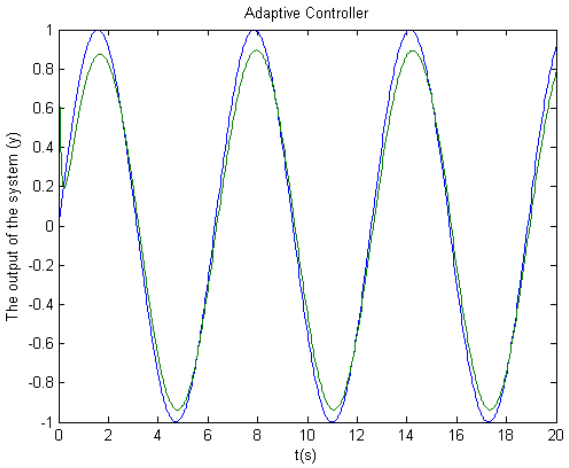

Fig. 1: The output of the system under adaptive controller.

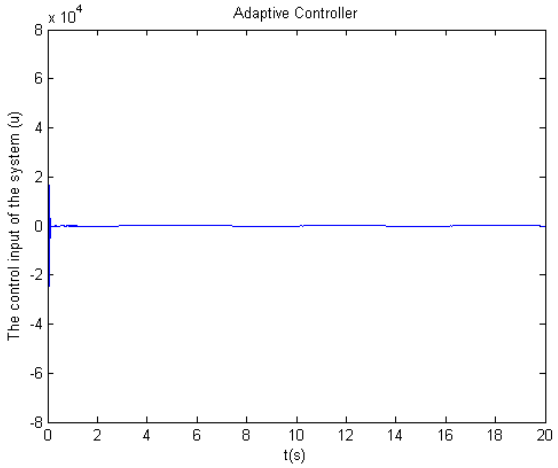

Fig. 2: The trajectory of the adaptive controller.

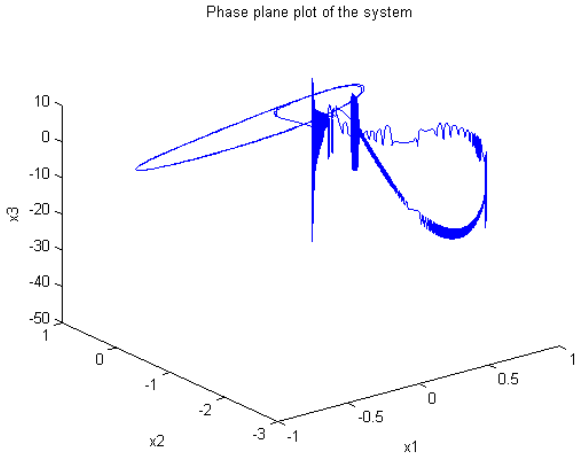

Fig. 3: The phase plane plot of the system.

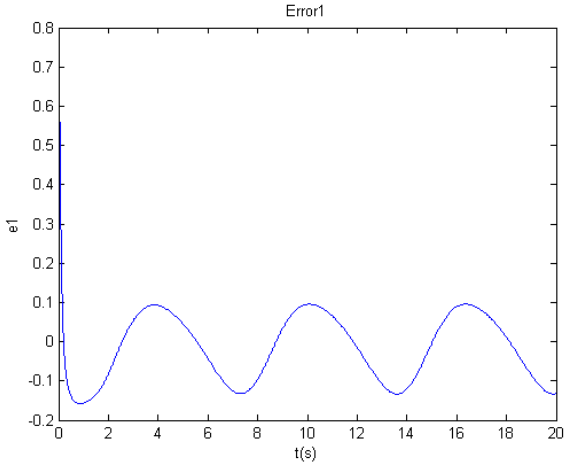

Fig. 4: Error e_1

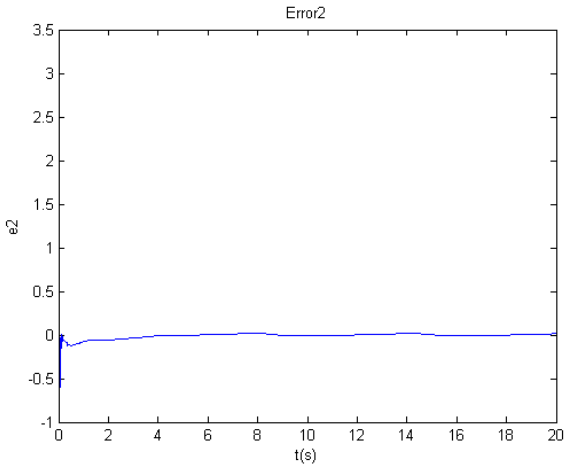

Fig. 5: Error e_2

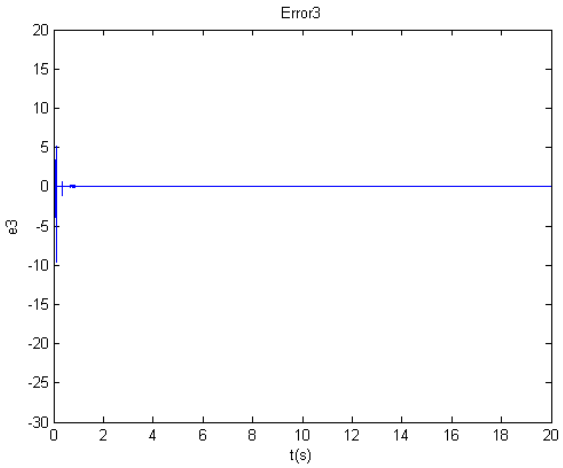

Fig. 6: Error e_3

4. Conclusion

In this paper, we recognize a new form of systems that we call mixed interlaced form. We apply the well known backstepping and forwarding techniques via specific steps. Also Lyapunov functions can be selected to approve convergence and stability. A lot of systems have the mixed interlaced form. For example we can think systems in biological models that have many terms from different states. After the appropriate selection of the controller we can apply adaptive control to make the systems follow a desired trajectory.

The tracking error is bounded and is established on the basis of the Lyapunov approach. Finally, only the states of the unknown plant which are related to the reduced order model are assumed to be available for measurement.

The authors hope that the proposed approach would serve as a promising tool to analyze more complex systems.

References

[1] O. Kaynak, S. Qiang, X. Zhuang, and L. Yahui, "Robust and Adaptive Backstepping Control for Nonlinear Systems Using RBF Neural Networks," *IEEE Trans. Neural Networks*, vol 15, pp 693-701, 2004.

[2] M Krstic, I. Kanellakopoulos, and P. V. Kokotovic, Nonlinear and Adaptive Control Design, New York: Wiley, 1995

[3] M. Krstic, "Feedback Linearizability and Explicit Integrator Forwarding Controllers for Classes of Feedforward Systems," IEEE Trans. on Automatic Control, vol. 49, pp. 1668-1682, 2004.

[4] F. L. Lewis, S. Jagannathan and A. Yesildirek, Neural Network Control of Robot Manipulators and Nonlinear Systems, Taylor & Francis, 1999.

[5] G. A. Rovithakis and M. A. Christodoulou, Adaptive Control with Recurrent high-order Neural Networks, Springer Verlag, New York, USA, 2000.

[6] G. A. Rovithakis, "Tracking Control of multi-inputs affine nonlinear dynamical systems with unknown nonlinearities using dynamical neural networks, "IEEE Trans. Syst., Man, Cybern., vol. 29, pp. 447-451, 1999.

[7] P. A. Ioannou and J. Sun, Robust Adaptive Control, Englewood Cliggs, NJ: Prentice-Hall 1993.

[8] M. Polycarpou and P. A. Ioannou, "Identification and Control Using Neural Network Models: Design and Stability Analysis," Dept. Elect. Eng. Syst., Univ. Southern California, Los Angeles, Tech. Rep. 91-09-01, 1991.

[9] P. V. Kokotovic, R. Sepulchre and M. Jankovic, Constructive Nonlinear Control. New York: Springer Verlag, 1997.

[10] A. R. Teel, "Feedback stabilization: Nonlinear solutions to inherently nonlinear problems," Ph.D., Univ. California, Berkeley, CA, 1992.

[11] R. M. Sanner and J. E. Slotine, "Gaussian networks for direct adaptive control," IEEE Trans. Neural Networks, vol. 3, pp. 837-863, Nov. 1992.

[12] Kyriakos G. Vamvoudakis, Manolis A. Christodoulou, "Adaptive Backstepping Control for MAPK Cascade Models Using RBF Neural Networks," Proc. Mediterranean Conf. Control & Automation, Athens, Greece, June 2007.


Proceedings, 4th Chaotic Modeling and Simulation International Conference
31 May – 3 June 2011, Agios Nikolaos, Crete Greece

Linear-inversive congruential generator of PRN's.

Pavel Varbanets[1] and Sergey Varbanets[2]

[1] I.I. Mechnikov Odessa National University, Dvoryanskaya,2 , 65026, Odessa, Ukraine
(E-mail: varbanetspd@mail.ru)
[2] I.I. Mechnikov Odessa National University, Dvoryanskaya,2 , 65026, Odessa, Ukraine
(E-mail: varb@sana.od.ua)

Abstract. Generalization of the inversive congruential generator of pseudorandom numbers with prime-power modules is considered and the exponential sums on sequence of pseudorandom numbers are estimated. Also we obtained the estimate of the average value of exponential sums over initial value y_0. The estimates for discrepancy of s-dimensional "overlapping" points are obtained.
Keywords: inversive congruential pseudorandom numbers, exponential sum, discrepancy.

1 Introduction

Nonlinear methods of generating uniform pseudorandom numbers in the interval $[0, 1)$ have been introduced and studied during the last twenty five years. The development of this attractive fields of research is described in the survey articles (Chou[1], Eichenauer and Lehn[2], Eichenauer-Herrmann and Topuzoğlu[3], Niederreiter Shparlinski[5]) and in the Niederreiter's monograph[4]. Inversive congruential generators employ the particular place among nonlinear generators by virtue of simplicity of the realization of calculations. In the case of an odd prime-power modulus the inversive congruential generator is defined in the following way:

Let p be a prime, $p \geq 3$, m be a natural number. For given $a, b \in \mathbb{Z}$ we take an initial value y_0, and let y_n^{-1} denotes a multiplicative inverse for y_n in $\mathbb{Z}_{p_m}^*$ if $(y_n, p) = 1$, and $y_n^{-1} = 0$ if $m = 1$ and $y_n \equiv 0(mod\ p)$. Then the recurrence relation

$$y_{n+1} \equiv ay_n^{-1} + b(mod\ p^m) \tag{1.1}$$

generates a sequence $y_0, y_1, \ldots$ which we call the inversive congruential sequence modulo p^m.
The case $p \geq 3$, $m = 1$ studied in [2].

In sequel we will account that $m \geq 3$. In such case the generated sequence $\{y_n\}$, $n \geq 0$, may exists only if $(y_n, p) = 1$ for all $n = 0, 1, 2, \ldots$. In the work [1] indicated the conditions at which the sequence $\{y_n\}$ does not break.

Let $\{y_n\}$ be an infinite sequence generated by the congruence (1.1). By the normalization

$$x_n = \frac{y_n}{p^m}$$

we obtain a sequence of numbers in the interval $[0, 1)$.

The sequence $\{x_n\}$ calls the sequence of pseudorandom numbers in $[0, 1)$ (denoted as PRN's) if it satisfies the requirements of equidistribution and unpredictability (statistical independence). The property of statistical independence is a very important requirement of cryptography to PRN's.

The next important description of the sequence of PRN's $\{x_n\}$ is its period τ. Clearly that $\tau \leq p^{m-1}(p-1)$.

In the works of Chou[1], Eichenauer and Lehn[2], Eichenauer and Topuzöglu[3], Niederreiter[4] have been studied the problem of when the sequence of PRN's (generated by (1.1)) has the maximal period.

In the present paper we study a nonlinear generator similar to (1.1):

$$y_{n+1} \equiv ay_n^{-1} + b + cy_n (mod\ p^m), \tag{1.2}$$

moreover, $(a, p) = (y_0, p) = 1$, $b \equiv c \equiv 0 (mod\ p)$.

Note, that the conditions $(a, p) = 1$, $b \equiv c \equiv 0 (mod\ p)$ guarantee infinite of the process of generation.
The generator (1.2) with the conditions $a \equiv b \equiv 0 (mod\ p)$, $(c, p) = 1$, can be study similarly. The generator (1.2) we call the linear-inversive congruential generator of PRN's.

It is purpose of the present work to demonstrate that the sequence of PRN's $\{x_n\} = \left\{\frac{y_n}{p^m}\right\}$, $n = 0, 1, \ldots$, generated by the recursion (1.2), satisfies the requirements of equidistribution on $[0, 1)$ and passes the serial test on unpredictability.

Notation. Variables of summation automatically range over all integers satisfying the condition indicated. The letter p denotes a prime number, $p \geq 3$. For $m \in \mathbb{N}$ the notation $\mathbb{Z}_{p^m}$(respectively, $\mathbb{Z}^*_{p^m}$) denotes the complete(respectively, reduced) system of residues modulo p^m. We write $gcd(a, b) = (a, b)$ for notation a great common divisor of a and b. For $z \in \mathbb{Z}$, $(z, p) = 1$ let z^{-1} be the multiplicative inverse of a modulo p^m. We write $\nu_p(A) = \alpha$ if $p^\alpha | A$, $p^{\alpha+1} \not| A$. For real t, the abbreviation $e(t) = e^{2\pi it}$ is used.

2 Auxiliary results

We need the following statements.

LEMMA 1. *Let p be a prime number and let $f(x)$, $g(x)$ be polynomials over $\mathbb{Z}$*

$$f(x) = A_1 x + A_2 x^2 + p(A_3 x^3 + \cdots),$$
$$g(x) = B_1 x + + p(B_2 x^2 + \cdots),$$

and let, moreover, $\nu_p(A_2) = \alpha > 0$, $\nu_p(A_j) \geq \alpha$, $j = 3, 4, \ldots$.
Then we have the following estimates

$$\left| \sum_{x \in \mathbb{Z}_{p^m}} e\left(\frac{f(x)}{p^m}\right) \right| \leq \begin{cases} 2p^{\frac{m+\alpha}{2}} & \text{if} \quad \nu_p(A_1) \geq \alpha, \\ 0 & \text{else;} \end{cases} \tag{2.1}$$

$$\left| \sum_{x \in \mathbb{Z}^*_{p^m}} e\left(\frac{f(x) + g(x^{-1})}{p^m}\right) \right| \leq \begin{cases} (\overline{N} \cdot p)^{\frac{m}{2}} & \text{if } (B_1, p) = 1 \\ 2p^{\frac{m+\alpha}{2}} & \text{if } \nu_p(A_1) \geq 0,\ \nu_p(B_j) \geq \alpha, \ldots, \\ 0 & \text{if } \nu_p(A_1) < \alpha \leq \nu_p(B_j),\ j \geq 1, \end{cases} \tag{2.2}$$

where $\overline{N} = \overline{N}(A_1, B_1; p)$ *is the number of solutions of the congruence* $A_1 - B_1 u^2 \equiv 0 (mod\ p)$ *in* $\mathbb{Z}^*_p$.
(This assertion is corollary of the estimates of the Gauss sum and the Kloosterman sum).

Let $\{y_n\}$ generated by the recursive congruence (1.2). Using the arguments as in Varbanets and Varbanets[6] we obtain the following results.

LEMMA 2. *Let* $\{y_n\}$ *is the sequence of PRN's generated by the recursion (1.2) with conditions* $(y_0, p) = (a, p) = 1$, $0 < \nu_p(b) < \nu_p(c)$. *There exist the polynomials* $F_0(u, v, w)$, $G_0(u, v, w)$ *over* $\mathbb{Z}$, $F_0(0, v, w) = G_0(0, v, w) = 0$ *such that for any* $k \geq 2m + 1$*:*

$$\begin{aligned} y_{2k} = {} & kb + kacy_0^{-1} + (1 - k(k-1)a^{-1}b^2)y_0 + (-ka^{-1}b)y_0^2 + \\ & + (-ka^{-1}c + k^2a^{-2}b^2)y_0^3 + p^\alpha F_0(k, y_0, y_0^{-1}), \end{aligned} \tag{2.3}$$

$$\begin{aligned} y_{2k+1} = {} & (k+1)b + (a - k(k+1)b^2)y_0^{-1} + (-kab)y_0^{-2} + \\ & + (-ka^2c + k^2ab^2)y_0^{-3} + (k+1)cy_0 + p^\alpha G_0(k, y_0, y_0^{-1}), \end{aligned} \tag{2.4}$$

where $\alpha := \min(\nu_p(b^3), \nu_p(bc))$*;*
$F_0(u, v, w)$, $G_0(u, v, w) \in \mathbb{Z}[u, v, w]$, $F_0(0, v, w) = G_0(0, v, w) = 0$.

COROLLARY 1. *Let the conditions of Lemma 4 satisfy. Then for* $p > 2$ *the sequence* $\{y_n\}$ *is purely periodic with period* $2p^{m-\ell}$*, where*

(i) $\ell = \nu_p(b) + \nu_p(a - y_0^2)$ *if* $\nu_p(a - y_0^2) < \nu_p(b) \leq \frac{1}{2}m$*;*
(ii) $\ell = 2\nu_p(b)$ *if* $\nu_p(a - y_0^2) > \nu_p(b)$, $\nu_p(b) \leq \frac{1}{2}m$.

For $p = 2$ we can obtain the similar assertion and the following corollary.

COROLLARY 2. *Let* $p = 2$, $m \geq 3$. *Then the sequence* $\{y_n\}$ *defined by recursion (1.2) is purely periodic, where* $b = 2^\nu b_0$, $(b_0, 2) = 1$, $c = 2^\mu c_0$,

$(c_0, p) = 1$, $\mu > \nu > 0$; $\nu_2(a - y_0^2) = \nu_0 \geq 1$. *And its period* τ *is equal*

$$\begin{array}{ll} (i) & 2^{m-2\nu+1} \quad if\ m \geq 2\nu,\ \nu_0 > \nu; \\ (ii) & 2^{m-2\nu-\beta_0+1}\ if\ m > 2\nu,\ \nu_0 = \nu, \beta_0 = \nu_p\left(\frac{y_0^2-a}{2^{\nu_0}} + b_0\right); \\ (iii) & 2^{m-\nu-\nu_0+1} \quad if\ m \geq \nu + nu_0,\ \nu_0 < \nu. \end{array}$$

3 Exponential sums on sequence of PRN's

In this section we get the estimates of certain exponential sums over the linear-inversive congruential sequence $\{y_n\}$ which was defined in (1.2).

For $h_1, h_2 \in \mathbb{Z}$ we denote

$$\sigma_{k,\ell}(h_1, h_2; p^m) := \sum_{y_0 \in \mathbb{Z}_{p^m}^*} e\left(\frac{h_1 y_k + h_2 y_\ell}{p^m}\right),\ (h_1, h_2 \in \mathbb{Z}). \tag{3.1}$$

Here we consider y_k, y_ℓ as a functions at y_0 generated by (1.2) (see, formulas (2.3)-(2.3)).

THEOREM 1. *Let* $(h_1, h_2, p) = 1$, $\nu_p(h_1 + h_2) = \beta$, $\nu_p(h_1 k + h_2 \ell) = \gamma$. *We have the following estimates*

$$|\sigma_{k,\ell}(h_1, h_2; p^m)| \leq \begin{cases} N(h_1, ah_2; p)^{\frac{m}{2}} p^{\frac{m}{2}} & if \quad k \not\equiv \ell (mod\ 2); \\ 0 & if \quad k \equiv \ell (mod\ 2) \\ & and\ \beta < \gamma + \nu,\ m - \beta - \nu > 0; \\ p^{m-1}(p-1) & if \quad k \equiv \ell (mod\ 2) \\ & and\ \beta \geq \gamma + \nu,\ m - \nu - \gamma \leq 0; \\ 2p^{\frac{m+\nu+\gamma}{2}} & if \quad k \equiv \ell (mod\ 2) \\ & and\ \beta \geq \gamma + \nu,\ m - \nu - \gamma > 0. \end{cases}$$

PROOF. We consider two cases:
(I) Let k and ℓ be non-negative integers of different parity, for example, $k := 2k$, $\ell := 2\ell + 1$. By (2.6), (2.7) we have

$$\begin{aligned} h_1 y_{2k} + h_2 y_{2\ell+1} = A_0 + A_1 y_0 + A_2 y_0^2 + A_3 y_0^3 + \\ + A_{-1} y_0^{-1} + A_{-2} y_0^{-2} + A_{-3} y_0^{-3} + \\ + p^\alpha H(y_0, y_0^{-1}) := F_1(y_0, y_0^{-1}), \end{aligned}$$

where

$$\begin{aligned} & A_1 \equiv h_1 (mod\ p^\nu),\ A_2 \equiv -h_1 kab (mod\ p^{\nu+1}), \\ & A_{-1} \equiv ah_2 (mod\ p^\nu),\ A_{-2} \equiv -h_2 ab\ell (mod\ p^{\nu+1}), \\ & A_3 \equiv A_{-3} \equiv 0 (mod\ p^\mu),\ \mu = \nu_p(c) > \nu_p(b) = \nu. \end{aligned}$$

Applying Lemma 1 we at once obtain the assertion of Theorem 1 for $k \not\equiv \ell(mod\ 2)$.
(II) Let k and ℓ be integers of identical parity. Then for $k := 2k$, $\ell := 2\ell$, we have modulo p^m:

$$h_1 y_{2k} + h_2 y_{2\ell} = B_0 + B_1 y_0 + B_2 y_0^2 + B_3 y_0^3 + B_{-1} y_0^{-1} + p^\alpha K(y_0, y_0^{-1}) = \\ := F_2(y_0, y_0^{-1}),$$

where

$$B_1 = h_1 + h_2 + p^{2\nu} B_1'$$
$$B_2 = -ab(h_1 k + h_2 \ell) + p^\alpha B_2'$$
$$B_3 = -a^{-2} b^2 (h_1 k^2 + h_2 \ell^2) - a^{-1} c(h_1 k + h_2 \ell) + p^\alpha B_3'$$
$$B_{-1} = ac(h_1 k + h_2 \ell) + p^\alpha B_{-1}',$$

moreover, B_1', B_2', B_3', B_{-1}' and coefficients of $K(y_0, y_0^{-1})$ contain multipliers of form $h_1 k^j + h_2 \ell^j$, $j \geq 0$.

Now, in order to apply the estimate of complete linear exponential sum to the sum

$$\sum_{y_0 \in \mathbb{Z}_{p^m}^*} e\left(\frac{h_1 y_{2k} + h_2 y_{2\ell}}{p^m}\right) = \sum_{y_0 \in \mathbb{Z}_{p^m}^*} e\left(\frac{F_2(y_0, y_0^{-1})}{p^m}\right)$$

we must define the values $\nu_p(B_1)$, $\nu_p(B_2)$, $\nu_p(B_3)$, $\nu_p(B_{-1})$.
For $\nu_p(h_1 + h_2) = \beta \geq \nu$, $\nu_p(h_1 k + h_2 \ell) = 0$ we obtain

$$|\sigma_{k,\ell}(h_1, h_2, p^m)| \leq 2p^{\frac{m+\nu}{2}}.$$

For $\nu_p(h_1 + h_2) = \beta \geq \nu$, $\nu_p(h_1 k + h_2 \ell) = \gamma > 0$ we denote $\delta = \min(\beta, \gamma)$. Moreover, in such case we have

$$h_1 k^j + h_2 \ell^j = (h_1 k^{j-1} + h_2 \ell^{j-1})(k + \ell) - k\ell(h_1 k^{j-2} + h_2 \ell^{j-2})$$

and then by induction on j we infer

$$\nu_p(h_1 k^j + h_2 \ell^j) \geq \delta, j = 2, 3, \ldots$$

Thereby we can apply the estimate of complete linear exponential sum.
Hence,

$$|\sigma_{2k,2\ell}(h_1, h_2; p^m)| \leq \begin{cases} 0 & if\ \beta < \gamma + \nu,\ m - \beta - \nu > 0, \\ 2p^{\frac{m+\nu+\gamma}{2}} & if\ \beta \geq \gamma + \nu,\ m - \nu - \gamma > 0, \\ \varphi(p^m) & if\ \beta \geq \gamma + \nu,\ m - \nu - \gamma \leq 0, \end{cases}$$

where $\varphi(n)$ is the totient Euler function.
For $k \equiv \ell \equiv 1(mod\ 2)$ we have the analogous result.
This finishes the proof of Theorem 1.

□

Let h be integer, $(h, p^m) = p^s$, $0 \le s < m$, and let τ be a least period length of the sequence of PRN's $\{y_n\}$, $n = 0, 1, \ldots$, defined in (1.2). For $1 \le N \le \tau$ we denote

$$S_N(h, y_0) = \sum_{n=0}^{N-1} e\left(\frac{hy_n}{p^m}\right). \tag{3.2}$$

The sum $S_N(h, y_0)$ calls the exponential sum on the sequence of PRN's $\{y_n\}$.

THEOREM 2. *Let the linear-inversive congruential sequence generated by the recursion (1.2) has the period τ, and let $\nu_p(b) = \nu$, $\nu_p(a - y_0^2) = \nu_0$, $2\nu \le m$. Then we have the following bounds*

$$|S_\tau(h, y_0)| \le \begin{cases} O(m) & if \quad p > 2 \text{ and } \nu_0 < \nu,\ \nu_p(h) < m - \nu - \nu_0 \\ & or \quad p = 2,\ \nu_0 < \nu,\ \nu_2(h) < m - 2\nu; \\ 4 \cdot p^{\frac{m+\nu_p(h)}{2}} & if \quad \nu_0 \ge \nu,\ \nu_p(h) < m - 2\nu; \\ \tau & else, \end{cases}$$

PROOF. By analogy with the proof of theorem 1 we have

$$\begin{aligned} |S_\tau(h, y_0)| &= \left|\sum_{n=0}^{\tau-1} e\left(\frac{hy_n}{p^m}\right)\right| = \left|\sum_{n=0}^{p^\ell-1} e\left(\frac{hy_n}{p^m}\right)\right| \le \\ &\le \left|\sum_{\substack{k_1=0 \\ k=2k_1}}^{p^\ell-1} e\left(\frac{hy_{2k_1}}{p^m}\right)\right| + \left|\sum_{\substack{k_1=0 \\ k=2k_1+1}}^{p^\ell-1} e\left(\frac{hy_{2k_1+1}}{p^m}\right)\right| = \\ &= \left|\sum_{k=0}^{p^\ell-1} e\left(\frac{hF(k)}{p^m}\right)\right| + \left|\sum_{k=0}^{p^\ell-1} e\left(\frac{hG(k)}{p^m}\right)\right| + O(m). \end{aligned} \tag{3.3}$$

In the last part of the formula (3.3) we into account that the representation y_n as a polynomial on k holds only for $k \ge 2m + 1$.

By the Corollaries 1 and 2 and Lemma 1 we easy obtain

$$|S_\tau(h, y_0)| \le \begin{cases} O(m) & if \quad p > 2,\ \nu_0 < \nu,\ \nu_p(h) < m - \nu - \nu_0, \\ O(m) & if \quad p = 2,\ \nu_0 < \nu,\ \nu_2(h) < m - 2\nu, \\ 4p^{\frac{m+\nu_p(h)}{2}} & if \quad \nu_0 \ge \nu,\ \nu_p(h) < m - 2\nu, \\ \tau & else. \end{cases}$$

The constants implied by the O-symbol are absolute.

□

THEOREM 3. *Let a, b, c be parameters of the linear-inversive congruential generator (1.2) and let $(a,p)=1$, $0<\nu=\nu_p(b)<\nu_p(c)$, $1\le N\le 2p^{m-1}$, $\nu_p(h)=p^s$, $s<m$. Then the average value of the $S_N(h,y_0)$ over $y_0\in\mathbb{Z}_{p^m}^*$ satisfies*

$$\overline{S}_N(h)=\frac{1}{\varphi(p^m)}\sum_{y_0\in\mathbb{Z}_{p^m}^*}|S_N(h,y_0)|\le N^{\frac{1}{2}}p^{-\frac{m}{4}}\left(2(\varepsilon_p(a))^{\frac{m}{4}}+\sqrt{10}p^{\frac{\nu+s}{4}}\right),$$

where $s=\nu_p((h,p^m))$, $h=h_0p^s$,

$$\varepsilon_p(a)=\begin{cases}1 & if\ p=2\\ 1+\left(\frac{-a}{p}\right) & if\ p>2,\ \left(\left(\frac{-a}{p}\right)\ be\ the\ Legendre\ symbol\right)\end{cases}.$$

PROOF. First we will consider the case $s=0$, i.e. $(h,p)=1$. By the Cauchy-Schwarz inequality we get

$$\begin{aligned}|\overline{S}_N(h)|^2&\le\frac{1}{\varphi(p^m)}\sum_{y_0\in\mathbb{Z}_{p^m}^*}|S_N(h,y_0)|^2=\\&=\frac{1}{\varphi(p^m)}\sum_{k,\ell=0}^{N-1}\sum_{y_0\in\mathbb{Z}_{p^m}^*}e\left(\frac{h(y_k-y_\ell)}{p^m}\right)\le\\&\le\frac{1}{\varphi(p^m)}\sum_{k,\ell=0}^{N-1}|\sigma_{k,\ell}(h,-h;p^m)|=\\&=N+\frac{1}{\varphi(p^m)}\sum_{\gamma=0}^{m-1}\sum_{\substack{k,\ell=0\\ \nu_p(k-\ell)=\gamma}}^{N-1}|\sigma_{k,\ell}(h,-h;p^m)|.\end{aligned}$$

Next

$$|\overline{S}_N(h)|^2\le$$

$$\le N+\frac{1}{\varphi(p^m)}\sum_{\gamma=0}^{m-1}\left(\sum_{\substack{k,\ell=0\\ k\not\equiv\ell(mod\ 2)\\ \nu_p(k-\ell)=\gamma}}^{N-1}|\sigma_{k,\ell(h,-h;p^m)}|+\sum_{\substack{k,\ell=0\\ k\equiv\ell(mod\ 2)\\ \nu_p(k-\ell)=\gamma}}^{N-1}|\sigma_{k,\ell}(h,-h;p^m)|\right)$$

Using Theorem 1 after the simple calculations we obtain

$$\begin{aligned}|\overline{S}_N(h)|^2&\le N\left(4\varepsilon_p(a)^{\frac{m}{2}}p^{-\frac{m}{2}}+8p^{\frac{-m+\nu}{2}}+2p^{\nu-m}\right)\le\\&\le Np^{-\frac{m}{2}}\left(4(\varepsilon_p(a))^{\frac{m}{2}}+10p^{\frac{\nu}{2}}\right),\end{aligned}$$

Thus, we infer for $(h,p)=1$:

$$|\overline{S}_N(h)|\le N^{\frac{1}{2}}p^{-\frac{m}{4}}\left(2(\varepsilon(a))^{\frac{m}{4}}+\sqrt{10}p^{\frac{\nu}{4}}\right)\tag{3.4}$$

Now an argument similar to the one used to prove (3.4) leads to general bound

$$|S_N(h)| \le N^{\frac{1}{2}} p^{-\frac{m-s}{4}} \left(2(\varepsilon_p(a))^{\frac{m}{4}} + \sqrt{10} p^{\frac{\nu}{4}}\right).$$

□

The estimates of exponential sums obtained in this section can be used to study the properties of the sequence PRN's $\{y_n\}$.

From our sequence $\{x_n\}$ we derive the sequence $\{X_n^{(s)}\}$ of points in $[0,1)^s$ putting $X_n^{(s)} := (x_n, x_{n+1}, \ldots, x_{n+s-1})$. From the theorems 1 and 2 and inequality for discrepancy (see, Niederreiter[4], ch.8) we have

THEOREM 4. *The discrepancy $D_N^{(s)}$, $s = 2,3,4$, of points constructed by linear-inversive congruential generator (1.2) with parameters a, b, c, which satisfy the condition*

$$0 < \nu_p(b) = \nu,\ 2\nu < \mu = \nu_p(c),\ a \not\equiv y_0^2 (mod\ p),$$

has the following bound

$$D_\tau^{(s)} \le \frac{s}{2p^{m-\nu}} + p^{-\frac{m-2\nu}{2}} \log^s p^m. \tag{3.5}$$

Finally note that Theorem 3 shows that for almost all $y_0 \in \mathbb{Z}_{p^m}^*$ the estimate of discrepancy can be improved.

The estimate (3.5) of discrepancy $D_\tau^{(s)}$ means that the sequence $\{x_n\}$ generated by recursion (1.2) passes s-dimensional serial test on independence(unpredictability) (for $s = 2,3,4$).

References

1.W.-S. Chou, The period lengths of inversive congruential recursions, Acta Arith., 73:325-341, 1995.

2.J. Eichenauer and J. Lehn, A non-linear congruential pseudorandom number generator, Statist. Hefte, 27:315-326, 1986.

3.J. Eichenauer-Herrmann and A. Topuzoğlu, On the period of congruential pseudorandom number sequences generated by inversions, J. Comput. Appl. Math., 31:87-96, 1990.

4.H. Niederreiter, Random Number Generation and Quasi-Monte Carlo Methods. SIAM, 1992, Philadelphia,Pa.

5.H. Niederreiter and I. Shparlinski, Exponential sums and the distribution of inversive congruential pseudorandom numbers with prime-power modulus, Acta Arith., 90:89-98, 2000.

6.P. Varbanets and S. Varbanets, Exponential sums on the sequences of inversive congruential pseudorandom numbers with prime-power modulus, Vorono's Impact on modern science, Proceedings of the 4th International Conference on Analytic Number Theory and Spatial Tessellations, Book 4, Volume 1, Kyiv, Ukraine, September 22-28, pages 112-130, Kyiv, 2008.

Proceedings, 4th Chaotic Modeling and Simulation International Conference
31 May – 3 June 2011, Agios Nikolaos, Crete Greece

Study of complex dynamics in an pH-oscillatory chemical reaction

T. Veber, I. Schreiber, and L. Schreiberová

Institute of Chemical Technology Prague, Department of Chemical Engineering and Center for Nonlinear Dynamics of Chemical and Biological Systems, Technická 5, 166 28 Prague 6, Czech Republic
E-mail: tomas.veber@vscht.cz
Telephone: +420-220443033, fax: +420-220444320

Abstract: The reaction system hydrogen peroxide-thiosulphate-sulfite in acidic solution belongs to the extensive family of pH-oscillators marked by significant pH variations in time implying autocatalytic nature of hydrogen ions. This system is known to display nonlinear behaviour in a continuous-flow stirred tank reactor. Dynamical regimes occurring in this system depend on external constrains such as temperature, flow rate or inlet concentrations of reactants. The hydrogen peroxide-thiosulphate-sulfite system displays strongly nonlinear dynamics as the flow rate k_0 is varied. The observed dynamical regimes of this reaction are periodic and aperiodic oscillations, chaotic behaviour and various stable steady states coexisting over a range of operating conditions. Presented work is focused on experimental study of aperiodic dynamics of the system and subsequent time series analysis. The analysis is based on the reconstruction of the attractor from the measured time series.
Keywords: Chemical reactor, aperiodic oscillations, time series analysis

1. Introduction

Nonlinear chemical dynamics represents an interdisciplinary branch of science that is specified by studying and understanding complex biological and natural processes through the chemical reaction observations [1]. These chemical reactions with appropriate chosen initial conditions, input parameters and well designed equipment for carrying out of chemical reactions can provide strange dynamical regimes which are closely associated with processes in human body or functions in plant and animal kingdom. Oscillations and other nonlinear phenomena in chemical reactions are can be studied particularly in special types of systems in which this dynamical behaviour can occur. One of them is open system represented by continuous-flow stirred tank reactor in which the reaction is kept far from equilibrium and thus give rise to complex behaviour indicated by a monitored quantity. As the dynamic system is specified by evolving in time, the monitored quantitity of interest is measured in time. The observed output signal can be then analyzes using the method of time series analysis. Analyze of dynamics of the system is based on phase space reconstruction from time series data points. Phase space reconstruction was first introduced to nonlinear dynamic theory by Packard [2] and Takens [3] involving building multidimensional phase space from scalar time series using time delay coordinates.

In this contribution, the phase space reconstruction based on singular value decomposition according Takens theorem is presented. In our study the time series analysis is applied to the experimental study of chaotic behaviour of inorganic pH-oscillatory reaction carried out in continuous stirred tank reactor. The observed quantity is the concentration of hydrogen ion, which plays an important role in the nature and living systems. The reaction between hydrogen peroxide-thiosulphate and sulfite ions is interesting in oxidation of sulfur solutions by hydrogen peroxide, many intermediates or complex reactive network with positive and negative feedbacks which leads to nonlinear dynamics such as oscillation or chaotic behaviour [4]. The reaction provides temperature sensitivity [5,6] as well as strong sensitivity to the presence of carbon dioxide in the ambient air [4]. Both influences also present possible ways to chaotic behaviour. In our experimental study we focused on finding array of chaotic dynamics if the influence of carbon dioxide is completely eliminated. The applied methods of time series analysis are based on delay reconstruction of matrix from measured timeseries and consequently important features from geometry interpretation of the measured behaviour are obtained. Decomposition of that matrix by calculation of eingevalues and eingevectors yields modes.

2. Dynamic system

Dynamic of the system (evolution process) is described with autonomous system of ordinary differential equations (ODEs) in an n-dimensional state (phase) space $\mathrm{G} \subset \mathrm{R}^n$, where R^n represents a set of all arranged tuplet real numbers which can be identified with e.g. a number of elements in a chemical reaction

$$\frac{\mathrm{dx}}{\mathrm{dt}} = \vec{\mathrm{f}}(\mathrm{x}),\ \mathrm{x} \in \mathrm{R}^n\ .$$

An expression on right side of the equation denotes a vector field. The solution of the equation can be interpreted as a function of two variables, a discrete time variable $t \in R$ and state (phase) variable $\mathrm{x} \in R^n$ and thus mentioned solution can be called as a phase flow $\varphi(t, \mathrm{x})$ of the system. Each state (phase) point is influenced by an abstract force causing a motion. The time evolution of real system is then described by motion of the state point along a trajectory considered as a smooth curve passing through the state point x. The vector field constitutes a driving force of the phase point along the trajectory and consequently determines the time evolution from the initial point. The system of all trajectories is consequently referred as phase portrait. The phase portrait can be interpreted as a geometry representation of a qualitative behaviour of all solutions of the system. The phase space reconstruction techniques by time delay embedding are most commonly based on embedding techniques according to Takens. Based on Takens's embedding theory, an attractor may be reconstructed with the embedding dimension $n \geq 2d + 1$.The embedding

dimension n is the lowest possible dimension of n-dimensional space R^n into which an attractor can be projected. d marks the dimension of the attractor.

2.2 Method of delay

Let us consider real data points $\mathrm{x}(\mathrm{t}_1), \mathrm{x}(\mathrm{t}_2), \mathrm{x}(\mathrm{t}_3),..., \mathrm{x}(\mathrm{t}_{\mathrm{N_T}}), \quad \mathrm{t} \in \mathrm{R}$ obtained from experimental time measurements. The data points can be arranged in the sequence of *m* vectors in an *n*-dimensional *embedding space* $\left\{ \nu_{\mathrm{j}} \in \mathrm{R}^{\mathrm{n}} \middle| \mathrm{j} = 1,2,..., \mathrm{m} \right\}$ (delay coordinate vectors)

$$\nu_{\mathrm{j}} = \left(\mathrm{x}_{\mathrm{j}}, \mathrm{x}_{\mathrm{j}+\tau_{\mathrm{d}}}, \ldots, \mathrm{x}_{\mathrm{j}+(\mathrm{n}-1)\tau_d} \right)$$

where *n* constitutes the dimension of the *embedding space* and *m* is defined as $m = \mathrm{N_T} - (n-1)\,\tau_{\mathrm{d}}$ and is number of points in the phase space. τ_{d} corresponds to a time delay in seconds and can be expressed as a multiple of sampling time τ_{S} and sampling frequency $\mathrm{f_S}$ of a time series.

$$\tau_{\mathrm{d}} = \tau_{\mathrm{S}}\, \mathrm{f_S}$$

2.2.1 Singular value decomposition

In the singular approach of this problem according to Broomhead and King [7], the corresponding time delay value $\tau_{\mathrm{d}} = 1$ is considered and such sequence of vectors in the *n*-dimensional space is used to generate *m x n trajectory matrix* X, whose components in the columns have same relationship to one another as do the rows [7]. Then introduce transpose matrix X^T of trajectory matrix X. If matrix X has the property $X = X^T$, then matrixes are symmetric. The *m x m* matrix $\Theta = X\,X^T$ and *n x n matrix* $\Omega = X^T X$ are real symmetric matrices, called *structural* and *covariance matrix* consequently. Let *trajectory matrix* X be a *m x n*, where $m \geq n$.

$$\mathrm{X} = \begin{bmatrix} \mathrm{x}_1 & \mathrm{x}_2 & \cdots & \mathrm{x}_{\mathrm{n}} \\ \mathrm{x}_2 & \mathrm{x}_3 & \cdots & \mathrm{x}_{\mathrm{n+1}} \\ \vdots & \vdots & \ddots & \vdots \\ \mathrm{x}_{\mathrm{m}} & \mathrm{x}_{\mathrm{m+1}} & \cdots & \mathrm{x}_{\mathrm{m+n-1}} \end{bmatrix} \quad \mathrm{X}^T = \begin{bmatrix} \mathrm{x}_1 & \mathrm{x}_2 & \cdots & \mathrm{x}_{m} \\ \mathrm{x}_2 & \mathrm{x}_3 & \cdots & \mathrm{x}_{\mathrm{m+1}} \\ \vdots & \vdots & \ddots & \vdots \\ \mathrm{x}_{\mathrm{n}} & \mathrm{x}_{\mathrm{n+1}} & \cdots & \mathrm{x}_{\mathrm{m+n-1}} \end{bmatrix}$$

The matrix X can be factorized using singular value decomposition (SVD) based on decomposition its eingevalues and eingevectors into a product of three matrices as fallows

$$\mathrm{X} = \mathrm{U}\,\Sigma\,\mathrm{V}^T$$

where U and V are orthogonal matrices, i.e., $U^T U = I$ and $V^T V = I$, whereas I is a *unit matrix*. The matrix U is *m x m* matrix containing eingevectors of structural matrix Θ and V is *n x n* matrix consists of eingevectors of *covariance matrix* Ω. The column vectors of the matrix U denoted by $\vec{u} = (u_1, u_2, \ldots, u_m)$ represent left singular vectors of originally *trajectory matrix* X, while the column vectors of the matrix V denoted by $\vec{v} = (v_1, v_2, \ldots, v_m)$ are the right singular vectors of X. The *m x n* diagonal matrix **Σ** carries corresponding *singular values* σ_i in the order of monotonically decreasing magnitude along its diagonal and all of them are nonnegative numbers

$$\Sigma = diag(\sigma_1, \sigma_2, \ldots, \sigma_n) \text{ where } \sigma_1 \geq \sigma_2 \geq \cdots \geq \sigma_n \geq 0$$

Because of close relation to eigenvalue decomposition, singular values σ_i are simply the square roots of eingevalues of the structural matrix Θ and the covariance matrix Ω according to

$$\Theta \vec{u} = \sigma_i^2 \vec{u} \qquad \Omega \vec{v} = \sigma_i^2 \vec{v}$$

Note, that trajectory matrix X can be written as a sum goes from 1 to *n*, where *n* is the rank of X

$$X = \sum_{i=1}^{n} \sigma_i u_i v_i^T$$

3. Experimental setup and conditions

3.1 Reactor. An experimental estimation was performed in cylindrical-shaped plexiglass cell under the conditions of the continuous stirred tank reactor experiments. The reactor was closed to air with plexiglass cap. This upside cap was equipped with holes for the inlets and outlet for tubing and the input for pH-electrode probe. RTD probe (RTD-860) for measuring temperature was inbuilt in the reactor side. A liquid in the flow cell was change through four inlet teflon tubes connected to the flexible silicon tubes (ID 1.30 mm) for peristaltic feeding (Ismatec IPC N). The cell was thermostated on required temperature of 26 ± 0.2°C from the bottom by circulating water from RM6 Lauda E103 thermostat. The liquid volume of the reactor was 17.6 mL. A teflon-covered magnetic stirred (1 cm long) was used to ensure a uniform mixing. The waste liquid was removed using canted position of the reactor. Two quantities were measured inside the reactor during the CSTR experiments. The pH-time data during the reaction were measured by a semi-micro combined pH-electrode (Theta ´90, type HC 139) connected to an Orion 525A pH-meter and an A\D converter and collected on a hard-disk of computer (Octek, Intel Pentium 200Mhz). The temperature inside the reactor was measured by RTD-860 probe connected to A\D converter and storaged on a hard-disk of computer. The computer also controlled pump speed change and recorded its actual value on a hard-disk.

3.2 Solutions. H_2O_2 (30% aqueous solution, Penta, Chrudim), Na_2SO_3 (Penta, Chrudim), NaS_2O_3 (Sigma-Aldrich) and H_2SO_4 (Lachema a.s., Neratovice) are chemicals used in this study. Two reactant solutions were prepared daily from fresh demineralized water and commercial available chemicals. One solution contained diluted hydrogen peroxide and the other contained the mixture of thiosulphate with sulfite and sulfuric acid. Input concentrations of the reactants were: $[H_2O_2]_0$=0.0135 mol/L, $[Na_2S_2O_3]_0$=0.005 mol/L, $[Na_2SO_3]_0$=0.0025 mol/L, $[H_2SO_4]_0$=5.10^{-4} mol/L. The initial concentration ($[\ ]_0$) is defined for each species to be the concentration of the species on the entrance to the reaction cell. Both reactant solutions were bubbled with nitrogen for at least 12 hours before the experiment for elimination of carbon dioxide impurities.

3.3 Procedure. Maximum pumping rate was used to fill the reactor with the input solutions. Then the pump speed was reduced to the desired lower speed k_0 = 0.0028 s^{-1} for the experiments and thermostated on required temperature at 26 ± 0.2°C. The rate of flow (proportional to reciprocal residence time) is conveniently characterized by $k_0 = \dot{V} / V$ (s^{-1}), where $\dot{V}$ (mL s^{-1}) is the total flow rate and V (mL) is the volume of the reaction mixture in the cell. Residence reciprocal time k_0 is the average time that a molecule spends in the reactor and presents that fast flow rate through a large reactor is equivalent to a slow rate through a small reactor [8]. The flow rate was systematically increased up in regular time steps by to the higher flow rate. Sufficient time was allowed at each flow rate for the system to keep the dynamical behaviour. By increasing the flow rate gradually until the maxium desired flow rate was obtain chaotic behaviour. Throughout the flow experiments reactant solutions were bubbled with nitrogen.

4. Results and discussion

The system at the flow rate k_0 = 0.0035 s^{-1} exhibit chaotic behaviour as is clearly shown in Fig. 1. Presented time series is characterized by occurrence of irregular large amplitude peaks with considerably smaller peaks. This figure represents interesting feature of the system when stock solutions are bubbled by nitrogen and the influence of carbon dioxide is eliminated. This feature reveals a complex nature of the reaction system in a short range of flow rate. Undesirable effect of carbon dioxide was suppressed for reasons of creating reaction intermediated leading to activation more closely unspecified secondary oscillators in reaction mechanism. This secondary oscillator may be a source of period-doubling or complex oscillations as is noted in [4, 9]. Our attention was focused on finding a region with aperiodic dynamic and obtaining geometric visualization of trajectories in phase space. For this purpose collection of many data points was necessary. The experimental data shown in Fig.1 provided 7200 data points which are used at the present analysis. For the reconstruction of the attractor using singular value decomposition the minimal time delay τ_d=1 (corresponding to 0.333 s) is applied to the original measured data. The main

concept of this method is to extract minimum embedding dimension n_S of embedding space.

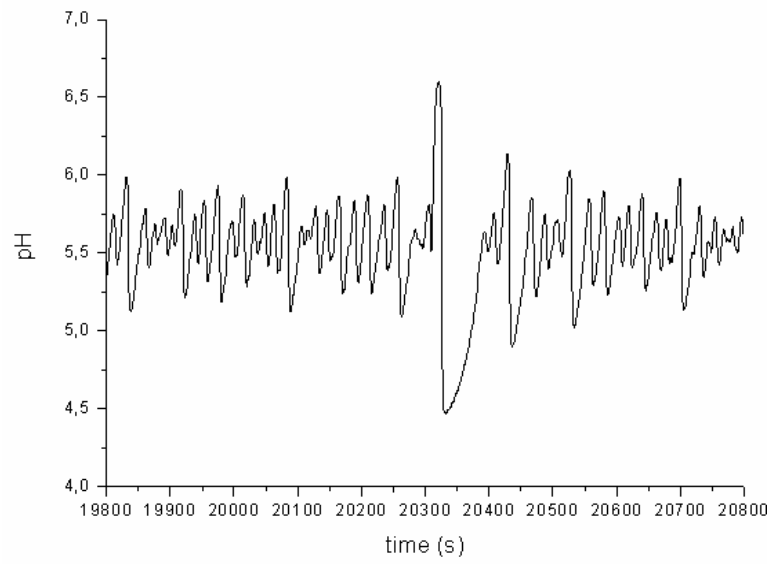

Fig. 1 Seguence of a time series measured at a flow rate k_0=0.0035 s^{-1}.

For the calculations we created am Matlab program. Measured time series in the form of column data points in Excel program were loaded to the Matlab m-file project and a decomposition of trajectory matrix was realized using Matlab SVD toolbox. For the reconstruction we chosen initial embedding dimension n_S=200. Figure 2 illustrates spectrum of corresponding 200 singular values, where horizontal axis corresponds to ordinal number of singular values and on the ordinate axis is a logarithm of the normalized singular value is plotted. The gradual decline of the dependence is evident and thus no distinct sudden change for determination of minimum embedding dimension n_S is clearly discernable. However, a slight jump in plotted singular values at the ordinal number about 13 may be taken as an indicator of the minimum embedding dimension n_S. Singular values above this break point constitute information about all essential parts of decomposed signal. These values are significant for the reconstruction of attractor. Singular values below the break point are associated with minor modes and may indicate either small-scale deterministic or noise level of measured signal. Such values are insignificant. When replaced by zero value and modified diagonal matrix is multiplied with original matrix U and V^T a filtrated version of originally trajectory matrix is created.

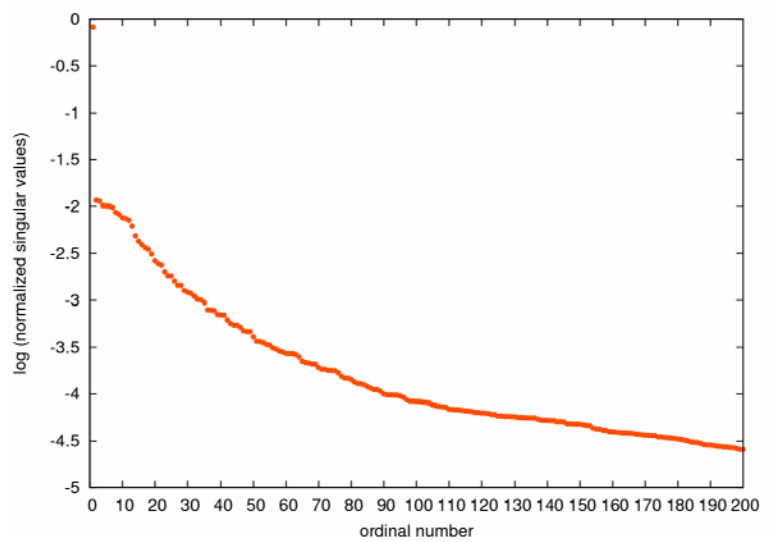

Fig. 2 Spectrum of normalized singular values.

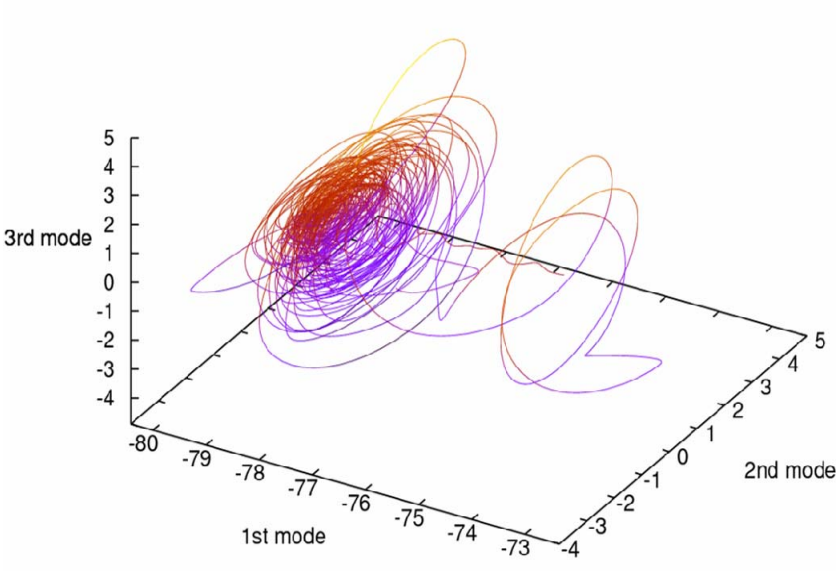

Fig. 3 Reconstructed attractor from singular value decomposition using first three modes.

The importance of each significant singular value is interpreted in the form of corresponding modes.

Modes are determined by columns of left singular vectors $\vec{u}$ representing directions and significant singular values representing the lengths of principal axes of an ellipsoid [7]. When the first three modes of singular value decomposition are plotted in 3D phase space, the reconstruction of atrractor obtained as is shown in Fig. 3

5. Conclusions

The autonomous dynamics of our chemical system of hydrogen peroxide-thiosulphate-sulfite was experimentally investigated in the continuous stirred tank reactor under the constant temperature. The flow rate k_0 was used as a bifurcation parameter in our experiments. Our intention was to find a region with aperiodic oscillations and successive time series analysis based on singular value decomposition. From measured experimental data of pH value in time a preliminary geometric structure of the dynamic was illustrated. Singular decomposition of measured signal was used to determine a minimum embedding dimension, but there is problem with clear indication where to cut off the modes used for the reconstruction of attractor. In future work, other methods of determination of embedding dimension, appropriate time delay or determination of Lyapunov exponents are object of interest.

Acknowledgements

This work was supported by GACR 104/08/H055, GACR 203/09/2091, project MSM 6046137306 and by financial support from specific university research (MSMT No 21/2011).

References

1. I. R. Epstein, K. Showalter: Nonlinear Chemical Dynamics: Oscillations, Patterns, and Chaos, *J. Am. Chem.* 100: 13132-13147, 1996.
2. N.H. Packard, J.P. Crutchfield, J.D. Framer, R.S. Shaw. Geometry from time series data, *Physica D* 45: 712-716, 1980.
3. F. Takens, Detecting Strange Attractors in Turbulence. Lecture Notes in Mathematics, *Springer, Berlin*, vol. 898: 366-381, 1981.
4. G. Rábai, I. Hanazaki. Chaotic pH Oscillations in the Hydrogen Peroxide – Thiosulfate – Sulfite Flow System, *J. Phys. Chem. A* 103: 7268-7273, 1999.
5. G. Rábai, T. G. Szántó, K. Kovács. Temperature - Induced Route to Chaos in the H_2O_2-HSO_3^--$S_2O_3^{2-}$Flow reaction system, *J. Phys. Chem. A* 112: 12007-12010, 2008
6. G. Rábai, I. Hanazaki. Temperature compensation in the oscillatory hydrogen peroxide – thiosulfate – sulfite flow system, *Chem. Commun. 19*: 1965-1966, 1999
7. D.S. Broomhead, G.P. King. Extracting qualitative dynamics from experimental data, *Physica D* 20: 217-236, 1986.
8. D. Kaplan, L. Glass. Understanding Nonlinear Dynamics, *Springer-Verlag, New York, Inc*., ISBN 0-387-94440-0, 1995.
9. Bakes D.. Study of Complex Dynamics of Chemical Reactions and Applications of Dynamical Responses Methods, Disertation thesis, VSCHT Prague, 2008.